MEASURED AND SIMULATED SOIL WATER REDISTRIBUTION AND EXTRACTION PATTERNS OF DRIP-IRRIGATED TOMATOES ABOVE A SHALLOW WATER TABLE

By

GEORGE VELLIDIS

A DISSERTATION PRESENTED TO THE GRADUATE SCHOOL
OF THE UNIVERSITY OF FLORIDA IN PARTIAL FULFILLMENT
OF THE REQUIREMENTS FOR THE DEGREE OF
DOCTOR OF PHILOSOPHY

UNIVERSITY OF FLORIDA

1989

UNIVERSITY OF FLORIDA
3 1262 08552 5862

Copyright 1989

by

George Vellidis

To my parents . . .

who encouraged me to reach for the stars

ACKNOWLEDGEMENTS

I would like to express special appreciation and thanks to Dr. Allen G. Smajstrla for his guidance, assistance, and encouragement throughout this research. His reliable support and sound advice formed the basis of a rewarding and enjoyable experience at the University of Florida. I would also like to thank the other members of my committee, Dr. D.Z. Haman, Dr. F.S. Zazueta, Dr. G.A. Clark, and Dr. J.J. Delfino for their support.

Special thanks go to Dr. Ken Stone for his friendship and help and to Mr. Danny Burch for his technical assistance and practical advice during the experimental phase of this research.

Finally, I would like to thank my wife Tracey who helped me collect data, weigh samples, irrigate tomatoes, repair shelters, and edit my writing. Her encouragement and her beautiful smile made the problems I encountered much easier to overcome.

TABLE OF CONTENTS

page

ACKNOWLEDGEMENTS iv

LIST OF TABLES vii

LIST OF FIGURES ix

ABSTRACT xii

CHAPTERS

1 INTRODUCTION 1

2 REVIEW OF LITERATURE 3

Soil Water Potential 3
Measurement of Soil Water 4
Soil-Moisture Content Measurements 4
Matric Potential Measurements 5
Automation of Matric Potential Measurements 6
Soil Hydraulic Properties 8
Soil-Moisture Retention Curve 8
Hydraulic Conductivity Curve 8
Water Flow in Unsaturated Soils 11
Numerical Solutions 14
Infiltration From a Line Source 15
Water Extraction by Plant Roots 17
Lysimetry 23

3 EXPERIMENTAL PROCEDURE 24

The Field Lysimeter System 24
Lysimeter Construction 24
The Data Acquisition System 31
Lysimeter System Operation 36
Soil Characteristics 38
Bulk Density 39
Soil-Moisture Retention Curves 40
Saturated Hydraulic Conductivity 40
Hydraulic Conductivity Curve 41

4 EXPERIMENTAL RESULTS 45

Plant Growth 45
Measurement Accuracy 46
Water Budget Accuracy 46

Weekly, Monthly, and Seasonal Water Use Accuracy 46
Crop Water Use 47
Partitioning of Crop Water Use 47
Weekly, Monthly, and Seasonal Water Use 49
Redistribution and Extraction Patterns 58
Evaporation from the Soil 66

5 NUMERICAL SOLUTION 69

One-Dimensional Model Development 69
Boundary Conditions 73
Solution 76
Time Step 77
Updating of Soil Parameters 78
Mass Balance 78
One-Dimensional Model Verification 79
Two-Dimensional Model Development 84
Boundary Conditions 87
Solution 91
Water Extraction by Plant Roots 92
Two-Dimensional Model Verification 97
Simulation of the Lysimeter Study 102
Estimated Daily ET 105
The Root Distribution Term, RDT 106
Simulation Results 109
Model Applications 118

6 SUMMARY AND CONCLUSIONS 119

The Lysimeter System 119
Field Data 120
Numerical Simulation 121
Model Applications 121

APPENDICES

A SOIL TEST REPORTS 122

B NUMERICAL MODEL PROGRAM LISTING 134

C TABULATED SOIL PARAMETERS 181

REFERENCES 192

BIOGRAPHICAL SKETCH 197

LIST OF TABLES

table		page
3.1.	Volumes of Irrigation Applications and Equivalent Depths Over the Lysimeter Areas.	38
3.2.	Characteristic Soil Properties.	39
3.3.	Parameters for van Genuchten's Equation.	41
4.1.	Canopy Dimensions (m)	45
4.2.	Monthly and Seasonal Water Use.	56
5.1.	Measured and Modified Saturated Hydraulic Conductivity.	110
A.1.	Routine Test Report and Standard Fertilization Recommendations: Builder's sand sample 1.	123
A.2.	Routine Test Report and Standard Fertilization Recommendations: Builder's sand sample 2.	124
A.3.	Routine Test Report and Standard Fertilization Recommendations: Builder's sand sample 3.	125
A.4.	Routine Test Report and Standard Fertilization Recommendations: Astatula f.s. sample 1.	126
A.5.	Routine Test Report and Standard Fertilization Recommendations: Astatula f.s. sample 2.	127
A.5.	Routine Test Report and Standard Fertilization Recommendations: Astatula f.s. sample 3.	128
A.7.	Routine Test Report and Standard Fertilization Recommendations: Pomona sand sample 1.	129
A.8.	Routine Test Report and Standard Fertilization Recommendations: Pomona sand sample 2.	130
A.9.	Routine Test Report and Standard Fertilization Recommendations: Pomona sand sample 3.	131
A.10.	Micronutrients, Organic Matter, Copper Toxicity Test, and Soluble Salts.	133
C.1.	Hydraulic Properties of Arredondo Fine Sand.	181
C.2.	Hydraulic Properties of Rehevot Sand.	184

C.3. Hydraulic Properties of Adelanto Loam. 186
C.4. Hydraulic Properties of Pachappa Loam. 188
C.5. Hydraulic Properties of Yolo Light Clay. 190

LIST OF FIGURES

figure		page
3.1.	Field layout of the lysimeter system.	25
3.2.	Side view giving details of an individual lysimeter soil water status monitoring system.	27
3.3.	Float valve and sump used to control the water table level.	29
3.4.	End view of the float valve showing details of the mechanism used to mount the valve onto a threaded stand.	29
3.5.	Side view of a lysimeter showing the location of the 10 tensiometers.	33
3.6.	End view of a lysimeter showing the location of the 10 tensiometers.	33
3.7.	Calibration curves of output voltage versus pressure for transducer no. 4.	34
3.8.	Fluctuations in atmospheric pressure for the week of June 13-19.	35
3.9.	Arrangement of the three soils in the lysimeters.	36
3.10.	Soil-moisture retention curves for the three soils used in this study.	42
3.11.	Fitted and experimental soil-moisture retention curves for the three soils used in this study.	43
3.12.	Hydraulic conductivity curves for the three soils used in this study.	44
4.1.	Partitioning of crop water use in May.	48
4.2.	Partitioning of crop water use in June.	49
4.3.	Weekly crop water use in builder's sand, May, 1988.	50
4.4.	Weekly crop water use in builder's sand, June, 1988.	51
4.5.	Weekly crop water use in Astatula f.s., May, 1988.	52
4.6.	Weekly crop water use in Astatula f.s., June, 1988.	53
4.7.	Weekly crop water use in Pomona sand, May, 1988.	54
4.8.	Weekly crop water use in Pomona sand, June, 1988.	55
4.9.	Cumulative water use for the plants growing in builder's sand.	56

4.10. Cumulative water use for the plants growing in Astatula f.s. 57

4.11. Cumulative water use for the plants growing in Pomona sand. 57

4.12. Tensiometer readings versus time on a daily scale. 59

4.13. Tensiometer readings versus time on an hourly scale. 59

4.14. Tensiometer readings versus time on a daily scale for the week of June 6. ... 61

4.15. Side view of a lysimeter showing the bed, the water table, and the tensiometer locations. 61

4.16. Equipotential lines in a Pomona sand profile at irrigation (kPa). 63

4.17. Equipotential lines in a Pomona sand profile during redistribution (kPa). 63

4.18. Equipotential lines in a Pomona sand profile during redistribution (kPa). 64

4.19. Equipotential lines in a Pomona sand profile following redistribution (kPa). .. 64

4.20. Equipotential lines in a Pomona sand profile during extraction (kPa). 65

4.21. Equipotential lines in a Pomona sand profile during extraction (kPa). 65

4.22. Comparison of Penman ET and observed bare soil evaporation from the lysimeters. 67

4.23. Comparison of Penman ET and estimated daily bare soil evaporation from the lysimeters during the final two months of the growing season. 68

5.1. The finite difference grid system used for the one-dimensional model. Adapted from Stone (1987), p.38. 70

5.2. Simulated, analytical, and experimental results of steady-state evaporation at a rate of 0.033 mm/hr from a water table in Yolo light clay. 80

5.3. Simulated results of soil water content profiles for infiltration into Rehevot sand under constant rain intensity of 12.7 mm/hr. 81

5.4. Simulated results of soil water content profiles for infiltration into Rehevot sand under constant rain intensity of 47 mm/hr. 81

5.5. Simulated and analytical results of steady-state infiltration above a shallow water table at rates of 0.0 and 1.5 mm/hr. 83

5.6. Simulated and analytical results of steady-state infiltration above a shallow water table with a constant extraction rate of 0.42 mm/hr. 83

5.7. Schematic diagram of the finite-difference grid system for the two-dimensional model of water movement and extraction. 85

5.8. Effect of the relative available soil water and four ET rates on the predicted soil water extraction rate. 95

5.9. Simulated distribution of the daily ET over a 24-hr period. 96

5.10. Two-dimensional model simulated results of soil water content profiles for infiltration into Rehevot sand under constant rain intensity of 12.7 mm/hr. . . 98

5.11. Two-dimensional model simulated results of soil water content profiles for infiltration into Rehevot sand under constant rain intensity of 47 mm/hr. . . . 98

5.12. Lines of constant pressure head, ψ (mm), for parallel buried line sources 1220 mm apart. 100

5.13. Lines of constant pressure head, ψ (mm), for a buried line source with a water table 300 mm below the soil surface. 100

5.14. The vertical water content distribution at (0,z) for a line source discharge of 11442 mm^2/hr after 0.40 hrs. 103

5.15. The horizontal water content distribution at (x,210) for a line source discharge of 11442 mm^2/hr after 0.40 hrs. 103

5.16. Finite difference mesh for the lysimeter problem. 104

5.17. Comparison of Penman ET and estimated daily ET from the lysimeters during the final two months of the growing season. 105

5.18. The number of cells contained by each soil compartment. 107

5.19. Distribution of extraction in Astatula f.s. for the week of May 2. 108

5.20. Distribution of extraction in Pomona sand for the week of June 6. 108

5.21. Comparison of simulated and observed pressure heads at a depth of 100 mm in Astatula f.s. for the week of May 2. 111

5.22. Comparison of simulated and observed pressure heads at a depth of 200 mm in Astatula f.s. for the week of May 2. 112

5.23. Comparison of simulated and observed pressure heads at a depth of 300 mm in Astatula f.s. for the week of May 2. 113

5.24. Comparison of simulated and observed pressure heads at a depth of 100 mm in Pomona sand for the week of June 6. 114

5.25. Comparison of simulated and observed pressure heads at a depth of 200 mm in Pomona sand for the week of June 6. 115

5.26. Comparison of simulated and observed pressure heads at a depth of 300 mm in Pomona sand for the week of June 6. 116

Abstract of Dissertation Presented to the Graduate School
of the University of Florida in Partial Fulfillment of the
Requirements for the Degree of Doctor of Philosophy

MEASURED AND SIMULATED SOIL WATER REDISTRIBUTION AND EXTRACTION PATTERNS OF DRIP-IRRIGATED TOMATOES ABOVE A SHALLOW WATER TABLE

By

GEORGE VELLIDIS

May, 1989

Chairman: Allen G. Smajstrla
Major Department: Agricultural Engineering

In Florida, the greatest use of fresh water resources is for supplemental irrigation of agricultural crops. Because of increasing competition for the consumptive use of this water, there has been a rapid increase in the use of micro irrigation, and in particular, line source drip irrigation systems which are increasingly being used to irrigate high cash value crops such as fruits, vegetables, and ornamentals.

Throughout Florida, vegetables are often grown on mulched beds in soils that commonly require irrigation even if they are subject to naturally occurring high water tables. The contribution of high water tables to soil water extracted by agricultural crops had not been accurately determined, especially in combination with line source drip irrigation systems. This soil-plant-water relationship problem lent itself well to a study conducted in lysimeters.

A set of six rain-sheltered field lysimeters was developed to simulate these conditions. Each drainage lysimeter contained a water table regulation device and was irrigated with a

line source drip irrigation system. Soil pressure potential data were collected continuously using a microcomputer-based tensiometer-pressure transducer data acquisition system.

Experiments were conducted in the lysimeters to measure crop water use and redistribution and extraction patterns of a tomato crop. The design of the lysimeters permitted crop water use to be partitioned into irrigation and water table recharge components. Results indicated that a significant portion of daily plant water use was provided by the water table. Redistribution and extraction patterns calculated from the soil water potential measurements showed that very little change in soil water status took place at horizontal distances of more than 200 mm from the irrigation lateral and at depths greater than 300 mm.

A two-dimensional finite difference model was developed to simulate water infiltration, redistribution, and extraction under the above conditions. The simulated results were in excellent agreement with the field observations. The model can be used to investigate many different irrigation strategies without the cost normally associated with field experiments.

CHAPTER 1
INTRODUCTION

The greatest use of Florida's fresh water resources is for supplemental irrigation of agricultural crops. Harrison et al. (1983) reported that 41% of the state's total fresh water use was for irrigation. In 1987, 728,000 ha were irrigated in Florida by all types of irrigation systems (Goldstein, 1988).

There are three main methods used for supplemental irrigation in Florida: sprinkler, seepage, and micro irrigation. In the past 10 years there has been a rapid increase in the use of micro irrigation in Florida. This is due to energy and water savings offered by these systems in a time of increasing fuel costs, the ability to apply nutrients and chemicals directly to the crop, and increasing competition for the consumptive use of available fresh water. Of special interest are line source drip irrigation systems which are increasingly being used to irrigate high cash value crops such as fruits, vegetables, and ornamentals.

Line source systems consist of irrigation laterals with closely-spaced discharge points or emitters. These differ from other micro irrigation systems in that they generate a wetted band of soil along the lateral, as opposed to a series of nonoverlapping wetted bulbs. When well designed and managed, and in absence of rainfall, they provide adequate water for crop growth and minimize losses from percolation below the root zone and evaporation from the soil surface.

Florida soils commonly require irrigation even if they are subject to naturally occurring high water tables (0.5-1.5 m below the bed surface). The contribution of high water tables to soil water extracted by agricultural crops has not been accurately determined, especially in combination with line source drip irrigation systems. This soil-plant-water relationship problem lends itself well to studies conducted in lysimeters if the lysimeter system is designed to adequately approximate the physical system (Chow, 1964).

A sound knowledge of the dynamics of water movement from line sources into the soil, and of the extraction patterns observed under agricultural crops is needed to minimize irrigation input while optimizing production returns. The dynamics of interactions must be studied mathematically using numerical methods because analytical solutions are applicable to only a few specific cases due to the nonlinear nature of the governing equations. Many researchers have developed numerical models to use in the study of soil water movement (Smajstrla, 1982; and Feddes et al., 1978). These models allow many different irrigation strategies to be investigated without the cost normally associated with field experiments (Stone, 1987). These models, however, do not address the unique conditions often encountered in Florida.

The purpose of this research was to obtain a clear understanding of the dynamic soil-plant-water relationships that occur when agricultural crops are grown on sandy soils, irrigated by line source drip systems, and subjected to naturally occurring high water tables. To achieve this goal, three objectives were established:

1. To develop and test a set of field lysimeters in which irrigation studies could be conducted under high water table conditions.
2. To use real-time monitoring of soil water potentials to record the dynamics of soil water redistribution and extraction under line source micro irrigation systems and high water table conditions.
3. To develop a mathematical model that describes the redistribution and extraction of soil water governed by the above conditions and formulate a numerical procedure for evaluating the model.

CHAPTER 2
REVIEW OF LITERATURE

Soil Water Potential

In the soil, water moves from points where it has a high energy status to points where it has a lower one. It is constantly in pursuit of that elusive state known as equilibrium (Hillel, 1980). Therefore, soil water moves constantly in the direction of decreasing potential energy. The energy status of water in soil is called the water potential Ψ and is composed of several components

$$\Psi = \psi + \psi_g + (\psi_{osm} + \psi_{gas}) \tag{2.1}$$

where

ψ = matric potential, resulting from capillary and adsorptive forces due to the soil matrix,

ψ_g = gravitational potential, resulting from the gravitational force,

ψ_{osm} = osmotic potential, resulting from osmotic forces, and

ψ_{gas} = pneumatic potential, resulting from changes in ambient gas pressure.

In studies of soil moisture flow, the osmotic and pneumatic potentials can usually be neglected. The influence of ψ_{osm} is low because, in general, solute concentrations in the soil solution will not significantly affect liquid flow. Pneumatic pressure can be disregarded because atmospheric pressure remains nearly constant and gas pressures in natural soil generally do not differ from the atmospheric pressure. Equation (2.1) then reduces to

$$\Psi = \psi + \psi_g \tag{2.2}$$

Soil water potential can be expressed in terms of mass, volume, or weight, and it is most often expressed as energy per unit weight of soil water. Soil water potential then has

units of length, i.e. mm, which can easily be translated to hydrostatic pressure. For example, 100 mm of water is equivalent to about 1 kPa or 0.01 bar.

The matric potential (ψ) in unsaturated soil is negative, because work is needed to withdraw water against the soil matric forces. At the phreatic surface, ψ=0 mm, while it is positive below the water table.

The gravitational potential (ψ_g) at each point is determined by the height of the point relative to some arbitrary reference level, z. If the origin of z is taken at the soil surface with z positive in the downward direction, ψ_g=-z mm anywhere below the soil surface.

When dealing only with the sum of matric and gravitational potential expressed in units of length, the sum is referred to as the hydraulic head, H. Equation (2.2) becomes

$$H = \psi - z \quad (mm) \tag{2.3}$$

with ψ now called the soil moisture pressure head and z the gravitational head. It is convenient to refer to negative pressure head (ψ) as a positive suction or tension (h). Thus

$$h = -\psi \tag{2.4}$$

and the value of h ranges from 0 to 10^8 mm (Feddes et al., 1978).

Measurement of Soil Water

There are two general reasons for measuring soil water. One is to determine the moisture content of the soil (θ), and the other to determine the magnitude of the matric potential, or pressure head (ψ), in the soil.

Soil-Moisture Content Measurements

There are direct or indirect methods to measure θ. The gravimetric method involves removing a sample by augering into the soil and then determining the moist and dry weights (Hillel, 1980).

Neutron scattering allows the nondestructive measurement of soil-moisture content. Although the method is efficient and reliable, it has low spatial resolution. Gamma ray absorption, on the other hand, allows measurement in very thin layers of soil but is a rather difficult and erratic procedure.

Another approach involves the use of the electrical resistance of a soil volume to measure its moisture content. Colman and Hendrix (1949), among others, used electrical resistance blocks placed in the soil and left to equilibrate with soil moisture to produce a calibration curve of block resistance versus soil wetness. They found, however, that porous blocks placed in the soil equilibrate with matric potential rather than soil moisture.

Except for the gravimetric method, the techniques discussed produce indirect measurements of soil-moisture content and do not lend themselves to automation. Overall, the measurement of soil wetness does not provide a sufficient description of the state of soil water (Hillel, 1980). To obtain such a description, matric potential must be measured.

Matric Potential Measurements

To measure matric potential in the field, an instrument known as a tensiometer is used. The tensiometer consists of a closed tube with a porous ceramic cup on the end which is inserted into the soil. The cup/tube assembly is filled with deaerated water, sealed, and allowed to equilibrate with the soil water. Initially, moist soil at atmospheric pressure is placed in contact with pure water across the ceramic. Solutes then diffuse from the soil across the ceramic to the tensiometer solution until solute equilibrium is established. At that time, the solution in the instrument is called the equilibrium dialyzate (Taylor and Ashcroft, 1972). This effectively eliminates any osmotic potential component from consideration. Soil water, being generally at subatmospheric pressure, exercises a suction which draws out a certain amount of dialyzate from the rigid and airtight tensiometer, thus causing a drop in its hydrostatic pressure (Hillel, 1980). A pressure sensing device, usually a vacuum gage, a mercury manometer, or an electrical transducer, is used to measure the pressure in the tensiometer tube.

In a tensiometer, the matric potential is not measured directly. Instead, the negative pressure created within the tensiometer by the matric suction is measured. When the pressure head is divided by the density of liquid water, the pressure potential of the dialyzate in terms of energy per mass is obtained. Although the matric potential of the soil is not measured directly, it is assumed to be equal to the pressure potential of the dialyzate, which is directly determined (Taylor and Ashcroft, 1972). Tensiometers left in the soil for a long period of time tend to follow the changes in the matric potential. This potential is also the hydraulic potential that a plant must exert to extract water from the soil.

The hydraulic resistance of the ceramic cup, the surrounding soil, and the contact between the cup and soil cause tensiometer readings to lag behind the changes in the soil matric suction. Lags are also caused by the volume of water needed to be moved through the cup to register on the measuring device. This lag time can be minimized by the use of a null-type device or of a transducer-type pressure sensor with rigid tubing, so that practically no flow of water is required as the tensiometer adjusts (Hillel, 1980).

The useful range of tensiometers is from 0 to -80 kPa. Below -80 kPa, air enters through the ceramic cup or the water column in the tensiometer breaks, causing the tensiometer to fail. This measurement limitation is not serious for crops on sandy soils because 75% or more of the amount of soil water used by plants is depleted within the tensiometer range.

Automation of Matric Potential Measurements

Early methods of measuring tensiometer pressure heads used mercury manometers. Later, mechanical vacuum gauges were used. Both methods functioned well for manual applications but neither was readily automated (Stone, 1987). Recent interest in better understanding the dynamics of soil water movement has spurred the development of numerical models that simulate water flow through the soil. The large amounts of data required to validate and calibrate these models have resulted in the need for an automated system of recording tensiometer readings on a continuous real-time basis.

Most recent efforts have focused on using a transducer-type pressure sensor to read the pressure head. Marthaler et al. (1983) used a pressure transducer to read individual tensiometers. The upper end of the tensiometer was closed off with septum stoppers to provide an airtight seal. A needle connected to a pressure transducer was manually inserted through the septum into a pocket of entrapped air in the tensiometer and the pressure transducer output was obtained immediately. However, since the transducer had to be moved manually from tensiometer to tensiometer, this was not an automated system.

Thomson et al. (1982) used individual pressure transducers on tensiometers with all air purged from the system to monitor matric potentials. Thus, they were able to avoid lag times associated with air pockets in the tensiometers. They read the pressure transducers by electronically switching from one to another.

Stone et al. (1985) developed a low-cost microcomputer-based data acquisition system for continuous pressure head measurements. Their system consisted of tensiometer-mounted pressure transducers, a multiplexing system, an analog-to-digital converter, and a portable microcomputer. The system components were calibrated independently and the assembled data acquisition system was evaluated under laboratory and field conditions. They achieved excellent agreement between pressure heads read with the data acquisition system and those read manually using mercury manometers. Agreement was generally within 0.47 kPa. The system was tested under various field conditions and proved to be reliable and accurate.

Although the system developed by Stone et al. (1985) was inexpensive and reliable, it involved developing most of the system components. In the time since then, numerous data acquisition and control devices have become commercially available. These devices receive an analog signal from the instruments, convert the signal to digital form, and pass it on to a microcomputer. In addition, most of the devices have up to 32 channels available for data input. This enhanced ability allows a powerful microcomputer based data acquisition system for continuous soil water pressure measurement to be assembled from commercially available instruments.

Soil Hydraulic Properties

Solution of unsaturated flow problems requires the predetermination of the soil hydraulic properties, namely, the relationship between the pressure head, ψ, and the soil-moisture content, θ, and the dependence of the hydraulic conductivity, K, on ψ or θ. The most important single factor limiting the successful application of unsaturated flow theory to actual field problems is the lack of information on the parameters entering the governing flow equations (van Genuchten, 1980).

Soil-Moisture Retention Curve

The amount of water retained in the unsaturated zone at equilibrium is a function of the sizes and volumes of the water-filled pores. It is also, therefore, a function of the matric forces. This function can be determined experimentally, and is represented graphically by a curve known as the soil-moisture retention curve (Childs, 1940).

The soil-moisture retention curve is a plot of pressure head (ψ) versus soil-moisture content (θ) and is obtained by desorption or sorption. The equilibrium moisture content at a given ψ is greater in desorption (drying) than in sorption (wetting) (Hillel, 1980). This phenomenon is referred to as hysteresis. Poulovassilis (1962) presented a rigorous mathematical description of hysteresis. In many studies hysteresis is not considered since a soil's spatial variability is unknown and often exceeds the influence of hysteresis (Feddes et al., 1978). Desorption curves are also much easier to develop and are therefore typically used to describe the soil-moisture retention curve.

The desorption curve is usually determined by using a gas pressure extractor which provides a reliable means of removing soil moisture from soil samples, under controlled conditions, throughout the whole plant growth range.

Hydraulic Conductivity Curve

Hydraulic conductivity is defined as the ratio of the flux, q, to the hydraulic gradient, or the slope of the flux versus gradient curve (Hillel, 1980). For saturated flow, the total soil

pore space is available for water flow. With unsaturated flow, however, part of the pores are filled with air. Therefore, the unsaturated hydraulic conductivity, K, is smaller than the saturated hydraulic conductivity, K_s. So for unsaturated soils, K is not constant but depends on the soil moisture content θ or the pressure head ψ (Feddes et al., 1978).

$$K = f(\theta) \qquad \text{or} \qquad K = f(\psi) \tag{2.5}$$

Direct measurement of unsaturated hydraulic conductivity is desirable but difficult to obtain because experimental determination is time-consuming and costly, relationships between K, ψ, and θ are hysteretic and dependent upon previous wetting and drying histories, and soil variability is such that an enormous amount of data would be required to represent the hydraulic conductivity accurately (Mualem, 1986). To replace the missing information, several models have been developed to compute hydraulic conductivity. Mualem (1986) presented a review of several models.

One approach that has been successful involves calculating the unsaturated conductivity from the more easily measured soil-moisture retention curve. The Millington-Quirk method (Millington and Quirk, 1971) has been applied with good results by several researchers including Green and Corey (1971). The method's disadvantage is that it produces output in tabular form which is difficult to use when dealing with nonhomogeneous, multi-dimensional, unsaturated flow problems (van Genuchten, 1980).

Brooks and Corey (1966) developed a closed-form analytical expression for predicting unsaturated hydraulic conductivity whose predictions compared favorably with experimental results. However, a discontinuity which prevented rapid convergence in numerical simulations of unsaturated flow problems was encountered in their soil-moisture retention and hydraulic conductivity curves.

Mualem (1976) derived a simple integral formula from which closed form analytical solutions for predicting the hydraulic conductivity were derived, provided suitable equations for the soil-moisture retention curves were known. Van Genuchten (1980) derived such closed-form analytical solutions. The conductivity models he developed contained three

independent parameters which were obtained by matching a proposed soil-moisture retention function to experimental data. Agreement was excellent between observed and predicted conductivity curves for lighter soils such as sands and loams but higher conductivity values were seriously underpredicted for a clay soil.

The soil-moisture content as a function of the pressure head is given by van Genuchten (1980) as

$$\theta = \theta_r + \frac{(\theta_s - \theta_r)}{[1 + (\alpha |\psi|)^n]^m} \tag{2.6}$$

where

θ_s = saturated soil-moisture content,

θ_r = residual soil-moisture content,

$|\psi|$ = absolute value of the pressure head,

α, n = parameters to be determined, and

$m = 1 - 1/n.$ (2.7)

Equation (2.6) contains four independent variables (θ_s, θ_r, α, and n), which must be obtained from observed soil-moisture retention data. The most available of the four is θ_s, which is easily determined experimentally. The residual water content, θ_r, may be measured experimentally by determining the soil-moisture content on very dry soil. It is defined as the low end soil-moisture content for which the gradient ($d\theta/d\psi$) becomes zero, excluding the region near θ_s, which also has a zero gradient (van Genuchten, 1980). The remaining parameters, α and n, are determined by differentiating equation (2.6) to obtain

$$\frac{d\theta}{d\psi} = \frac{-\alpha m(\theta_s - \theta_r)}{1 - m} \left[\frac{1}{1 + (\alpha |\psi|)^n}\right] \left\{1 - \left[\frac{1}{1 + (\alpha |\psi|)^n}\right]\right\}^m \tag{2.8}$$

where the right hand side is expressed in terms of ψ. Further substitutions solve for α, n, and m. A step by step procedure was provided by van Genuchten (1980).

The hydraulic conductivity was expressed in terms of pressure head by the following expression

$$K(\psi) = K_s \frac{\{1 - (\alpha |\psi|)^{n-1} [1 + (\alpha |\psi|)^n]^{-m}\}^2}{[1 + (\alpha |\psi|)^n]^{m/2}} \tag{2.9}$$

where all variables are as defined for equation (2.6).

Water Flow in Unsaturated Soils

The general equations governing unsaturated flow in porous media are Darcy's law and the continuity of flow equation. Richards (1931) linked the two and presented a combined flow equation which he described as the general partial differential equation of soil water transfer.

Darcy's law for the flow of water in unsaturated porous media (Darcy, 1856), including soils, can be expressed as

$$q = -K(\psi) \nabla H \tag{2.10}$$

where

q = density flux or volume of water passing through a unit cross-sectional area per unit time,

K = unsaturated hydraulic conductivity of the soil as a function of ψ,

ψ = soil moisture pressure head,

∇ = differential operator, and

H = hydraulic head.

The continuity of flow equation according to Freeze and Cherry (1979) can be expressed as

$$\frac{\partial \theta}{\partial t} = - \nabla q - S \tag{2.11}$$

where

θ = soil-moisture content,

t = time, and

S = a sink or source term.

The sink term is used to represent the loss or gain of water from the soil by root extraction or by application of irrigation water.

Substitution of equation (2.10) into the continuity equation yields the combined flow equation or the Richards equation which can be expressed as

$$\frac{\partial \theta}{\partial t} = -\nabla [\, K(\psi)\, \nabla H \,] - S(\psi) \tag{2.12}$$

Full expansion of equation (2.12) in two dimensions yields the flow equation in terms of hydraulic head

$$\frac{\partial \theta}{\partial t} = \frac{\partial}{\partial x}\left[K(\psi) \frac{\partial H}{\partial x} \right] + \frac{\partial}{\partial z}\left[K(\psi) \frac{\partial H}{\partial z} \right] - S(\psi) \tag{2.13}$$

where x is the horizontal dimension and z is the vertical dimension with z positive in the downward direction.

Substitution of equation (2.3) into equation (2.13) yields the pressure head form of the flow equation

$$\frac{\partial \theta}{\partial t} = \frac{\partial}{\partial x}\left[K(\psi) \frac{\partial (\psi - z)}{\partial x} \right] + \frac{\partial}{\partial z}\left[K(\psi) \frac{\partial (\psi - z)}{\partial z} \right] - S(\psi) \tag{2.14}$$

Differentiating the internal terms of equation (2.14) with respect to x and z accordingly yields

$$\frac{\partial \theta}{\partial t} = \frac{\partial}{\partial x}\left[K(\psi) \frac{\partial (\psi)}{\partial x} \right] + \frac{\partial}{\partial z}\left[K(\psi) \left(\frac{\partial (\psi)}{\partial z} - 1 \right) \right] - S(\psi) \tag{2.15}$$

Childs (1957) used a different approach to obtain the same general flow equation.

Equation (2.15) is complicated by the appearance of two dependent variables θ and ψ. Rubin (1966) discussed three ways of reducing the equation to a single dependent variable, among which was the ψ-based approach which was selected for this study. This technique involves modifying equation (2.15) by introducing the specific water capacity, C, defined by

$$C = \frac{d\theta}{d\psi} \tag{2.16}$$

which was discussed in detail by Klute (1965). Because hysteresis is not included, ψ is considered a single-value function of θ and a normal instead of a partial derivative notation is used in equation (2.16) (Feddes et al., 1978).

Using the chain rule of calculus

$$\frac{\partial\theta}{\partial t} = \frac{d\theta}{d\psi} \cdot \frac{\partial\psi}{\partial t} \tag{2.17}$$

and substituting equation (2.16) into (2.17) yields

$$\frac{\partial\theta}{\partial t} = C \cdot \frac{\partial\psi}{\partial t} \tag{2.18}$$

which in turn is substituted into equation (2.15) to produce the final form of the general flow equation, commonly known as the two dimensional form of the Richards equation.

$$C(\psi)\frac{\partial\psi}{\partial t} = \frac{\partial}{\partial x}\left[K(\psi)\frac{\partial(\psi)}{\partial x}\right] + \frac{\partial}{\partial z}\left[K(\psi)\left(\frac{\partial(\psi)}{\partial z} - 1\right)\right] - S(\psi) \tag{2.19}$$

Written in this form, the flow equation is easier to solve and provides the basis for predicting soil water movement in saturated and unsaturated soils. The equation is a nonlinear, parabolic, second order, partial differential equation (PDE). It is nonlinear because the parameters $K(\psi)$, $C(\psi)$, and $S(\psi)$ depend on the solution of $\psi(x,z,t)$. Nonlinearity causes problems in the equation's solution and analytical solutions are complex and known for special

cases only (e.g., Gilley and Allred, 1974; Warrick et al., 1979). The nonlinearity of equation (2.19) and the typical variable boundary conditions associated with it have dictated the use of numerical methods to solve practical field problems of soil-plant-water relationships (Stone, 1987).

Numerical Solutions

The finite difference method is the numerical technique most commonly used to solve the Richards equation. Finite differences are expedient because solutions are obtained by working directly with the governing differential equations, and they apply to specific flow geometries with specific mesh spacings. Therefore, finite differences lend themselves well to the solution of soil-plant-water relationship problems in regularly shaped lysimeters.

Finite difference formulations may be solved explicitly or implicitly. Although the implicit approach is more complicated, it is preferable because it offers better stability and convergence. It also permits relatively larger time steps, thus allowing longer simulation periods.

The Richards equation has been successfully solved for one-dimensional flow by many researchers. Haverkamp et al. (1977) reviewed six numerical models of one-dimensional infiltration solved using both the water content based equation and the pressure head based equation. Each model employed different discretization techniques to approximate the nonlinear infiltration equation. They found that implicit models which solved the pressure head based infiltration equation had the widest range of applicability for predicting water movement in saturated or unsaturated soil.

Feddes et al. (1978) developed a one-dimensional implicit model that simulated infiltration and redistribution under high water table conditions. Plant growth and root extraction were also simulated. Field lysimeters were used to collect data for model calibration and special attention was paid to the influence of the groundwater table on the amount of water available for transpiration of red cabbage on sticky clay.

The most popular implicit procedure used in solving the two-dimensional form of the Richards equation has been the alternating direction implicit (ADI) method. Rubin (1968) developed a two-dimensional numerical model of transient water flow in unsaturated and partly unsaturated soils which utilized an ADI scheme. He studied horizontal infiltration and ditch drainage with the numerical model.

Hornberger et al. (1969) developed a model of transient water movement in a composite soil moisture ground water system. The model was used to study two-dimensional flow in response to a falling water table and used the Gauss-Sidel iterative method to solve the flow equations.

Amerman (1976) developed a computational scheme for solving the steady-state, two-dimensional form of the Richards equation using the successive overrelaxation (SOR) finite difference method. The model was developed using subsectioning which allowed application of the model, without internal modification, to a wide range of geometric shapes, hydraulic boundary conditions, and soil distributions.

Perrens and Watson (1977) studied a two-dimensional infiltration-redistribution sequence in which the surface flux was spatially nonuniform. They found that an ADI method described the flow process satisfactorily. Their program incorporated an interpolation-type hysteresis model and produced two-dimensional profile distributions of water content and pressure head.

Brandt et al. (1971) considered a plane flow and a cylindrical flow model in a study of two-dimensional transient infiltration from a trickle source. The water flow equation was solved numerically by an approach that combined the noniterative ADI procedure with Newton's iterative method. The numerical results compared favorably with data from the literature and indicated that the method was reliable and could be used with confidence.

Infiltration From a Line Source

A special two-dimensional water flow problem is infiltration from a line source. Researchers have presented several analytical and numerical solutions to this problem. Raats

(1970) was one of the earliest investigators to study steady infiltration from an array of equally spaced line sources or furrows at the surface of a semi-infinite soil profile. He used the steady-state assumption and the Kirchhoff transformation to obtain a straightforward analytical solution. He produced explicit expressions for the stream function, the flux, the matric flux potential, the pressure head, and the total head.

In a similar steady-state study, Zachmann and Thomas (1973) developed equations which can be used in the design of subsurface irrigation systems that lie in a horizontal plane and are parallel and equally spaced. The analytical solution described the flow from the line sources in the presence of uniform infiltration or evaporation at the soil surface.

Warrick and Lomen (1977) developed a two-dimensional analytical solution of the linearized flow equation for a buried line source with an underlying constant potential surface. Their geometry was appropriate for describing flow from a trickle or subsurface irrigation system of porous pipe, or emitters, spaced closely in a line above a shallow water table or in a lysimeter. They examined only the steady-state case and attained linearization by assuming that the unsaturated hydraulic conductivity was exponentially related to the pressure head. Warrick et al. (1979) further enhanced the model by adding a one-dimensional extraction term. Other analytical solutions of infiltration from a line source were provided by Gilley and Allred (1974), Lomen and Warrick (1974), and Thomas et al. (1974).

Fewer studies have provided numerical solutions to the line source problem. Oron (1981) linearized the steady-state nonlinear equation and then solved it numerically. His model included a continuous sink function which simulated water uptake by roots. Oron's results satisfactorily simulated the flow characteristics in the soil and were validated by experimental data.

Ragab et al. (1984) used a simulation model based on the matric flux potential concept to describe two-dimensional infiltration into sand from a line source. The model showed considerable stability with varying grid sizes and flow rates. Their simulated wetting patterns indicated close agreement with published experimental data, especially under higher flow rates.

An extensive literature review has shown that many researchers have investigated infiltration from line sources. Most however, limited their studies to the solution of the linearized, steady-state form of the flow equation. Those that solved for transient, two-dimensional infiltration from line sources did not include an extraction term to simulate water uptake by plants. Furthermore, the line source problem has not been investigated under high water table conditions. A general model simulating transient infiltration and extraction under line sources is lacking.

Water Extraction by Plant Roots

Hamon (1966) calculated that 70% of the 750 mm average annual precipitation of the contiguous United States is lost to evaporation and transpiration. Penman (1970) estimated that 2000 Mg of water must be extracted from the soil in order to produce 20 Mg of fresh weight of a crop. These observations indicate that the soil-plant-atmosphere pathway is a major component of the subsurface hydrologic system. Any serious attempt to model the pathway requires an understanding of the dynamics of soil moisture depletion by plants.

Most models of soil extraction by plant roots use the Ohm's law analogy which was originally introduced by Gradmann (1928) and enhanced by van den Honert (1948). The analogy suggests that the driving force for water uptake is the effective potential gradient between water in the plant and water in the soil. The resistance term is a summation of the hydraulic resistances of the soil as well as the root cortex and xylem along the flow path (Belmans et al., 1979). In simulating water extraction by plant roots, two methods have been used: the microscopic and the macroscopic approach.

A microscopic study examines the flow process in the vicinity of a single root. The root may be considered as a cylindrical sink of infinite length, uniform radius, and uniform water absorbing properties. The soil moisture flow equation is written in cylindrical coordinates and solved with appropriate boundary conditions at the root surface and at some distance r_{max} from the root (Molz and Remson, 1970). Moisture flux, moisture content, or a combination of both, may be specified as a boundary condition at the root surface. Gardner

(1960; 1964) developed one of the earliest detailed quantitative models of this type. Other microscopic studies were conducted by Molz et al. (1968), Newman (1969), Whisler et al. (1970), and Steinhardt et al. (1982).

As discussed by Molz and Remson (1970), microscopic models are impractical because flow to each individual rootlet of a complete root system must be considered. Furthermore, the entire root system is not uniformly permeable to water and its geometry is time dependent. As a result, most extraction functions have been developed using a macroscopic approach (Molz, 1981).

In the macroscopic approach, the flow to individual roots is disregarded and the entire root system is assumed to extract moisture from each differential volume, or cell, of the root zone at some rate S. At a given cell, the quantity S is interpreted as an extraction rate that may be a function of space, time, moisture content, or a combination of these variables (Slack, 1975). The total extraction rate is the summation of the water flow rates from each soil cell. In the soil moisture flow equations, the extraction rate is represented as a sink or a negative source term, S, and is simply added to the continuity equation (see equation 2.11). Boundary conditions are specific at boundaries of the composite soil-plant system such as the soil surface and the water table, and they do not involve the actual roots (Molz and Remson, 1970).

Gardner and Ehlig (1962) used the Ohm's law analogy to present a macroscopic extraction function of the form

$$S = \frac{\psi_{soil} - \psi_{plant}}{R_{soil} + R_{roots}} \tag{2.20}$$

where

S = the extraction function or the volume of water taken up by the roots per unit bulk volume of soil in unit time,

ψ_{soil}, ψ_{plant} = water potentials in the soil and plant respectively, and

R_{soil}, R_{roots} = the corresponding hydraulic resistances.

They conducted greenhouse experiments and found that the impedance to water movement in the soil is greater than the impedance to water movement into plant roots. Their experimental results were consistent with the uptake equation.

Molz and Remson (1970) developed a one-dimensional model which used a macroscopic extraction term to describe moisture removal from soil by the roots of transpiring plants. The extraction rate was given by

$$S(z,\theta) = T \frac{R(z)D(\theta)}{\int_0^{\nu} R(z)D(\theta)dz} \tag{2.21}$$

where

T = transpiration rate per unit area,

$R(z)$ = effective root density,

$D(\theta)$ = diffusivity, and

ν = root depth.

A numerical procedure based on the Douglas-Jones predictor-corrector method was used to solve the model. Solutions compared with experimental data indicated that the extraction term was computationally and physically feasible.

Belmans et al. (1979) used the extraction term proposed by Gardner and Ehlig (equation 2.20) in a mechanistic simulation model describing the process of soil moisture extraction by root systems. They conducted experiments to test the model's validity and found that root resistance was the dominant resistance term through most of the soil moisture availability range. The increase in soil hydraulic resistance resulting from soil moisture extraction did not become significant relative to root resistance until the soil moisture reserve was substantially depleted.

Nimah and Hanks (1973a) developed a model for estimating soil water, plant, and atmospheric interrelations. Their one-dimensional model predicted water content profiles,

root extraction, and root water potential under field conditions. It used a root extraction term of the form

$$S(z,t) = \frac{[H_{root} + (1.05z) - h(z,t) - s(z,t)]\, RDF(z)K(\theta)}{\Delta x \Delta z} \qquad (2.22)$$

where

H_{root} = the effective water potential in the root at the soil surface,

h = soil matric potential,

s = osmotic potential,

RDF = proportion of total active roots in depth increment Δz,

K = hydraulic conductivity, and

Δx = distance between the plant roots at the point where h and s are measured.

The model predicted significant changes in root extraction due to variations in pressure head-water content relations and root depth. A field test of the model (Nimah and Hanks, 1973b) with an alfalfa crop provided best agreement between predicted and computed values 48 hours after water addition. Poorest agreement was found immediately following irrigation.

Feddes et al. (1976) defined the extraction term in two different ways. The first extraction term was dependent on the hydraulic conductivity of the soil, the difference in pressure head between the soil and the root-soil interface, and a root effectiveness function. The second term was defined as a function of soil water content. The governing partial differential equations were solved by a finite difference and a finite element approach, and the computed values were verified against field measurements. Only slight discrepancies between the two numerical methods were found and these were attributed to the different manner in which they handle boundary conditions and water uptake by roots. Agreement between measured and computed values ranged from excellent to satisfactory.

Slack et al. (1977) developed a mathematical model of water extraction by plant roots as a function of leaf and soil water movement and water uptake. A two-dimensional radial flow model was used to describe water movement and estimate transpiration from corn grown in a controlled environment under soil drying conditions. A microscopic and a macroscopic approach was used to produce a combined extraction model which predicted daily transpiration adequately for the period modeled.

Feddes et al. (1978) developed an implicit finite difference model to describe water flow and extraction in a non-homogenous profile under the influence of groundwater. Their extraction term was considered to be a function of the soil moisture pressure head, ψ. The extraction rate was held at a maximum level if ψ was above a set limit, ψ_2. When the pressure head fell below ψ_2, water uptake decreased linearly with ψ until the wilting point, ψ_3, was reached. Below ψ_3 water uptake by roots was set at zero. The extraction term between ψ_2 and ψ_3 was defined by

$$S(\psi) = S_{max} \frac{\psi - \psi_3}{\psi_2 - \psi_3} \tag{2.23}$$

where

S_{max} = the maximum possible transpiration rate divided by the effective rooting depth.

The model yielded satisfactory results in predicting both cumulative transpiration and distribution of soil moisture content with depth.

Tollner and Molz (1983) developed a physically based extraction function for use in the general flow equation. The function assumes that water uptake per unit volume of soil is proportional to the product of contact length per unit soil volume, root permeability per unit length, and water potential difference between soil and root xylem potential. A factor which accounts for reduced root-soil-water contact as water is removed was included in the extraction term. Model predictions compared favorably with experimental results from the literature.

Studies conducted by Denmead and Shaw (1962) and Ritchie (1973) with field crops showed that during periods of high potential evapotranspiration (ET) demand, actual ET was considerably less than the potential rate even though the available soil water was considered adequate. They also observed that during periods of low potential ET demand actual ET equaled potential rates, even down to very low soil water contents.

Smajstrla (1982) developed an extraction function that was consistent with these observations. His function was based on potential extraction rate and soil water status and was defined as

$$S = T_p R^{(T_p/CR)} \tag{2.24}$$

where

T_p = potential transpiration rate, and

C = a calibration constant.

R was defined as the relative available soil water content and was given mathematically by

$$R = \frac{\theta - \theta_{wp}}{\theta_{fc} - \theta_{wp}} \tag{2.25}$$

where

θ = soil water content,

θ_{wp} = soil water content at the wilting point, and

θ_{fc} = soil water content at field capacity.

The model was calibrated using the rate of soil water content change observed during lysimeter field experiments with soybeans. The function permits a rapid rate of soil water extraction when soil water is readily available. As the water is depleted, the extraction rate declines logarithmically. Extraction is limited during periods of high potential ET and is allowed to recover to near potential rates during periods of low potential ET. The function limits extraction to very low rates as the permanent wilting point is approached.

Stone (1987) modified Smajstrla's extraction term to include a root distribution function and substituted potential transpiration (T_p) with actual ET, thus eliminating the calibration constant. The extraction term was used with success in a two-dimensional model simulating extraction patterns under agricultural crops.

Lysimetry

Lysimeters have been used for determining soil-plant-water relationships for many years. A review of lysimetry was published by Aboukhaled et al. (1982). Lysimeters can generally be described as weighing and nonweighing (or drainage) types whose advantages and disadvantages were discussed by Smajstrla (1985). He found that weighing lysimeters are more costly and difficult to maintain because of requirements for service and calibration. The tanks of weighing lysimeters must also be constructed with sufficient mechanical strength to support the soil profile without deformation and be supported by expensive load cells. They are ideally suited to studies in which hourly or daily soil water budgets are required.

Drainage lysimeters are cheaper to construct because the surrounding soil can be used to support the tanks (Aboukhaled et al., 1982). They are used for studies in which weekly or monthly soil water budgets are of interest because instrumentation to measure soil water status is not sufficiently accurate. Smajstrla (1985) developed a set of drainage-type field lysimeters for water management studies on deep sandy soils for Florida humid climatic conditions.

Feddes et al. (1978) studied the influence of the groundwater table on the amount of water available for transpiration of red cabbage on sticky clay with a drainage-type field lysimeter. Their system was designed to continuously maintain the water table in the lysimeter at approximately the same depth as it was in the surrounding field. Drainage-type lysimeters with water table controls for Florida conditions were described by Clayton et al. (1942), Speir (1962), and Shih et al. (1977).

CHAPTER 3
EXPERIMENTAL PROCEDURE

The Field Lysimeter System

A field lysimeter system was constructed to study soil water redistribution and extraction patterns of three different soil profiles irrigated by a line source under the influence of a shallow water table. The system consisted of 6 rain-sheltered drainage-type lysimeters arranged in tandem to simulate row-crop conditions. Rain shelters were used to eliminate unwanted rainfall from the lysimeters during water management studies (Figure 3.1). Soil water status data were collected with a microcomputer-based data acquisition system which consisted of tensiometer-mounted pressure transducers, a data acquisition and control device, and a portable microcomputer.

Lysimeter Construction

Each of the six lysimeters constructed for this facility provided a rectangular cross section of 0.7 m^2 and an effective surface production area of 1 m^2. Their profiles were 0.75 m deep.

The lysimeters were built from commercially available galvanized steel 3 x 0.9 x 0.75 m water troughs. Each trough was partitioned to create two lysimeters. The partitions were machined from sheets of aluminum and bonded into the troughs with an epoxy-resin-based metal filler. The strength and water tightness of each bond was tested by filling one of the lysimeters in each trough with water while leaving the other empty and inspecting for leaks. The aluminum was then covered with a primer, an epoxy-based paint, and an asphalt-based paint to prevent corrosion.

The lysimeters were installed at the Institute of Food and Agricultural Sciences Irrigation Research and Education Park at Gainesville, Florida. A trench was excavated to a depth of

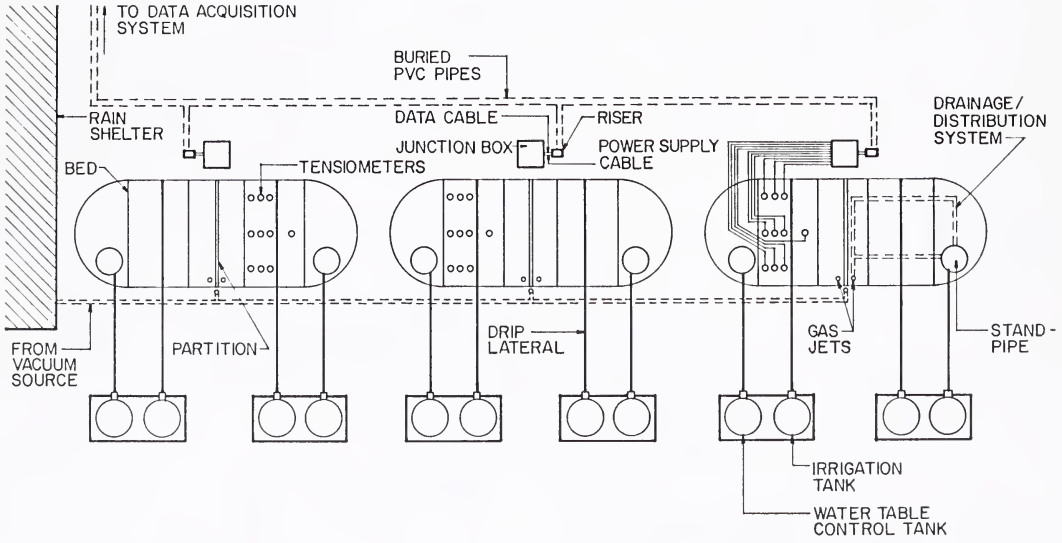

Figure 3.1. Field layout of the lysimeter system.

0.5 m with a backhoe and the remaining 0.25 m were excavated by hand to ensure that the bottom surface of the trench was level. A thin layer of coarse builder's sand was placed in the bottom of each trench, leveled, and tamped to ensure that the bottoms of the lysimeters were completely supported. The lysimeters were installed in tandem, with a 0.3 m spacing between troughs. A carpenter's level was used to ensure that they were level in order to avoid nonuniform water table heights within the lysimeters. A standpipe and a drainage/distribution system were placed in each of the lysimeters, and a 50 mm layer of builder's sand was laid over the distribution systems to facilitate drainage and water table control. Soil was backfilled around the lysimeters while soil profiles were simultaneously reconstructed in the lysimeters by hand packing to prevent the shapes of the lysimeters from distorting while they were being filled.

Three different soils were used to fill the lysimeters, with each of the soils occupying a pair of lysimeters. Because Florida agricultural soils are single-grained fine sands, the soils used in the lysimeters were chosen accordingly and further selected to provide high, intermediate, and low water-holding capacities. The soils used were Pomona sand, Astatula fine sand, and Builder's sand, respectively.

Profile reconstruction. Handpacking was used to assure that the individual soil profiles were as homogeneous as possible (Smajstrla, 1985). Lysimeter profiles were reconstructed in approximately 50 mm thick layers by a continual process of filling, tamping, and raking between layers.

To simulate row crop conditions, beds were formed within the lysimeters. One 0.9 m long trapezoidal bed ran across the width of each lysimeter as illustrated in Figures 3.1 and 3.2. The soil profiles were reconstructed uniformly for the first 450 mm and then the beds were shaped. Each bed was 1.0 m wide at its base, 300 mm wide on top, 300 mm tall, and side slope ratios were 3:2. Half the height of the bed (150 mm) protruded above the lip of the lysimeter. To contain the ends of the beds, sheets of galvanized steel, cut into trapezoidal shape, were pushed into the soil profile along the inner edges of the lysimeters. The irrigation laterals were then placed and the beds covered with black plastic mulch.

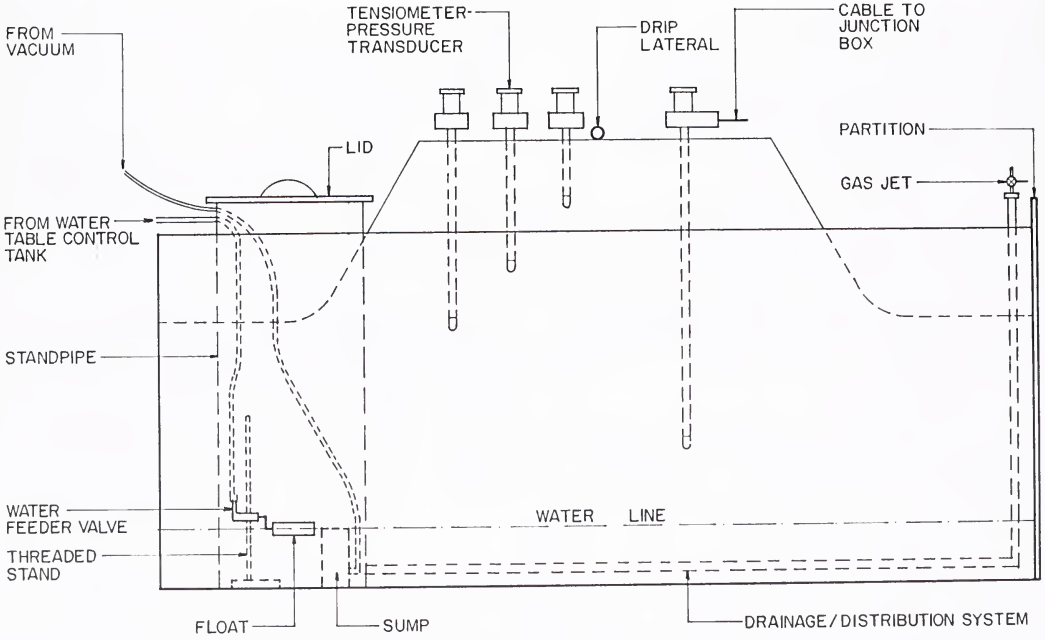

Figure 3.2. Side view giving details of an individual lysimeter soil water status monitoring system.

Lysimeter water table control. A system was designed to provide accurate regulation of the water table within the lysimeters. The design consisted of a float valve and a sump which were located in a standpipe.

The standpipes were constructed by cutting a 250 mm diameter polyvinyl chloride (PVC) pipe into lengths of 650 mm. Holes (3 mm) were drilled into the bottom 100 mm of each pipe to facilitate the flow of water. Very fine mesh nylon screen was used to cover the holes and prevent soil particle loss. The standpipes were then glued to the bottom of the lysimeters in an upright position (Figure 3.2). Lids were manufactured to keep out debris and insects.

Attached to the standpipe was a distribution system (Figures 3.1 and 3.2) to facilitate the movement of water along the bottom of the lysimeter. PVC pipe elbows were used to connect lengths of 26 mm well screen to form a rectangular distribution system. One corner of the distribution system led into the standpipe. On the opposite end of the distribution system, a reducing elbow was used to install a vertical 16 mm PVC pipe and a gas jet which allowed water to be extracted to the surface by vacuum. The gas jet was used for rapidly extracting water or for lowering the water table below the level allowed by the sump.

The water table in each lysimeter was recharged from the float valve (Figure 3.3) which consisted of a water feeder valve regulated by a float attached to the valve lever arm. A coupling and slip sleeve were used to connect 6.4 mm diameter copper tubing to the float valve. Tygon tubing was slipped over the copper tubing and led to the top of the standpipe. From there, 10 mm polyethylene (PE) tubing led to a 40 L water supply tank which provided the positive head required by the float valve. Two nuts, welded together, were used to mount the float valve onto a threaded stand and permitted fine adjustment of the water levels (Figure 3.4). A minimum level of 20 mm was required for the float valve to operate properly. Once calibrated, the float valve allowed the water level to be adjusted to within 3 mm of the desired depth setting. The volume of water added to each water table through a float valve was determined by measuring the volume of water depleted from the corresponding water tank. To accurately measure depletions, the water table tanks were replenished with the use of a graduated cylinder.

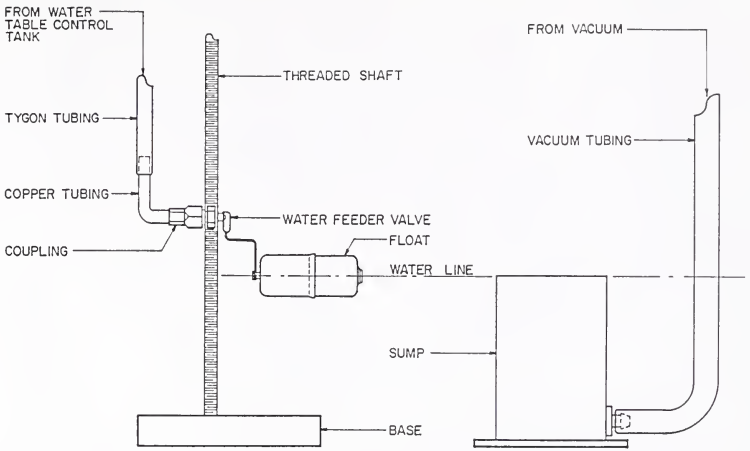

Figure 3.3. Float valve and sump used to control the water table level.

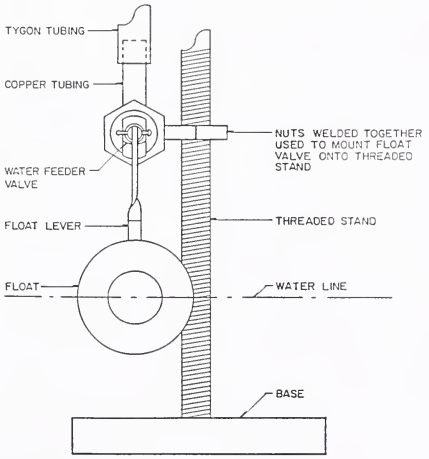

Figure 3.4. End view of the float valve showing details of the mechanism used to mount the valve onto a threaded stand.

The sumps were constructed to eliminate fluctuations in the water table caused by percolating irrigation water. Any water draining into the sumps was extracted by vacuum to individual drain traps. The sumps were made by gluing a bottom to one end of a 30 mm length of 50 mm PVC pipe. Each sump was then attached to the lysimeter bottom within the standpipe (Figures 3.2 and 3.3). Vacuum tubing, which led to individual drain traps, was connected to the sumps with a hose barb.

A portable drain trap was constructed for each lysimeter from 100 mm PVC pipe. PVC end-cups were then glued on a 600 mm length of pipe to form a cylindrical tank with a capacity of approximately 5 L. A graduated cylinder was used to accurately measure the volumes of water collected in the drain trap.

The vacuum system consisted of a 250 L/min vacuum pump, a 300 L vacuum tank, a regulator to start and stop the vacuum pump, and vacuum control valves to permit the desired vacuum to be set.

Irrigation system. The irrigation system was a low flow, manually operated line source drip irrigation system. Each lysimeter was irrigated by a separate lateral, which was supplied from a 60 L water tank. The tank, placed on a platform, provided the positive head required by the irrigation system. Laterals were placed along the centerlines of each bed (Figures. 3.1 and 3.2). Twelve drip emitters, closely spaced at 75 mm, in order to simulate a line source, were installed on each lateral. Spot Vortex emitters were used with flow rates of 2.4 L/hr or 32 L/hr per m lateral length. To accurately measure the irrigation volumes, a graduated cylinder was used to add water to the irrigation tanks.

Rain shelter. An automated rain shelter was used to cover the lysimeters in the event of rainfall. The system consisted of a shelter mounted on a rail system, electric motors and controls, and a rainfall detector and switch to activate the motors. The shelter was part of a preexisting lysimeter system (Smajstrla, 1985).

The Data Acquisition System

A microcomputer-based data acquisition system for continuous soil water potential measurements was developed. The system consisted of tensiometer-mounted pressure transducers, a Keithley System 570 work station data acquisition and control device, and a Zenith 161 portable microcomputer.

Pressure transducers were mounted on Model S Irrometer tensiometers by drilling 3 mm holes into the tensiometer reservoirs opposite the vacuum gage ports. The pressure transducers used were Micro Switch model 141PC15D transducers which measure pressures from 0 to -100 kPa. Each transducer produced an analog output of 1 to 6 volts which was proportional to the vacuum exerted on a membrane in the transducer. One side of the membrane was in contact with the tensiometer water while the other side was open to the atmosphere. As pressure on the water changed, the membrane deformed proportionally, and the voltage across the membrane changed. The pressure transducers required an 8-volt direct current (VDC) power supply at 8 mA each. These transducers were used because they were shown to be linear, temperature compensating, and adaptable to field use (Stone et al., 1985).

The System 570 data acquisition system had provisions for a maximum of 32 single-ended input channels. To provide flexibility, 12 conductor signal cable was installed, thereby providing 12 available signal leads for each pair of lysimeters. The signal cable was 22 American Wire Gage (AWG) with 6 pairs of stranded chrome conductors, each pair shielded to prevent induced voltage errors. A 12-gage power supply cable was installed to provide power to a junction box for each pair of lysimeters.

The microcomputer and the data acquisition system were housed in an air conditioned instrumentation building about 60 m from the lysimeters. Between the instrumentation building and the junction boxes, 3 signal cables and 3 power supply cables were buried in a 75 mm PVC pipe. One data cable and one power supply cable led into each junction box and a three conductor cable connected each transducer to its junction box. Two of the conductors were used for power supply, while the third carried the signal from the transducer.

Three of the 6 lysimeters were instrumented with 10 tensiometers per lysimeter, engaging 30 channels (Figure 3.1). One channel was used to monitor atmospheric pressure and the remaining channel was used as a backup. In order to provide a complete description of the soil profile in the lysimeter, the 10 tensiometers in each of the instrumented lysimeters were installed at depths and distributions as follows: 3 tensiometers were installed at each of 3 depths, 100 mm, 200 mm, 300 mm, and at distances of 50 mm, 150 mm, and 250 mm from the lateral. One tensiometer was installed at a depth of 500 mm (Figures 3.5 and 3.6).

The Keithley System 570 data acquisition and control device was the interface between the microcomputer and the tensiometer pressure transducers. It consisted of a chassis/mother board and an interface card for the microcomputer. The mother board had individually numbered screw terminals to which the pressure transducer data cables were attached.

The System 570 was supported by the Soft500 software package which is an extension of Advanced BASIC and provided foreground/background architecture, multitasking, array management, memory management, disk access and storage, and a library of input and output commands accessible directly from BASIC. Real time analog measurement was accomplished by writing a Basic program incorporating Soft500 commands.

Data Acquisition System Operation. The data acquisition system permitted soil matric potentials to be monitored nearly continuously. Data from the 30 tensiometer-pressure transducers were collected at one minute intervals and averaged over a 10-minute period. The average soil matric potential of each tensiometer for that period and the corresponding time were saved to disk. The 320 kbyte 5 1/4 inch floppy disks used for storage of the soil water potential data permitted 7 days of continuous data collection.

Instrument calibration. The 30 pressure transducers were individually calibrated to analyze their response characteristics. Transducer outputs were measured at decreasing pressures from 0 to -40 kPa and individual transducer calibration curves were produced. Regression analysis of the data indicated that the calibration curves were linear with R^2 values of 1.000.

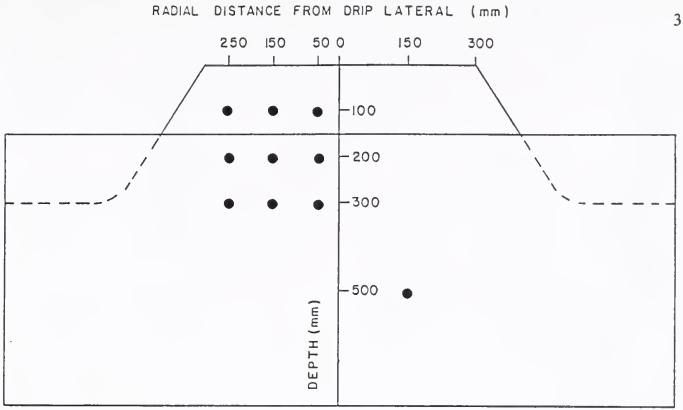

Figure 3.5. Side view of a lysimeter showing the location of the 10 tensiometers.

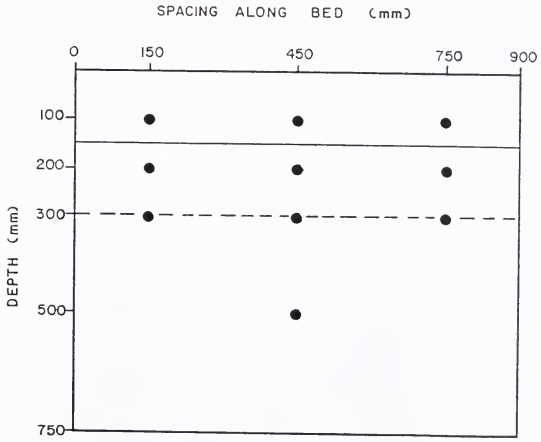

Figure 3.6. End view of a lysimeter showing the location of the 10 tensiometers.

Calibration curves of the assembled tensiometer-pressure transducer systems were also developed to take into account the effect of the hanging tensiometer column on the transducer output. The curves were developed by exerting a known vacuum on the tensiometer ceramic cups and reading the transducer outputs. The curves again proved to be linear with R^2 values ranging from 1.000 to 0.998. The net effect of the hanging column was to shift the output voltage of the transducer upwards by a an amount directly proportional to the column length. Figure 3.7 shows two typical calibration curves of transducer output voltage versus applied pressure. The lower curve shows the data and regression line of an individual transducer. The upper curve is the output of the same transducer mounted on an 18 inch (457 mm) tensiometer.

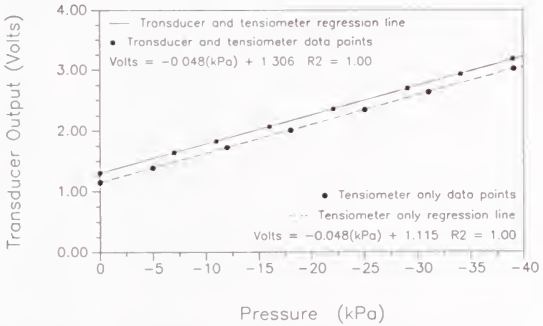

Figure 3.7. Calibration curves of output voltage versus negative pressure for transducer no. 4.

Pressure measurement accuracy. The analog-to-digital (A/D) board in the data acquisition system provided 12-bit resolution. This produced 4096 counts in the 0-5 volt range, 0.0012 volts per count, or a resolution of approximately 0.03 kPa. The relationship between voltage and pressure for transducer no. 4 is given by equation (3.1).

$$kPa = (volts - 1.1153) / -0.04766 \quad (3.1)$$

The above equation resulted in a maximum expected error of 0.06 kPa at 1 volt (-0.3 kPa of pressure) and 0.27 kPa at 5 volts (-83.7 kPa of pressure) (Stone et al., 1985). Stray voltages in the instrumentation building reduced resolution to 0.01 volts or 0.2 kPa. Instrumentation error of 0.2 kPa produces error of 20% to 4% in pressures from -1 kPa to -5 kPa, respectively. Therefore, it was important to recognize that significant errors could result when measuring soil water potentials near saturation.

Atmospheric pressure effects. Soil moisture matric potentials were measured using differential pressure transducers with atmospheric pressure as their reference. To determine the effects of atmospheric pressure changes on the performance of the differential pressure transducers, ambient pressure was measured using an absolute pressure transducer. It was found that atmospheric pressure did not vary enough to warrant correction of the matric potential measurements. Typical fluctuations varied from 0.1 to 0.3 kPa. These were well within the range of other variations in measurement accuracy. Figure 3.8 illustrates typical variation of ambient air pressure during a week in June, 1988.

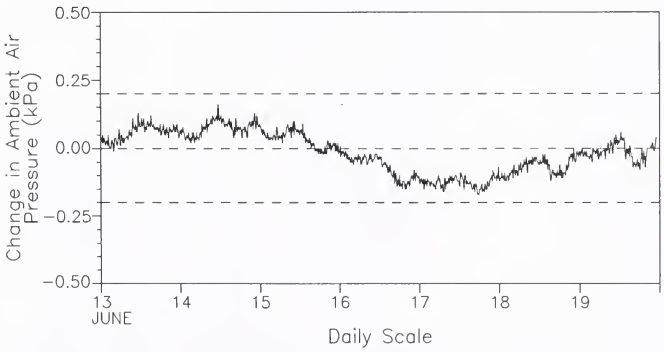

Figure 3.8. Fluctuations in atmospheric pressure for the week of June 13-19.

Lysimeter System Operation

In Florida, vegetables are typically grown under conditions similar to those that were simulated in the lysimeters. The tomato was chosen for this study for several reasons:

1. Tomatoes are one of the most important cash crops in the state.
2. Tomato plants have high transpiration rates which would allow measurable extraction rates and produce very definite redistribution and extraction patterns.
3. Information on redistribution and extraction patterns, contribution of the water table to crop water use, and water budgets was critically needed.

The Super Bush (VFN) hybrid (*Lycopersicon esculentum* Mill.) was selected for its vigorous growth and large, leafy bush. These were desirable traits because they increase the transpiration rate of the plant. Seedlings approximately 100 mm tall were purchased from a commercial nursery and transplanted to the lysimeters on March 15, 1988. Two seedlings were planted along the centerline of each bed, 450 mm apart, and each 225 mm from the edge of the lysimeter. Plant growth was monitored by taking biweekly canopy height and width measurements with a meter stick. Mature plants were removed from the lysimeters on June 26, 1988 which allowed for a three month growing season.

Irrigation scheduling. Three of the six lysimeters were instrumented. The two leftmost lysimeters in Figures 3.1 and 3.9 contained the Astatula f.s. and were labeled E1 and E2 (for East 1 and East 2). The two center lysimeters contained the Builder's sand and were labeled C1 and C2. Finally, the two rightmost lysimeters contained the Pomona sand and were labeled W1 and W2. The three instrumented lysimeters were E2, C1, and W1.

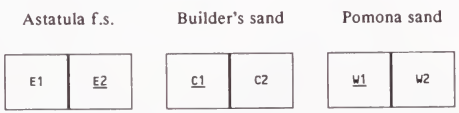

Figure 3.9. Arrangement of the three soils in the lysimeters.

An irrigation was applied when the soil water potential in a lysimeter dropped below -10 kPa. Soil water potential was used as the trigger point for irrigation instead of a percentage of water depletion from field capacity because potential is independent of soil type. Thus, the plants were subjected to a uniform stress level regardless of soil type. The -10 kPa value was chosen because it is consistent with the current practices used by growers who tend to keep the root zone moist and the plants stress-free.

The irrigation system was manually operated and the lysimeter system was serviced daily. Every morning the transducer outputs were monitored. If any of the instruments read below -10 kPa, the appropriate lysimeters were irrigated.

Permanent ink was used to mark reference levels on the irrigation and water table tanks. The reference level in the irrigation tanks was placed at the 40 L mark, or at 3/4 full. To provide the positive head required by the irrigation system, the irrigation tanks were always maintained at the reference level. The irrigation process began by adding the desired irrigation volume, carefully measured with a graduated cylinder, to the water already in the irrigation tanks. The valve on the irrigation tank was then opened and the water level in the tank allowed to drop to the reference level.

Immediately following irrigation with the drip emitters, the volume of water used to maintain the water table at the set level since the previous irrigation event was determined. Initially, the water table tanks were filled to the reference level (40 L mark). As the water table was recharged, the water level in the tanks dropped. After each irrigation event, water was added to the corresponding water table tank with a graduated cylinder until the tank was refilled to the reference level.

The vacuum system was left running continuously and the drain traps were checked daily. If any water had collected in the drain traps, it was measured and recorded.

Irrigation volumes. The objective in determining the irrigation volumes to be applied was that they should be large enough to wet the soil profile to field capacity but not so large that they would drain from the root zone. The approximate irrigation volumes for each soil type were estimated using the soil-moisture retention curves. The actual volumes were

determined through trial and error by incrementing the estimated volumes until drainage just began. Adjustments were made to the volumes over the growing season, because as the plants grew, they extracted larger volumes of soil water which had to be replenished.

Table 3.1 presents the irrigation volumes for the mature plants and their corresponding depths over the surface area of the lysimeters. These data demonstrated the need to apply small, frequent irrigations to minimize drainage. They also demonstrated that the volumes were a function of soil type and that the soils with low water-holding capacities (the Builder's sand and the Astatula f.s.) required much smaller irrigations than the Pomona sand. However, soil type does not necessarily influence the plant water requirement.

Table 3.1. Volumes of Irrigation Applications and Equivalent Depths Over the Lysimeter Areas.

Soil type	Volumes (L)	Depths (mm)
Builder's sand	4.00	3.46
Astatula f.s.	4.00	3.46
Pomona sand	8.00	6.93

Irrigation began immediately after the seedlings were transplanted but the volumes were not recorded until the data acquisition system became operational on April 1. By April 15, a water table 720 mm from the surface had been established in all the lysimeters and was being maintained by the float valves. On this date, collection of data on the contribution of the water table to crop water use began.

Soil Characteristics

Samples of each soil were taken and submitted for analysis to the University of Florida's IFAS Soil Testing Laboratory. Analyses were done on pH, percent organic matter, macro and micro nutrient concentrations, copper toxicity, and soluble salts. Organic matter and pH data are included in Table 3.2. Complete results can be found in Appendix A.

Analysis of the Pomona sand indicated that the soil had an initial pH of 4.6. Because the recommended soil pH for tomatoes is 6.0-6.8 (Stephens, 1984), 7.8 Mg/ha of dolomitic limestone was incorporated into the surface 25 cm of soil to adjust the pH level, as recommended by the Soil Testing Laboratory. The liming recommendation was based on the Adams-Evans lime requirement test.

Table 3.2. Characteristic Soil Properties.

Soil type	Bulk density (g/cm^3) ρ_b	Organic matter (g/g) %	Saturated water cont. (mm^3/mm^3) θ_s	Residual water cont. (mm^3/mm^3) θ_r	Saturated Hydraulic Cond. (mm/hr) K_s	pH
Builder's sand	1.68	0.01	0.35	0.01	536.07	6.8
Astatula f.s.	1.66	0.58	0.41	0.03	428.35	7.1
Pomona sand	1.10	5.34	0.54	0.08	169.77	4.6

The soil test reports also provided standard fertilization recommendations for each soil which were used to compute the appropriate fertilizer applications. The recommendations were similar for all three soils and called for 135 kg N, 180 kg P_2O_5, and 180 kg K_2O per ha. Half the requirement was met by mixing a complete fertilizer with a micronutrient supplement into the soil prior to planting. The remaining requirement was met by adding a complete water soluble fertilizer to the irrigation water tanks and applying it through the irrigation system at each irrigation. This fertilizer was supplemented with a micronutrient foliar spray.

Bulk Density

The bulk densities of the three soils used in the lysimeters were determined in the laboratory by packing five samples of each soil into fifteen aluminum cans which were 50 mm deep and had a 50 mm diameter. After oven drying at 105° C, the mass of each

sample was determined by subtracting the mass of the can from the total mass. The can volumes were found by determining the mass of water required to completely fill each can and converting that mass to volume. Excellent agreement was obtained between the five samples of each soil which were averaged to produce the bulk densities given in Table 3.2.

Soil-Moisture Retention Curves

Soil-moisture retention curves were developed for the three soils used in the study (Figure 3.10). A pressure plate extractor and the previously determined bulk densities were used to develop desorption curves of volumetric soil water content versus pressure potential. Five soil samples were used to determine the volumetric water content of the soil at a given pressure. Early results indicated that the time required for soil samples to reach equilibrium at a given pressure was much larger than the 24 hrs recommended in the literature. In this study, a five day period was used to ensure equilibrium. Saturated and residual water contents are given in Table 3.2.

The coefficients of variation of the water contents near saturation (-5 to -1 kPa) ranged from 2% to 8%, respectively, emphasizing the difficulty in obtaining these data in this pressure range. Some of this variability may have been due to normal sampling variability, while much was probably due to variation in control pressure in this range. The coefficients of variation generally decreased to less than 0.1% as potential decreased to -100 kPa.

Saturated Hydraulic Conductivity

Saturated hydraulic conductivity (K_s) was determined with a constant head permeameter. A soil core of length ΔL was packed into a permeameter and saturated with water from the bottom upwards. A constant depth of water was then established over the soil column and the system allowed to reach equilibrium. The outflow of water from the system, Q, was measured at fixed time intervals, t, to determine when equilibrium conditions were established. The constant head difference, $\Delta\psi$, was calculated by adding the depth of the standing water to ΔL. The saturated hydraulic conductivity was determined from

$$K_s = - \frac{Q}{At} \frac{\Delta L}{\Delta \psi} \tag{3.2}$$

where A is the cross-sectional area of the soil column. The saturated hydraulic conductivities of the three soils are given in Table 3.2.

Hydraulic Conductivity Curve

Hydraulic conductivity curves were developed for each of the three soils by the van Genuchten (1980) method because it has been extensively used to successfully predict conductivity curves of sandy soils. The observed data required by the method for each soil are the soil-moisture retention curve, the saturated and residual water contents, and the saturated hydraulic conductivity.

First, equation (2.6) was fitted to the data. The resulting parameters α, n, and m are tabulated below. To test the fit of the analytical functions, the predicted soil-moisture retention curves were plotted against the observed curves in Figure 3.11. The fits were excellent for the builder's sand and the Astatula f.s. and good for the Pomona sand. Equation (2.9) was then used to predict hydraulic conductivity which was plotted against pressure head in Figure 3.12.

Table 3.3. Parameters for van Genuchten's Equation.

Soil type	α	n	m
Builder's sand	0.032	6.59	0.848
Astatula f.s.	0.033	3.53	0.717
Pomona sand	0.029	3.01	0.668

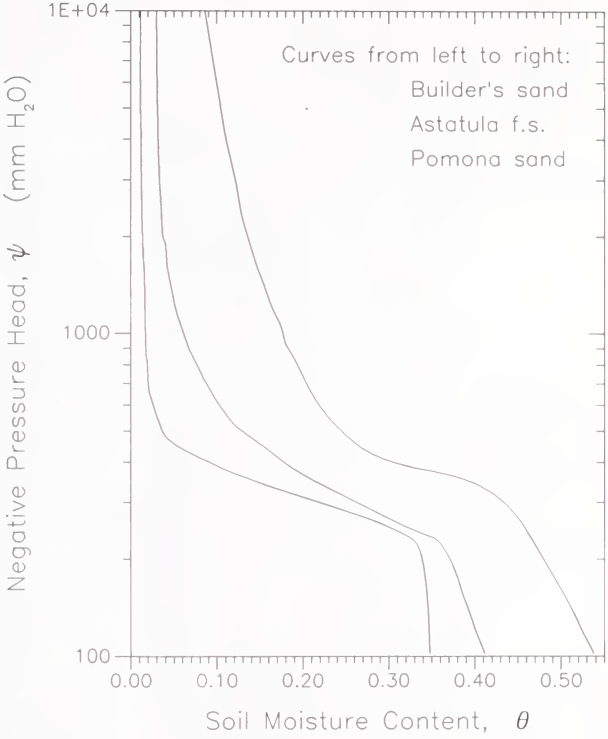

Figure 3.10. Soil-moisture retention curves for the three soils used in this study.

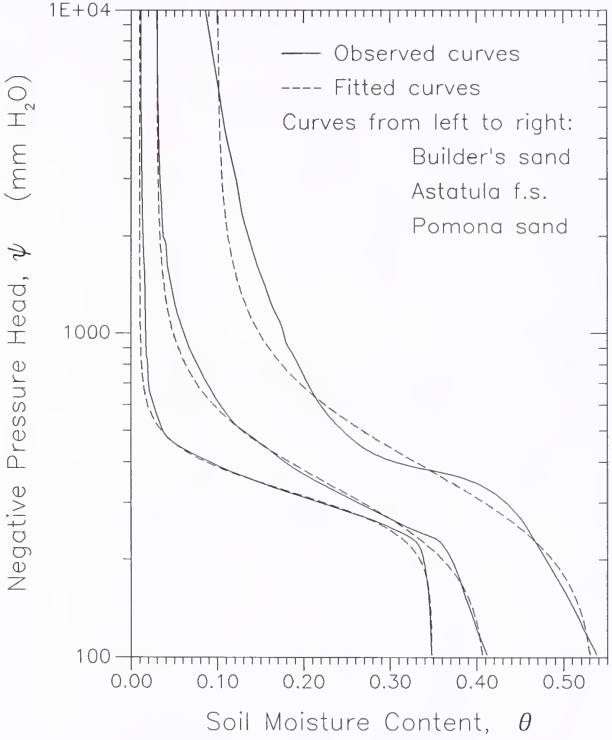

Figure 3.11. Fitted and observed soil-moisture retention curves for the three soils used in this study.

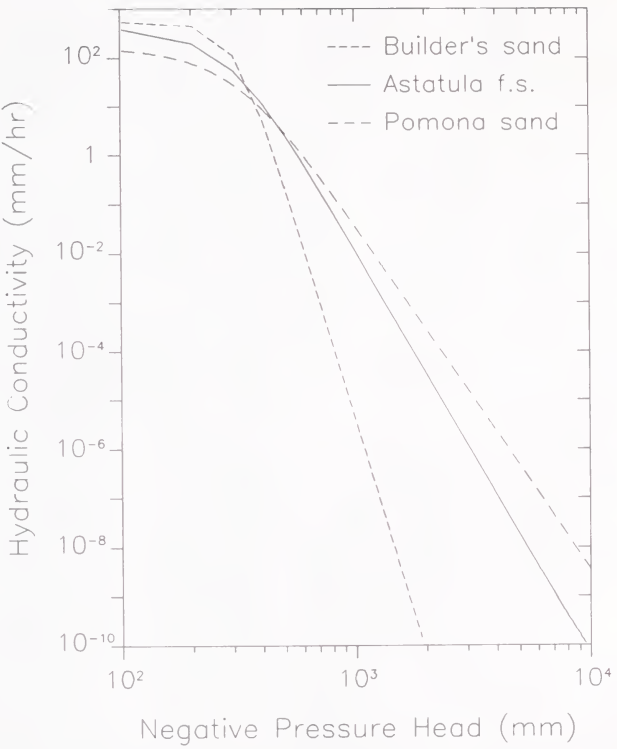

Figure 3.12. Hydraulic conductivity curves for the three soils used in this study.

CHAPTER 4
EXPERIMENTAL RESULTS

Plant Growth

The months of March and April, 1988, were unusually cool in Gainesville. Consequently, plant growth and water use were uncharacteristicly limited during those months. The majority of plant growth occurred in May and June (Table 4.1). For this reason, the discussion of water use was limited to these final eight weeks of the season.

Table 4.1. Canopy Dimensions (m).

Soil Type and Lysimeter	March 15		May 01		June 26	
	Height	Width	Height	Width	Height	Width
Builder's Sand C1	0.11	0.06	0.24	0.30	0.70	0.45
Builder's Sand C2	0.10	0.07	0.26	0.28	0.67	0.38
Astatula f.s. E1	0.12	0.05	0.25	0.31	0.73	0.55
Astatula f.s. E2	0.10	0.07	0.27	0.26	0.86	0.48
Pomona sand W1	0.10	0.07	0.26	0.29	0.93	1.06
Pomona sand W2	0.11	0.06	0.28	0.32	0.93	1.14

Despite efforts to maintain plant size uniform across all soil types, the plants in the Pomona sand grew considerably better than those in the Astatula f.s., while the smallest plants were produced in the builder's sand. Yield data were not collected because the fruit were afflicted by blossom end rot, particularly those in the Pomona sand. The disease, which is caused by calcium deficiency, was treated by spraying the plants with a foliar calcium supplement. The plants responded well to the treatment, but not quickly enough to produce a representative yield by the end of the experiment.

Measurement Accuracy

There are inherent limitations when drainage type lysimeters are used to conduct water use studies. These limitations which, along with other measurement errors, may reduce the accuracy of collected data, must be recognized and accounted for.

Water Budget Accuracy

All water volumes applied to or extracted from the lysimeters were measured with a graduated cylinder. The accuracy of the graduated cylinder and the ability to refill the water supply tanks reproducibly determined the accuracy of the measured water volumes. A 1 L graduated cylinder with accuracy to 10 mL was used to refill the supply tanks and measure drainage water extractions. Calibration tests indicated that the supply tanks were refilled reproducibly to within 50 mL which produced errors in water inflows and outflows of less than 2%.

Weekly, Monthly, and Seasonal Water Use Accuracy

For accurate short-term measurement of water use from a lysimeter, an accurate measurement of soil-water storage or soil-moisture content is required. Because drainage type lysimeters do not permit a direct determination of soil-moisture content, it was determined indirectly by monitoring soil water potential.

Soil-moisture content and water potential are related through the soil-moisture retention curve which was measured for each soil. But, as discussed earlier, the translation of soil water potential to soil-moisture content on the basis of the soil-moisture retention curves measured introduced errors up to 8% near saturation. The combination of instrumentation error of 0.2 kPa (20% to 4% of -1 to -5 kPa) and error resulting from the pressure extractor procedure were the causes of this error. The resulting error prevented accurate measurements of daily water use, although wetting or drying patterns were still determined. As the measurement period increased, the relative size of the error diminished with respect to the water used by the crop. Thus, weekly water use was accurately determined, especially during high water use periods.

Crop Water Use

Because the research was conducted in rain-sheltered lysimeters buffered by well watered grass, the water use data may not represent the water use requirements of an extensive tomato crop grown under field conditions in Gainesville, Florida. The data are primarily a comparison of crop water use contributions by the water table and the irrigation system with respect to soil type.

Partitioning of Crop Water Use

For the purposes of this study, measured crop water use was defined as

$$\text{crop water use} = \text{irrigation} - \text{drainage} + \text{water table recharge} \quad (4.1)$$

The design of the lysimeters permitted crop water use to be partitioned into irrigation and water table recharge components. Monthly values in terms of mm over the surface area of the lysimeter for each of the components are presented in Figures 4.1 and 4.2. The numbers over the irrigation and water table recharge bars represent the percentage of crop water use contributed by each component. The number over the drainage bar represents the percentage of irrigation water lost to drainage. Drainage was a function of soil type. The Pomona sand, with the greatest water holding capacity, consistently had the smallest drainage fraction. Overall, drainage volumes were small because, as discussed earlier, irrigation applications were designed to minimize deep percolation.

During May, when the plants were still maturing, the contribution of the water table to crop water use in the builder's sand, the Astatula f.s., and the Pomona sand was 16%, 19%, and 33%, respectively (Figure 4.1). In June, when the plants were mature, the water table contributions were 26%, 34%, and 31% (Figure 4.2). These data indicate that as the plant root systems developed and extended down towards the capillary fringe in the builder's sand and the Astatula f.s., the water table contribution increased significantly. In the Pomona sand, on the other hand, plant size had little effect on water table contribution. In fact, the contribution of the water table to crop water use in Pomona sand remained the same

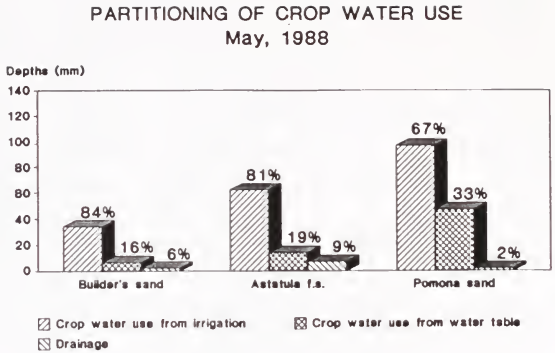

Figure 4.1. Partitioning of crop water use in May.

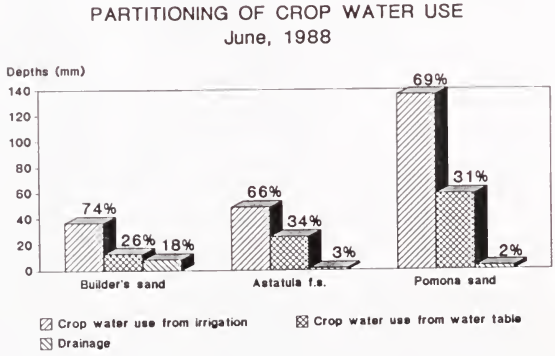

Figure 4.2. Partitioning of crop water use in June.

throughout the growing season. Consequently, it was concluded that the properties of the soil, and in particular the particle size distribution and organic matter content, allowed the capillary fringe to rise high enough in the Pomona sand to make water available to the plant roots, regardless of plant size.

It is also possible that the rate of growth of the plant root system towards the capillary fringe in the builder's sand and the Astatula f.s. was a function of the irrigation schedule. If these two soils could not hold the daily crop water requirement from only one irrigation event per day, the root system may have developed towards the water table in response to the water available there. Pressure transducer readings of up to 50 kPa indicate that the plants in all three soils may have experienced mild, daily short term water stresses during the hours preceding irrigation. At no time, however, did the plants show any visual signs of water stress such as wilting.

Weekly, Monthly, and Seasonal Water Use

Weekly crop water use for the final eight weeks of the growing season is presented in Figures 4.3-4.8. Each figure contains two graphs. The graph on the left shows weekly water use in the form of stacked bars where the lower bar depicts the contribution of irrigation water to crop water use and the upper bar the contribution of the water table. The other half of each figure presents potential evapotranspiration (computed by the Penman equation) over the same period. By comparing the two graphs, it can be clearly seen that the fluctuations in water use correspond closely with the fluctuations in potential ET.

The water use data indicate that crop water use was a function of plant size and that the plants' source of water (irrigation versus water table) was a function of soil type. The plant size data presented in Table 4.1 do not adequately illustrate the striking difference in appearance between the plants. This is more apparent in Figures 4.1-4.8 where it can be clearly seen that although the water use patterns were the same for all three soils, the total water use values varied dramatically from soil to soil.

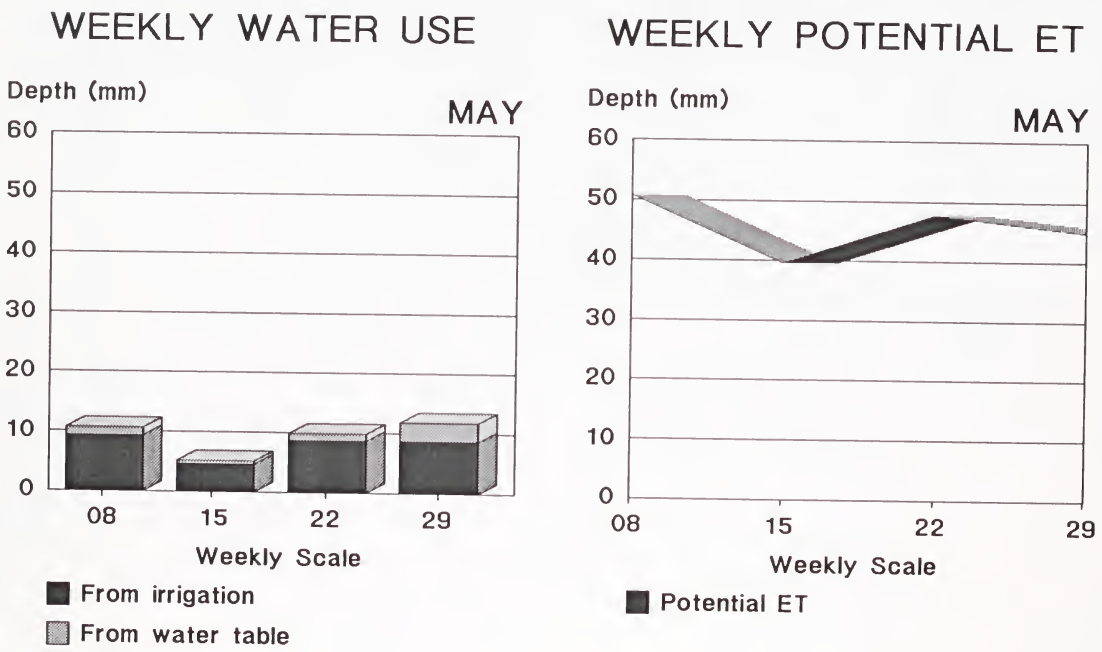

Figure 4.3. Weekly crop water use in builder's sand, May, 1988.

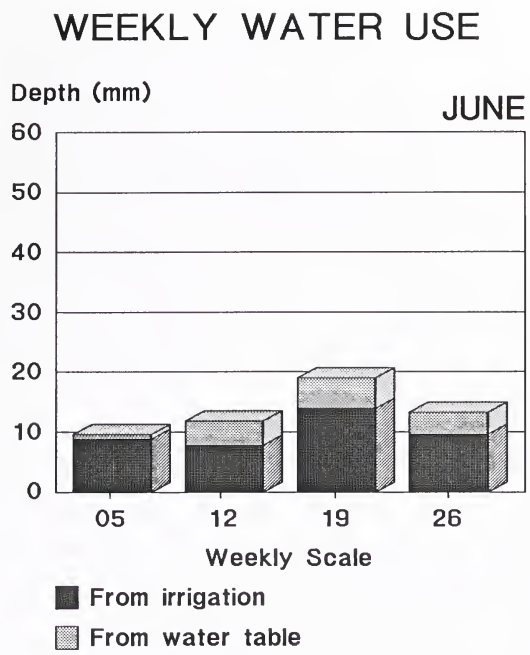

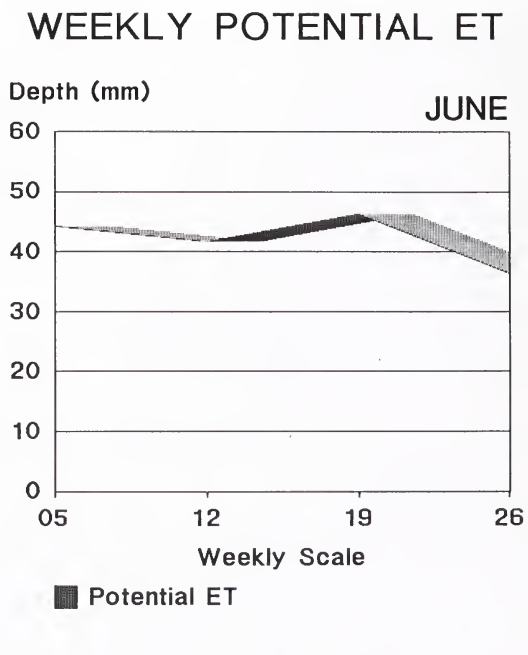

Figure 4.4. Weekly crop water use in builder's sand, June, 1988.

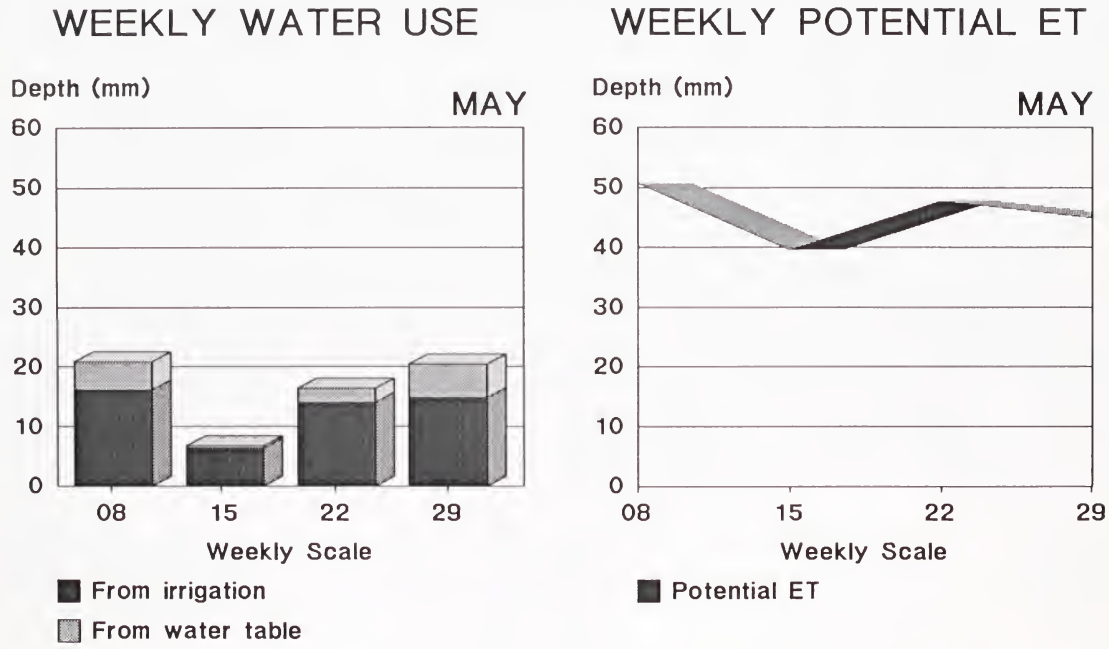

Figure 4.5. Weekly crop water use in Astatula f.s. May, 1988.

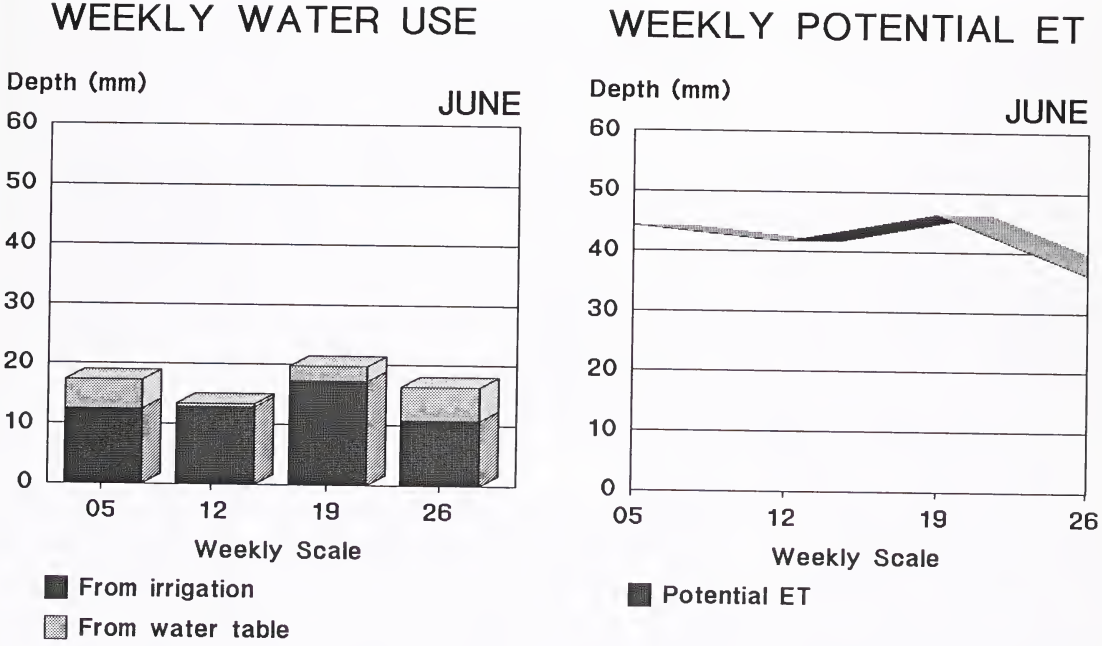

Figure 4.6. Weekly crop water use in Astatula f.s. June, 1988.

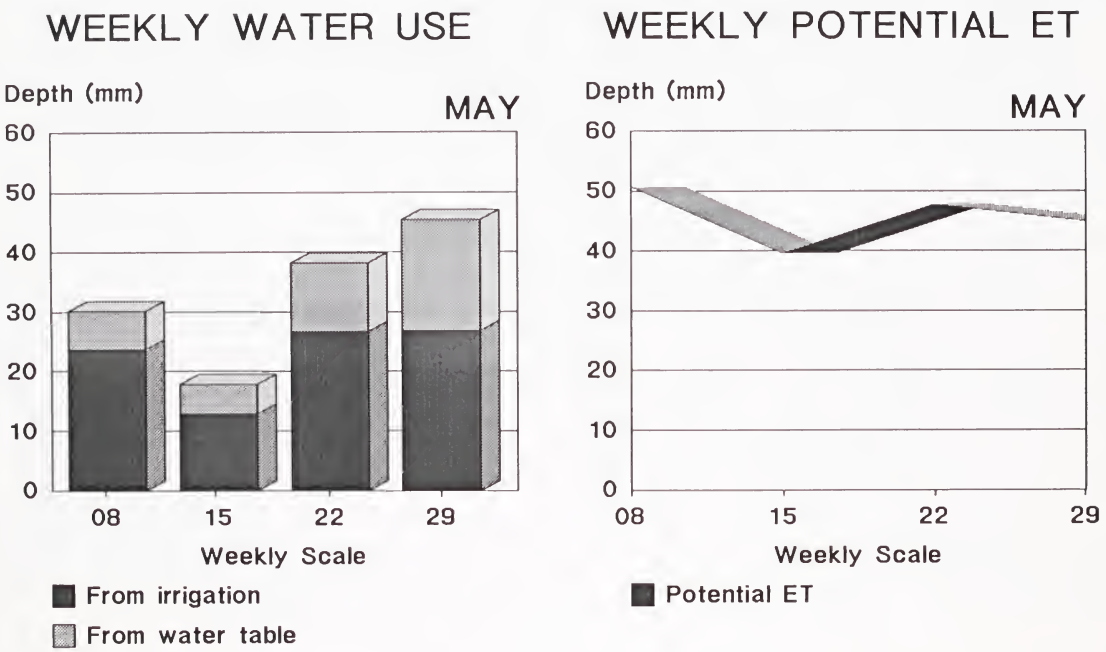

Figure 4.7. Weekly crop water use in Pomona sand, May, 1988.

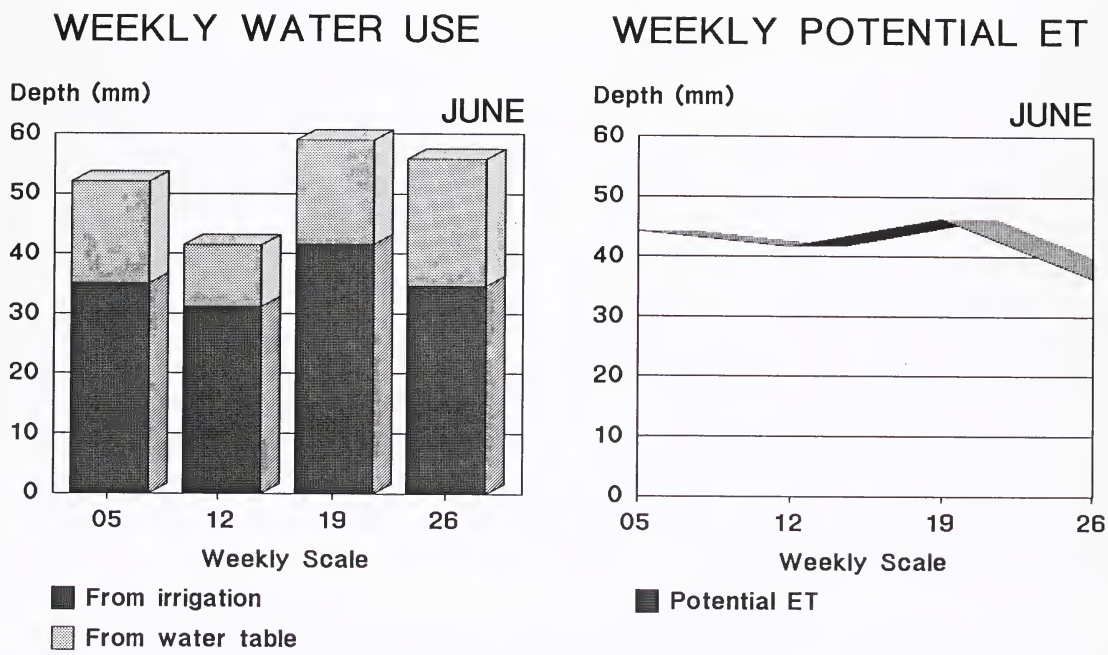

Figure 4.8. Weekly crop water use in Pomona sand, June, 1988.

Seasonal water use budgets varied greatly from soil to soil. These differences were attributed to differences in plant size. Values for total monthly crop water use and seasonal use are tabulated in Table 4.2. Cumulative use for the final eight weeks of the growing season are shown in Figures 4.9-4.11

Table 4.2. Monthly and Seasonal Water Use.

Soil Type	May		June		Seasonal	
	(mm)	(L/m)	(mm)	(L/m)	(mm)	(L/m)
Builder's Sand	41	53	50	64	91	117
Astatula f.s.	77	99	75	96	152	195
Pomona sand	145	186	195	250	340	436

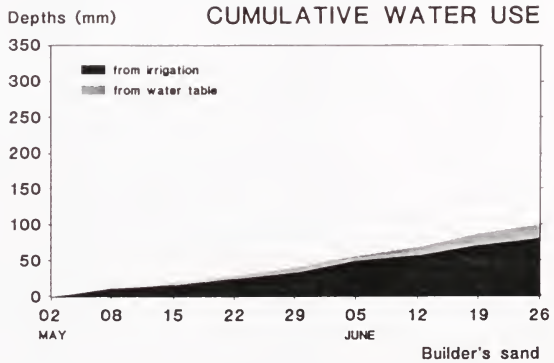

Figure 4.9. Cumulative water use for the plants growing in Builder's sand.

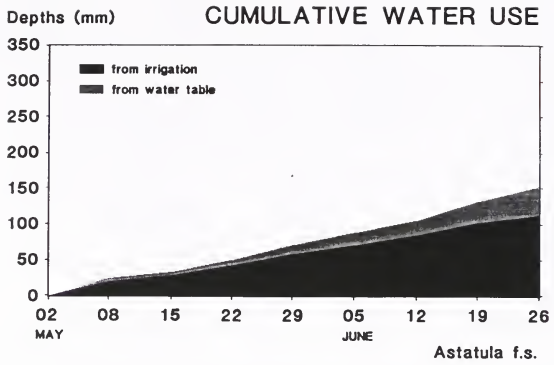

Figure 4.10. Cumulative water use for the plants growing in Astatula f.s.

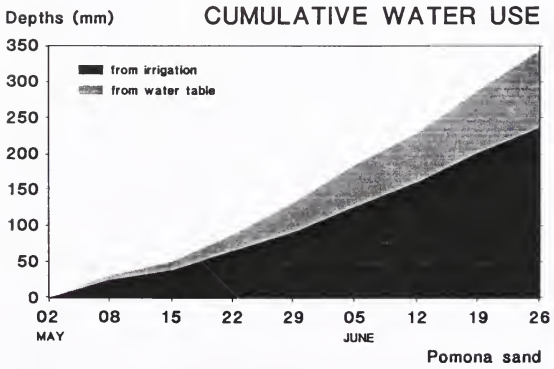

Figure 4.11. Cumulative water use for the plants growing in Pomona sand.

Redistribution and Extraction Patterns

The data acquisition system proved extremely effective in determining redistribution and extraction patterns in the soil profile. These patterns, however, were limited to the top 300 mm of the soil profile because that is where 9 of the 10 tensiometers were located (Figures 3.5 and 3.6)

The data acquisition system read the instruments at one minute intervals. These readings were passed on to the microcomputer where ten minute averages were computed and saved to disk. These data, graphed for weekly periods, provided excellent means of monitoring the changes in soil water status in the soil profile. Figure 4.12 is a graph of readings from the three tensiometers in the Astatula f.s. at the 100 mm depth and at radial distances 50, 150, and 250 mm from the irrigation lateral. This figure illustrates extraction, irrigation, and redistribution during a week in late April when the plants were small.

Since the 50 mm tensiometer was closest to the irrigation lateral and the plants, it was the first to respond to irrigation and extraction by plant roots. As a result, the extremes exhibited by this curve are much larger than those of the other two curves. The first high peak of the curve occurred in the late afternoon of April 27. Immediately following is a period of overnight redistribution of soil water succeeded by the reinitiation of extraction the next morning. These events are marked by the U shape in the curve. At the top of the second peak, an irrigation occurred, creating the sudden increase in soil water potential. Figure 4.13 isolates the 24-hour period around the irrigation event and permits a closer view of how the tensiometers reacted to the wetting front.

From Figure 4.13, there was a considerable time lag between the irrigation event and the tensiometers response to the wetting front. As expected, the lag was a function of distance. The tensiometer 50 mm from the lateral responded to the wetting front about 10 minutes after the irrigation event which occurred at 10:30 and the tensiometer 150 mm away responded to it about 40 minutes later. It was difficult to distinguish when the wetting front reached the 250 mm tensiometer because the tensiometer's response was only on the order of 2 kPa. However, the tensiometer did eventually react to the approaching wetting front.

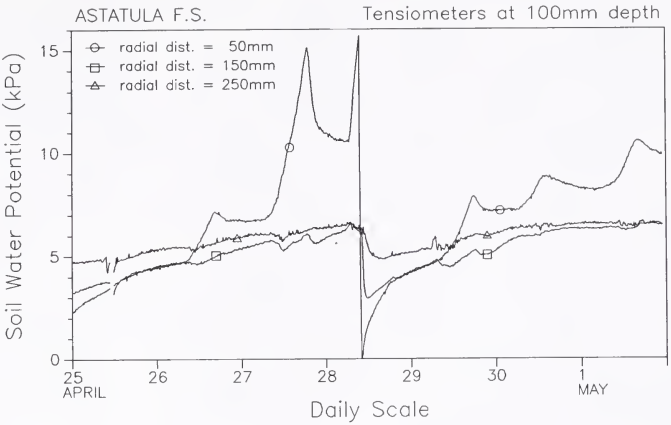

Figure 4.12. Tensiometer readings versus time on a daily scale.

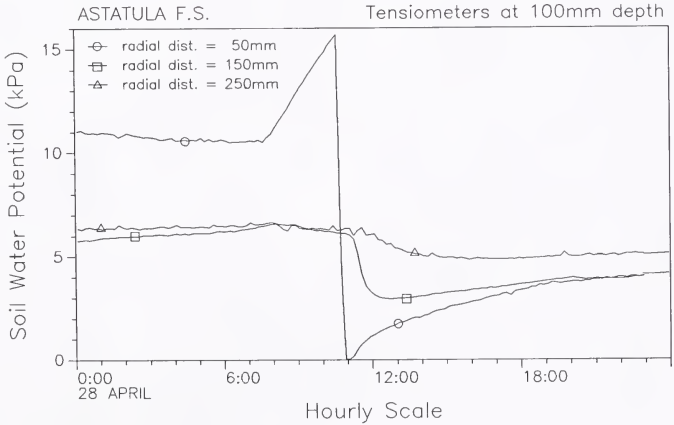

Figure 4.13. Tensiometer readings versus time on an hourly scale.

Another series of extraction-irrigation-redistribution cycles which occurred in the Pomona sand during the week of June 6 is shown in Figure 4.14. In this case, the plants were mature and once extraction began, low soil water potentials were reached very quickly. The events of June 11 and 12 were chosen for closer study because irrigation occurred late in the afternoon, shortly before sunset. This condition allowed redistribution and extraction to be studied independently. Redistribution proceeded overnight with minimal influence from extraction, while extraction was studied the following morning after most of the redistribution had been completed. All the sudden drops (increases in soil water potential) indicate irrigation events.

The extraction-redistribution cycle of June 11 and 12 was studied by using transducer readings over a 24-hour period to graph soil water equipotential lines in the bed profile. Equipotential lines were limited to the bed because, as can be seen in Figure 4.15, 9 of 10 tensiometers were located there. This, however, was not a serious limitation to this study because most of the redistribution and extraction events occurred in the bed. Only half of the lysimeter profile was instrumented because the irrigation lateral, which was located along the center line of the bed, created a plane of symmetry. For the same reason, the tensiometer at the 500 mm depth which was actually located on the opposite half of the lysimeter (Figure 3.5) from the other nine tensiometers, was used as shown in Figure 4.15.

Figures 4.16-4.21 depict the change in equipotential lines over a 24-hour period in the instrumented Pomona sand lysimeter for the June 11 and 12 irrigation, redistribution, and extraction cycle. Figure 4.16 shows the soil water status in the bed when the irrigation event occurred at 17:00. Low potentials were found mostly in the top left quadrant of the profile where, as expected, most of the roots were concentrated. The tensiometers on the right hand side of the bed were in relatively moist soil at -10 kPa.

The next figure (4.17) shows the equipotential lines 20 minutes after the irrigation event. By that time, the wetting front had moved past the shallowest tensiometer 50 mm from the lateral and was beginning to affect the shallowest tensiometer at the 150 mm radial distance. The front had not yet penetrated to the 200 mm depth.

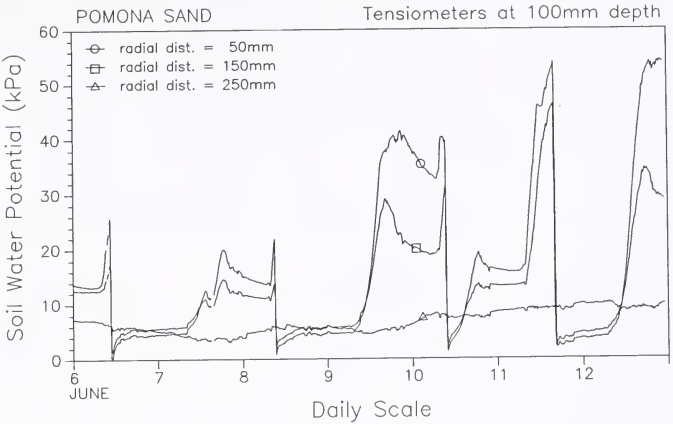

Figure 4.14. Tensiometer readings versus time on a daily scale for the week of June 6.

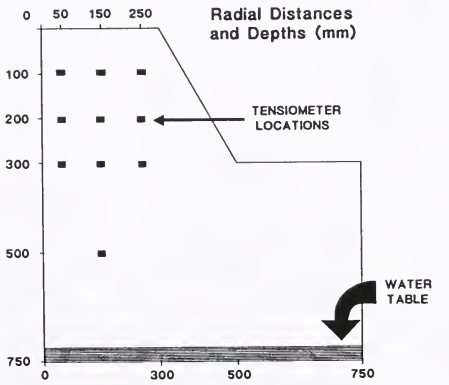

Figure 4.15. Side view of a lysimeter showing the bed, the water table, and the tensiometer locations.

Figure 4.18 shows the equipotential lines at 18:00, one hour after irrigation. By that time, the wetting front had clearly reached the 6 tensiometers closest to the plane of symmetry. The equipotential lines in this figure appear to be in some disarray. This was caused by assuming that this line source problem was two-dimensional. In fact, it was not completely so because the wetting front did not move uniformly through the soil profile along the whole length of the bed. Since the tensiometers were not located in a single plane as shown in the figures, but were located along the length of the bed, some instruments responded to the wetting front earlier or later than they would have in a true 2-dimensional homogeneous, isotropic soil. This situation occurred only shortly after an irrigation event when most of the instruments were affected by the moving wetting front.

Figure 4.19 shows the equipotential lines following overnight redistribution. This figure distinctly shows which sections of the soil profile were affected by the irrigation event. The potentials in the top right quadrant of the bed remained unchanged despite irrigation while the remainder of the bed returned to field capacity. Clearly, the radial movement of the wetting front was limited to less than 250 mm. The vertical movement of the front, on the other hand, was more than 300 mm.

Figures 4.20 and 4.21 show the effects of extraction. At 12:00, the effects of extraction are apparent. At 17:00, 24 hours after the irrigation event, soil water status in the profile was very similar to the conditions that existed before irrigation. What is also apparent from these figures is that there was very little extraction taking place near the edges of the bed.

Overall, very little change in soil water status took place at radial distances of more than 200 mm from the irrigation lateral. On the other hand, redistribution and extraction were evident for at least 300 mm in the vertical direction. Similar redistribution and extraction patterns were obtained for the builder's sand and the Astatula f.s. Radial movement of the wetting fronts in these two soils, however, was less than in the Pomona sand. These observations were a function of the hydraulic properties of the sandy soils studied.

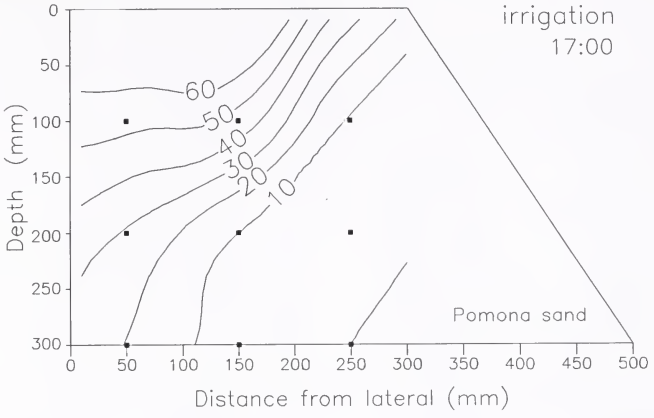

Figure 4.16. Equipotential lines in a Pomona sand profile at irrigation (kPa).

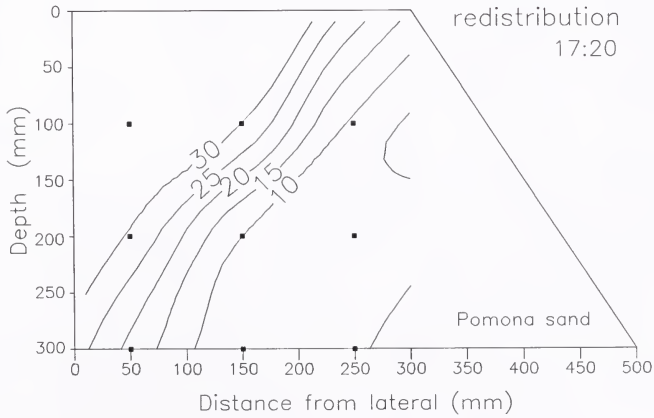

Figure 4.17. Equipotential lines in a Pomona sand profile during redistribution (kPa).

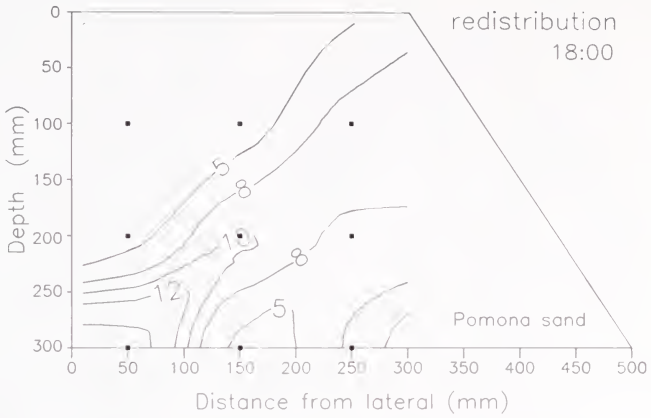

Figure 4.18. Equipotential lines in a Pomona sand profile during redistribution (kPa).

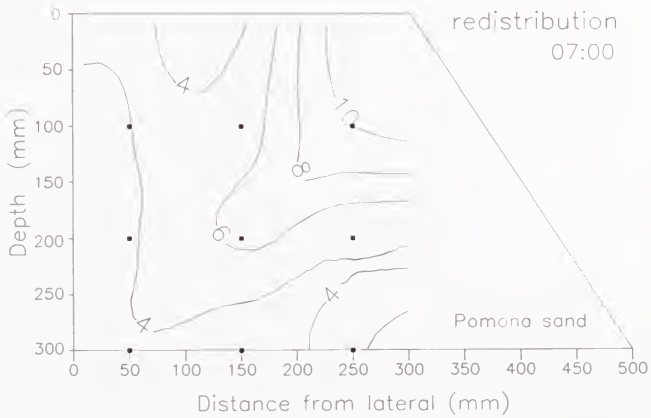

Figure 4.19. Equipotential lines in a Pomona sand profile following redistribution (kPa).

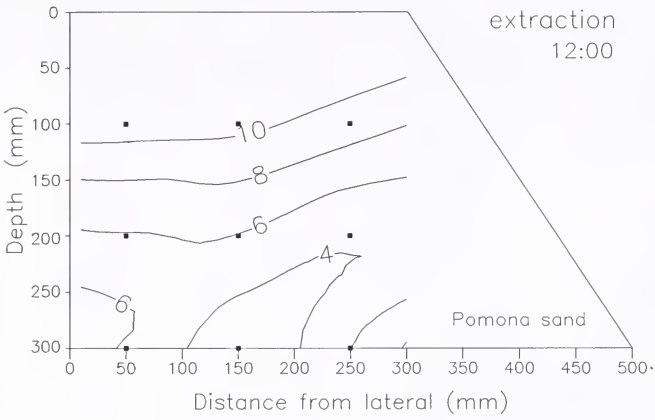

Figure 4.20. Equipotential lines in a Pomona sand profile during extraction (kPa).

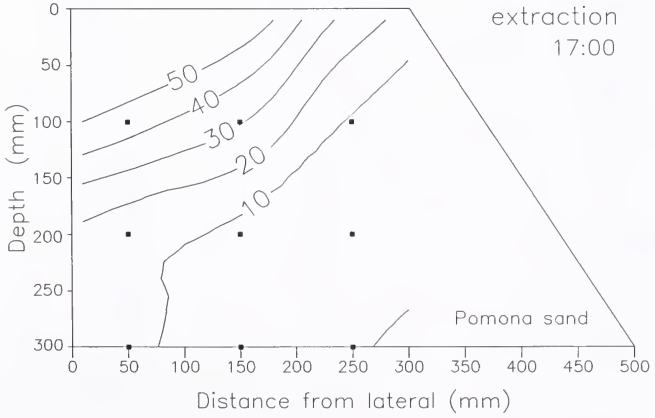

Figure 4.21. Equipotential lines in a Pomona sand profile during extraction (kPa).

Evaporation from the Soil

Evaporation from the bare soil (furrows) between the mulched beds of each lysimeter could not be calculated from ET data collected during the growing season. A short experiment was therefore conducted after the growing season to determine the magnitude of the evaporation term.

The plants were removed from the lysimeters and perforations in the plastic mulch were sealed to eliminate transpiration or evaporation losses from the bed. The water table was continuously recharged by the float valves, and the water table tanks were replenished after two or three day measurement periods.

The depths of water lost to evaporation from each lysimeter was calculated by dividing the volumes required to refill the water table tanks by the furrow surface areas of the lysimeters (0.255 m^2). The evaporation depths were then compared to Penman ET values. Figure 4.22 presents the data for approximately three weeks in October and November, 1988. The data are given as depths of water lost to evapotranspiration as computed by the Penman equation and depths of water lost to evaporation from the three soils used in the study during the two or three day measurement periods. The evaporation depths of all three soils were generally an order of magnitude smaller than the corresponding ET values but followed the same trend. The evaporation values were the largest for Pomona sand, followed by Astatula f.s., and builder's sand. Consequently, it was concluded that the evaporation values were a function of the soil properties, and in particular the particle size distribution and organic matter content. Because the two replications of each soil produced almost identical data, only the average data are presented in Figure 4.22.

Soil evaporation coefficients, C_s, were developed for each of the soils. The coefficient of each soil was computed by dividing the observed evaporation by Penman ET for each of the nine measurement periods discussed above and averaging the nine values to obtain a mean. The coefficients were C_s = 0.037, 0.070, and 0.097, for builder's sand, Astatula f.s., and Pomona sand, respectively. Daily bare soil evaporation from the furrows

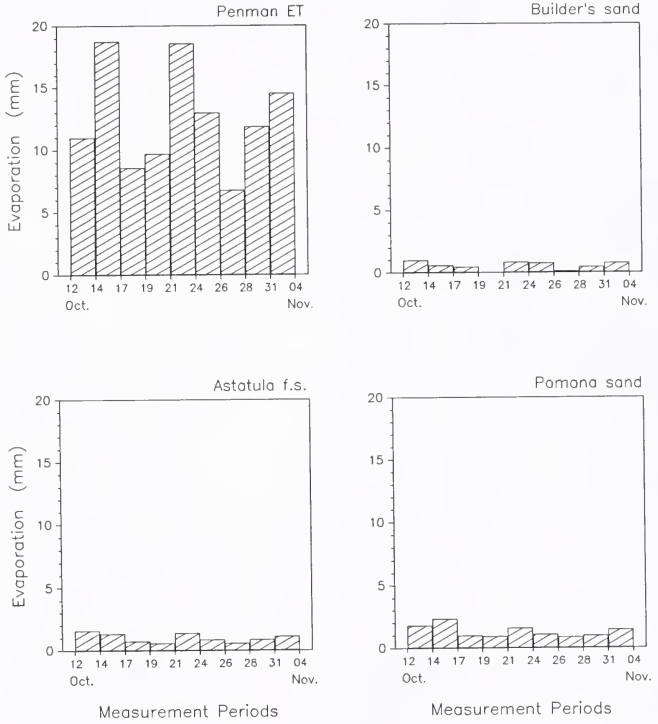

Figure 4.22. Comparison of Penman ET and observed bare soil evaporation from the lysimeters.

during the growing season was approximated by multiplying the corresponding daily Penman ET values by the appropriate coefficients. Figure 4.23 presents daily Penman ET pan values and estimated bare soil evaporation values from the lysimeters for each of the three soils during the last two months of the growing season.

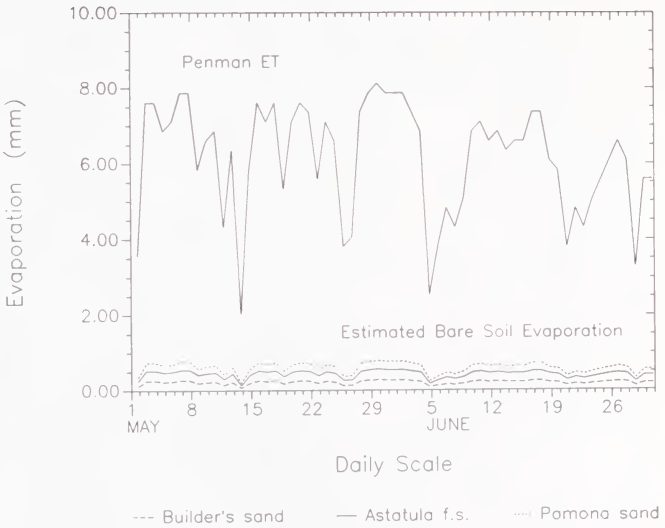

Figure 4.23. Comparison of daily Penman ET and estimated daily bare soil evaporation from the lysimeters during the final two months of the growing season.

CHAPTER 5
NUMERICAL SOLUTION

The Richards equation was solved with a finite difference approximation. Because line sources produce a continuous wetted band along the length of the lateral (the y-axis), they can be studied as two-dimensional problems in the x-z plane. A two-dimensional numerical model was therefore developed to simulate infiltration, redistribution, and extraction of water in the soil profile.

Several assumptions were employed in the development of the numerical model to simplify the complexities associated with mathematically describing water movement in unsaturated porous media. These assumptions were:

1. Physical properties of the soil were homogeneous, isotropic, and nondeforming under varying moisture content and pressure head.
2. Physical and chemical properties of the soil were constant in time.
3. Hydraulic conductivity, $K(\theta)$, and pressure head, ψ, were single-valued functions of water content, θ, (nonhysteretic).

One-Dimensional Model Development

A one-dimensional vertical simulation model was developed as the precursor of the two-dimensional model. Its purpose was to verify that the finite difference equations closely approximated the governing partial differential equation. For one-dimensional flow, equation (2.19) reduces to

$$C(\psi)\frac{\partial \psi}{\partial t} = \frac{\partial}{\partial z}\left[K(\psi)\left(\frac{\partial(\psi)}{\partial z} - 1\right)\right] - S(\psi) \tag{5.1}$$

where z = the vertical dimension.

Equation (5.1) was discretized with an implicit finite difference scheme that used explicit linearization of the soil parameters as suggested by Haverkamp et al. (1977). Application of equation (5.1) to the soil was accomplished by superimposing a mesh over the soil profile with a finite number of grids or cells as shown in Figure 5.1. For simplicity, the parameters $K(\psi)$, $C(\psi)$, and $S(\psi)$ were represented by K, C, and S, respectively. The superscript j was used as the space increment and Δz as the grid spacing in space.

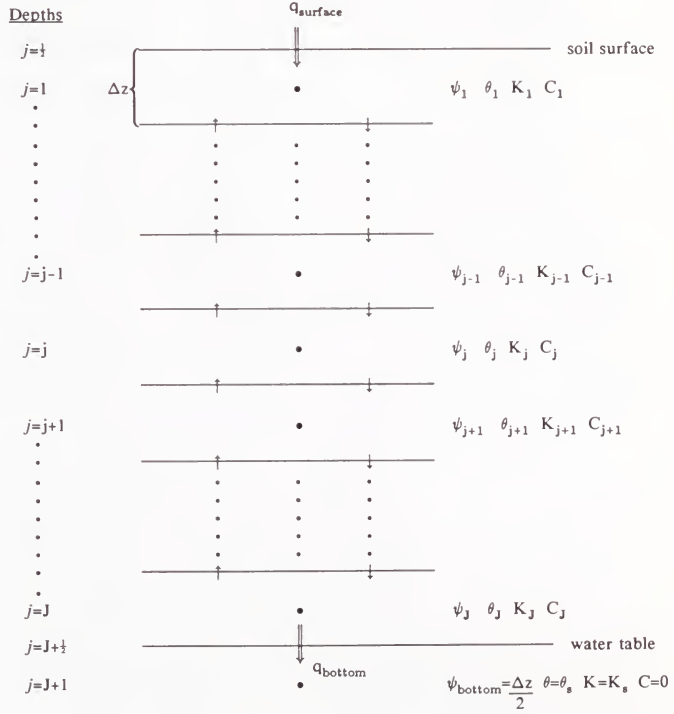

Figure 5.1. The finite difference grid system used for the one-dimensional model. Adapted from Stone (1987), p.38.

The pressure head and soil parameters of each cell were computed and assigned to the node located at the center of each cell. The total number of interior nodes was J with the water table, which acted as the lower boundary, located at $j=J+\frac{1}{2}$. The exterior node, at $j=J+1$, was used in the finite difference equation that described the lower boundary condition.

The numerical form of equation (5.1) was obtained by letting

$$\frac{\partial}{\partial z}\left[K(\psi)\left(\frac{\partial(\psi)}{\partial z} - 1\right)\right] = \frac{\partial W}{\partial z} \tag{5.2}$$

and discretizing the right hand side of equation (5.2) around j to obtain

$$\left[\frac{\partial W}{\partial z}\right]_j = \frac{W_{j+\frac{1}{2}} - W_{j-\frac{1}{2}}}{\Delta z} \tag{5.3}$$

Equation (5.3) was then substituted into equation (5.2) to give

$$\frac{1}{\Delta z}\left\{\left[K_{j+\frac{1}{2}}\left(\frac{\partial \psi}{\partial z} - 1\right)_{j+\frac{1}{2}}\right] - \left[K_{j-\frac{1}{2}}\left(\frac{\partial \psi}{\partial z} - 1\right)_{j-\frac{1}{2}}\right]\right\} \tag{5.4}$$

The derivatives of ψ with respect to z were approximated as

$$\left(\frac{\partial \psi}{\partial z} - 1\right)_{j+\frac{1}{2}} = \frac{\psi_{j+1} - \psi_j}{\Delta z} - 1 \tag{5.5}$$

$$\left(\frac{\partial \psi}{\partial z} - 1\right)_{j-\frac{1}{2}} = \frac{\psi_j - \psi_{j-1}}{\Delta z} - 1 \tag{5.6}$$

which when substituted back into equation (5.4) gave

$$\frac{1}{\Delta z}\left\{\left[K_{j+\frac{1}{2}}\left(\frac{\psi_{j+1} - \psi_j}{\Delta z} - 1\right)\right] - \left[K_{j-\frac{1}{2}}\left(\frac{\psi_j - \psi_{j-1}}{\Delta z} - 1\right)\right]\right\} \tag{5.7}$$

The superscript n was used as the time coordinate and Δt as the grid spacing in time. The implicit formulation of equation (5.7) was obtained by evaluating at the *n+1* time level. The time derivative in equation (5.1) was then replaced by a backward-difference approximation relative to the *n+1* time level. By using explicit linearization, the soil parameters are known at each time step and are evaluated using the values of ψ at the n time step (ψ^n).

$$C_j^n \frac{\psi_j^{n+1} - \psi_j^n}{\Delta t} = \frac{1}{\Delta z}\left\{\left[K_{j+\frac{1}{2}}^n \left(\frac{\psi_{j+1}^{n+1} - \psi_j^{n+1}}{\Delta z} - 1\right)\right] - \left[K_{j-\frac{1}{2}}^n \left(\frac{\psi_j^{n+1} - \psi_{j-1}^{n+1}}{\Delta z} - 1\right)\right]\right\} - S_j^n \tag{5.8}$$

The hydraulic conductivity $K(\psi_{j\pm\frac{1}{2}}^n)$ was taken as the arithmetic mean for all interior nodes $1 \leq j \leq J$ where

$$K_{j-\frac{1}{2}}^n = \frac{K_j^n + K_{j-1}^n}{2} \tag{5.9}$$

$$K_{j+\frac{1}{2}}^n = \frac{K_j^n + K_{j+1}^n}{2} \tag{5.10}$$

Since explicit linearization was used to evaluate the soil parameters, the only unknowns in equation (5.8) were terms containing ψ^{n+1}. The equation was then rearranged so that the unknowns were on the left hand side and the knowns on the right hand side

$$-\left[\frac{K_{j-\frac{1}{2}}^n}{\Delta z^2}\right]\psi_{j-1}^{n+1} + \left[\frac{C_j^n}{\Delta t} + \frac{(K_{j-\frac{1}{2}}^n + K_{j+\frac{1}{2}}^n)}{\Delta z^2}\right]\psi_j^{n+1} - \left[\frac{K_{j+\frac{1}{2}}^n}{\Delta z^2}\right]\psi_{j+1}^{n+1} = \frac{C_j^n \psi_j^n}{\Delta t} + \frac{(K_{j-\frac{1}{2}}^n - K_{j+\frac{1}{2}}^n)}{\Delta z} - S_j^n \tag{5.11}$$

or in a more usable form

$$A_j \psi_{j-1}^{n+1} + D_j \psi_j^{n+1} + B_j \psi_{j+1}^{n+1} = R_j \tag{5.12}$$

where

$$A_j = - \frac{K_{j-\frac{1}{2}}^n}{\Delta z^2} \tag{5.13}$$

$$D_j = \frac{C_j^n}{\Delta t} - A_j - B_j \tag{5.14}$$

$$B_j = - \frac{K_{j+\frac{1}{2}}^n}{\Delta z^2} \tag{5.15}$$

$$R_j = \frac{C_j^n \psi_j^n}{\Delta t} + \frac{(K_{j-\frac{1}{2}}^n - K_{j+\frac{1}{2}}^n)}{\Delta z} - S_j^n \tag{5.16}$$

Equation (5.12) was written for each of the interior nodes $2 \leq j \leq J-1$ in the soil profile. The top and bottom grids of the system required equation (5.11) to be modified so that it would describe the boundary conditions.

Boundary Conditions

Two types of boundary conditions are usually associated with the flow equation in a soil profile. A Dirichlet condition specifies the dependent variable (in this case the pressure head, ψ). A Neuman condition specifies the derivative of the dependent variable which for the soil water problem means a specification of the flow through the boundary (Feddes et al., 1978). To simulate the conditions encountered in this study both types of boundary conditions were specified.

Top boundary. Physically, the top boundary of the soil profile consisted of the plastic mulch. The only flow through the soil surface allowed by the mulch was surface infiltration due to irrigation. Mathematically, this was modeled by a flux boundary condition with a

surface flux, $q_{surface}$ (q_s). The surface flux during irrigation was set equal to the water application rate until the irrigation event was completed. At all other times, q_s was set to zero. The total depth of water infiltrated at any time was calculated as the summation of the incremental infiltration volumes at all previous time steps. A flux across a boundary in the vertical direction is described by the partial differential equation

$$q = -K(\psi)\left[\frac{\partial\psi}{\partial z} - 1\right] \tag{5.17}$$

When equation (5.16) was discretized around j it became

$$q_j = -K_j\left[\frac{\psi_{j+\frac{1}{2}} - \psi_{j-\frac{1}{2}}}{\Delta z} - 1\right] \tag{5.18}$$

which when evaluated at $j = \frac{1}{2}$, the soil surface (Figure 5.1), gave

$$q_{\frac{1}{2}} = -K_{\frac{1}{2}}\left[\frac{\psi_1 - \psi_0}{\Delta z} - 1\right] = q_s \tag{5.19}$$

When equation (5.7) was evaluated at the first node, j=1, it became

$$C_1^n\frac{\psi_1^{n+1} - \psi_1^n}{\Delta t} = \frac{1}{\Delta z}\left\{\left[K_{3/2}^n\left[\frac{\psi_2^{n+1} - \psi_1^{n+1}}{\Delta z} - 1\right]\right] - \left[K_{1/2}^n\left[\frac{\psi_1^{n+1} - \psi_0^{n+1}}{\Delta z} - 1\right]\right]\right\} - S_1^n \tag{5.20}$$

The third term of equation (5.20) is the same as equation (5.19). Substitution of q_s for the term reduced equation (5.20) to

$$C_1^n\frac{\psi_1^{n+1} - \psi_1^n}{\Delta t} = \frac{1}{\Delta z}\left\{\left[K_{3/2}^n\left[\frac{\psi_2^{n+1} - \psi_1^{n+1}}{\Delta z} - 1\right]\right] + q_s\right\} - S_1^n \tag{5.21}$$

When the equation (5.21) was rearranged so that unknowns were on the left and knowns on the right it became

$$\left[\frac{C_1^n}{\Delta t} + \frac{K_{3/2}^n}{\Delta z^2}\right]\psi_1^{n+1} - \left[\frac{K_{3/2}^n}{\Delta z^2}\right]\psi_2^{n+1} = \frac{C_1^n\psi_1^n}{\Delta t} + \frac{q_s - K_{3/2}^n}{\Delta z} - S_1^n \tag{5.22}$$

or in a more usable form

$$D_1\psi_1^{n+1} + B_1\psi_2^{n+1} = R_1 \tag{5.23}$$

where

$$D_1 = \frac{C_1^n}{\Delta t} - B_1 \tag{5.24}$$

$$B_1 = -\frac{K_{3/2}^n}{\Delta z^2} \tag{5.25}$$

$$R_1 = \frac{C_1^n\psi_1^n}{\Delta t} + \frac{q_s - K_{3/2}^n}{\Delta z} - S_1^n \tag{5.26}$$

Bottom boundary. A constant potential boundary condition was used to simulate the water table. When equation (5.11) was evaluated for the last node, j = J, it became

$$-\left[\frac{K_{J-\frac{1}{2}}^n}{\Delta z^2}\right]\psi_{J-1}^{n+1} + \left[\frac{C_J^n}{\Delta t} + \frac{(K_{J-\frac{1}{2}}^n + K_{J+\frac{1}{2}}^n)}{\Delta z^2}\right]\psi_J^{n+1} - \left[\frac{K_{J+\frac{1}{2}}^n}{\Delta z^2}\right]\psi_{J+1}^{n+1}$$

$$= \frac{C_J^n\psi_J^n}{\Delta t} + \frac{(K_{J-\frac{1}{2}}^n - K_{J+\frac{1}{2}}^n)}{\Delta z} - S_J^n \tag{5.27}$$

Because J+1 was the exterior node at the lower boundary which was held at a constant pressure head, ψ_{bottom}, $\psi_{J+1}^{n+1} = \psi_{J+1}^n = \psi_{bottom}$. Therefore, the term containing ψ_{J+1}^{n+1} in equation (5.27) was known and could be moved to the right hand side of the equation, which when simplified, became

$$A_J \psi_{J-1}^{n+1} + D_J \psi_J^{n+1} = R_J \tag{5.28}$$

where

$$A_J = - \frac{K_{J-\frac{1}{2}}^n}{\Delta z^2} \tag{5.29}$$

$$D_J = \frac{C_J^n}{\Delta t} - A_J + \frac{K_{J+\frac{1}{2}}^n}{\Delta z^2} \tag{5.30}$$

$$R_J = \frac{C_J^n \psi_J^n}{\Delta t} + \frac{(K_{J-\frac{1}{2}}^n - K_{J+\frac{1}{2}}^n)}{\Delta z} + \frac{K_{J+\frac{1}{2}}^n}{\Delta z^2} \psi_{bottom} - S_J^n \tag{5.31}$$

The flux across the lower boundary, q_{bottom}, (q_b) was calculated by evaluating equation (5.18) at the lower boundary (j=J+½). Physically, q_b represented the rate at which water moved from the water table into the soil profile or drained to the sump.

An equation for a flux boundary condition at the lower boundary was also developed to allow the model to be compared to solutions developed by other researchers. The equation was derived by following the same steps used to develop equation (5.22).

Solution

The system of equations which were formed by applying equations (5.28), (5.12), and (5.23) to the appropriate nodes produced a tridiagonal matrix equation which was implicit in terms of pressure head, ψ.

$$\begin{vmatrix} D_1 & B_1 & & & & & & \\ A_2 & D_2 & B_2 & & & & & \\ & \cdot & \cdot & \cdot & & & & \\ & & \cdot & \cdot & \cdot & & & \\ & & & \cdot & \cdot & \cdot & & \\ & & & & A_{J-1} & D_{J-1} & B_{J-1} & \\ & & & & & A_J & D_J & \end{vmatrix} \begin{vmatrix} \psi_1 \\ \psi_2 \\ \cdot \\ \cdot \\ \cdot \\ \psi_{J-1} \\ \psi_J \end{vmatrix} = \begin{vmatrix} R_1 \\ R_2 \\ \cdot \\ \cdot \\ \cdot \\ R_{J-1} \\ R_J \end{vmatrix} \tag{5.32}$$

The tridiagonal matrix was readily solved by a Gaussian elimination method. In this work, a very concise algorithm utilizing recursion formulas for the solution of the tridiagonal system which was presented by Carnahan et al. (1969), was used.

A computer program used the finite difference equations and solved the tridiagonal matrix to simulate infiltration, redistribution, extraction, and upward flow from a water table. The program was written in Microsoft FORTRAN and designed to run on microcomputers.

Time Step

Implicit numerical techniques generally permit the use of much larger time steps than explicit techniques while maintaining stability. A suitable time step may be determined by trial and error and kept constant throughout the simulation. A much more efficient approach, however, is to have a variable time step which decreases in size during periods of increased soil water movement (infiltration) and increases during periods of relative inactivity (redistribution). Zaradny (1978) proposed that the time step be estimated by

$$\Delta t < \frac{\zeta \, \Delta z}{|q_{max}|} \tag{5.33}$$

where

Δt = the variable time step (hrs),

Δz = grid spacing in space (mm),

$|q_{max}|$ = the maximum net flux into any grid (mm/hr), and

ζ = the maximum permissible change in water content, θ, for any grid in the soil profile where $0.015 < \zeta < 0.035$.

Feddes et al. (1978) used the lower value of ζ to accommodate the rapid movement of water during infiltration and early stages of redistribution. Higher values of ζ were used during slow changes in boundary conditions such as continuous upward flow of water or during the

later stages of redistribution. Clark (1982) and Stone (1987) also used this method to compute time steps.

Updating of Soil Parameters

The soil parameters θ, C, and K corresponding to the new values of ψ at the end of every time step were determined from equations (2.6), (2.8), and (2.9), respectively, for the three soils used in the lysimeters (builder's sand, Astatula f.s., and Pomona sand). Because the observed soil-moisture retention curves and those predicted by equation (2.6) were well matched (Figure 3.11), this approach was much more efficient and about as accurate as a table lookup procedure.

The tabulated parameters of five other soils presented by Clark (1982) were included in the model to give it more flexibility. A tabulated data search was used to determine the corresponding values of K, C, and θ for these soils. Because the search had to be conducted for each grid at the end of every time step, the logarithmic interpolation method used by Clark (1982) was employed to reduce computer time. The table was set up with linearly increasing multiples of the logarithmic value of ψ. Since the tabulated soil parameters were discrete values, errors arose from the interpolation procedure. The errors however, proved to be less than 1% and were neglected. The tabulated parameters of the five soils, (Arredondo f.s., Rehevot sand, Adelanto loam, Pachappa loam, and Yolo light clay), are presented in Appendix C.

Mass Balance

A mass balance was computed at the end of every time step and used to check the stability of the simulation model. The water stored in each grid was integrated throughout the profile and compared to the cumulative inflows and outflows. Inflows consisted of surface infiltrations and upward flow from the water table. Outflows included drainage, root extractions, and evaporation from the soil surface which was a component of the surface grids' root extraction term. The mass balance error was calculated as the difference between the water stored in the profile at any time and the sum of inflows and outflows.

One-Dimensional Model Verification

The accuracy of the one-dimensional model was determined by comparing it to experimental data and analytical and numerical solutions found in the literature. The comparisons were selected to test every aspect of the model with soils that had widely varying hydraulic properties.

Analytical solutions of the Richards equation generally deal with steady-state situations or simplified boundary conditions or geometries, but are useful because they provide a true solution against which numerical simulations can be compared. Gardner (1958) developed several analytical solutions based on the matric flux potential concept (Philip, 1959) to describe steady-state evaporation from a water table in soils whose hydraulic conductivity function could be described by

$$K(\psi) = \frac{a}{(\psi^n + b)} \tag{5.34}$$

where a, n, and b are constants.

Gardner and Fireman (1958) used one of these analytical solutions to calculate steady-state evaporation from a Yolo light clay with a water table 1050 mm from the soil surface. To obtain the solution, they empirically fitted equation (5.34) to the Yolo light clay hydraulic conductivity data that Moore (1939) presented in his landmark paper. From the resulting curve they determined that $a = 400\ cm^3/day$, $b = 400\ cm^2$, and $n = 2$ and used these constants in the analytical solution that they presented. They simulated steady-state evaporation at the rate of 0.033 mm/hr (0.08 cm/day) and compared their results to the data given by Moore (1939) for steady-state evaporation from a column of Yolo light clay with a water table at a depth of 1050 mm.

The one-dimensional model developed in this study was used to simulate steady-state evaporation for the same conditions. For this validation, the evaporation rate was simulated as a negative surface flux and $K(\psi)$ was computed from equation (5.34). The other soil

parameters were updated with the tabulated data search. The numerical solution was in excellent agreement with the analytical solution and the experimental data as shown in Figure 5.2.

Simulated infiltration into an initially very dry soil profile was compared to a study by Rubin and Steinhardt (1963). They developed a model to study constant intensity rainfall infiltration into Rehevot sand by implicitly solving the θ-form of the Richards equation. They presented results for rainfall intensities of 12.7 and 47 mm/hr on a semi-infinite soil profile with a uniform initial soil-moisture content of 0.005.

The one-dimensional model developed in this work was used to simulate infiltration and redistribution for identical initial and boundary conditions. Soil parameters were updated with the tabulated data search using the Rehevot sand soil hydraulic characteristics table (Appendix C). Results were in excellent agreement with Rubin and Steinhardt (1963) and are presented in Figures 5.3 and 5.4 in terms of soil water content profiles.

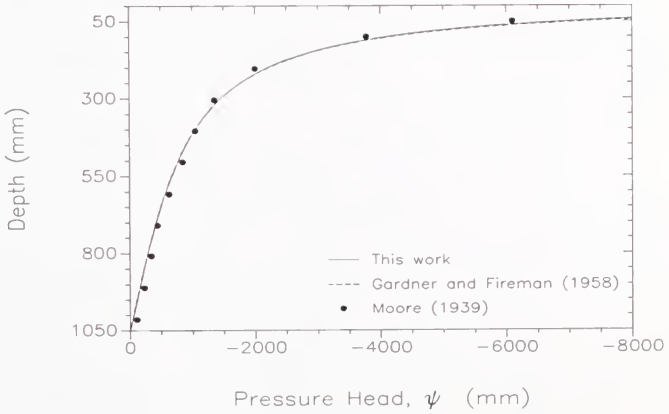

Figure 5.2. Simulated, analytical, and experimental results of steady-state evaporation at a rate of 0.033 mm/hr from a water table in Yolo light clay.

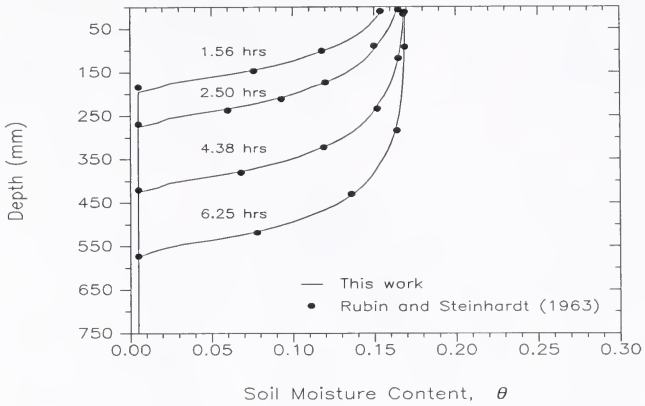

Figure 5.3. Simulated results of soil water content profiles for infiltration into Rehevot sand under constant rain intensity of 12.7 mm/hr.

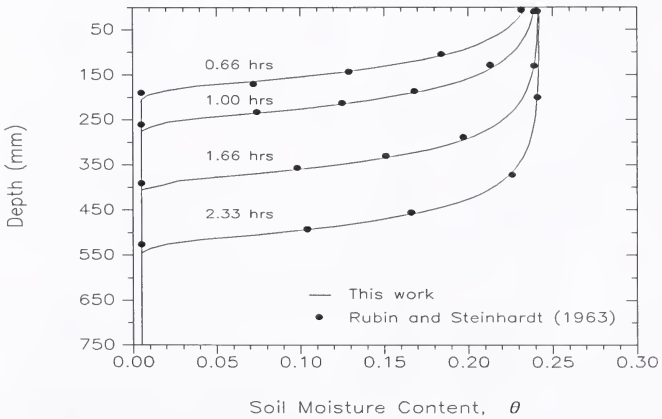

Figure 5.4. Simulated results of soil water content profiles for infiltration into Rehevot sand under constant rain intensity of 47 mm/hr.

Warrick (1974) also solved the one-dimensional, steady-state moisture flow equation using the matric flux potential to obtain a linearized form. He presented solutions for a semi-infinite flow medium and a finite-depth medium overlying a shallow water table with a flux surface boundary condition and arbitrary plant water withdrawal functions. He assumed unsaturated hydraulic conductivity, $K(\psi)$, to be of the form

$$K(\psi) = K_s e^{(\alpha\psi)} \tag{5.35}$$

where K_s is the saturated hydraulic conductivity and α is an empirical constant depending on soil texture.

Warrick (1974) used an arbitrary soil with K_s = 4.17 mm/hr and α = 0.001 mm^{-1} to present numerical examples of his analytical solutions. One set of numerical results was developed for a soil profile with a water table 1000 mm from the soil surface. The arbitrary extraction function was set to 0 and surface fluxes of 0.0 mm/hr and 1.5 mm/hr were used.

Equation (5.35) and a linear soil-moisture release function were incorporated into the one-dimensional model to allow comparison with Warrick's solutions. Steady-state pressure head were simulated for identical boundary conditions and they were in excellent agreement with the analytical solutions. Both solutions and are shown in Figure 5.5.

In order to evaluate the performance of extraction in the model, the simplest water extraction function given by Warrick (1974) was chosen and coded into the model. This was a constant sink term give by

$$S(z) = a \tag{5.36}$$

where a is the constant extraction rate per unit length. The total soil profile water extraction rate used by Warrick (1974) was 0.42 mm/hr (S=aL where L is the depth to the water table).

The numerical simulations were run to steady-state using the same conductivity function and initial and bottom boundary conditions as before but with infiltration rates of 0.42 and 0.63 mm/hr. The results were in excellent agreement with the analytical solution and are shown in Figure 5.6.

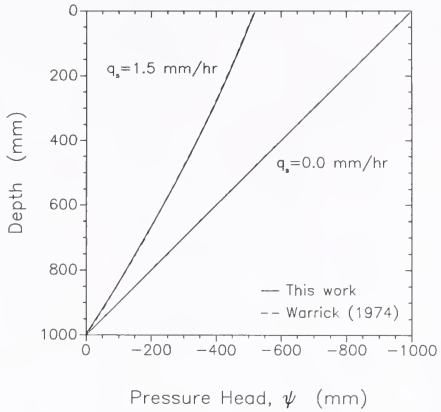

Figure 5.5. Simulated and analytical results of steady-state infiltration above a shallow water table at rates of 0.0 and 1.5 mm/hr.

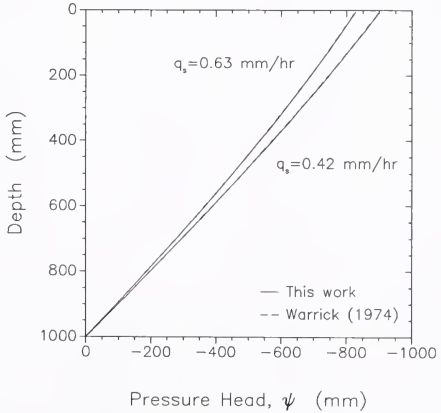

Figure 5.6. Simulated and analytical results of steady-state infiltration above a shallow water table with a constant extraction rate of 0.42 mm/hr.

Two-Dimensional Model Development

The process of infiltration, redistribution, and extraction under line sources or closely spaced emitters can be treated as a two-dimensional problem. The governing equation for two-dimensional flow in a porous medium is

$$C(\psi)\frac{\partial \psi}{\partial t} = \frac{\partial}{\partial x}\left[K(\psi)\frac{\partial(\psi)}{\partial x}\right] + \frac{\partial}{\partial z}\left[K(\psi)\left(\frac{\partial(\psi)}{\partial z} - 1\right)\right] - S(\psi) \tag{5.37}$$

where x represents the horizontal dimension along the x-axis and z represents the vertical dimension along the z-axis.

As shown in Figure 5.7, the line source lies on the soil surface along the y-axis and intercepts the x-z plane at the origin. The trickle discharge per unit length of the line source is given by Q(t) in $mm^3/(mm\text{-}hr)$.

Equation (5.37) was solved numerically with a Gaussian elimination implicit finite difference scheme and explicit linearization of soil parameters. The flow domain was divided into a mesh of rectangular cells having dimensions Δx, Δz, and unity in the y direction. The index i (i=1, 2, ..., I) was used to locate the cells in the x-direction with respect to the line source, and j (j=1, 2, ..., J) was used to number the cells in the vertical direction (Figure 5.7).

Horizontal flow in equation (5.37) is described by

$$\frac{\partial}{\partial x}\left[K(\psi)\left(\frac{\partial(\psi)}{\partial x}\right)\right] = \frac{\partial W}{\partial x} \tag{5.38}$$

The finite difference approximation of this equation was obtained by discretizing the right hand side of equation (5.38) around i to obtain

$$\left[\frac{\partial W}{\partial x}\right]_{i,j} = \frac{W_{i+\frac{1}{2},j} - W_{i-\frac{1}{2},j}}{\Delta x} \tag{5.39}$$

Equation (5.39) was then substituted into equation (5.38) to give

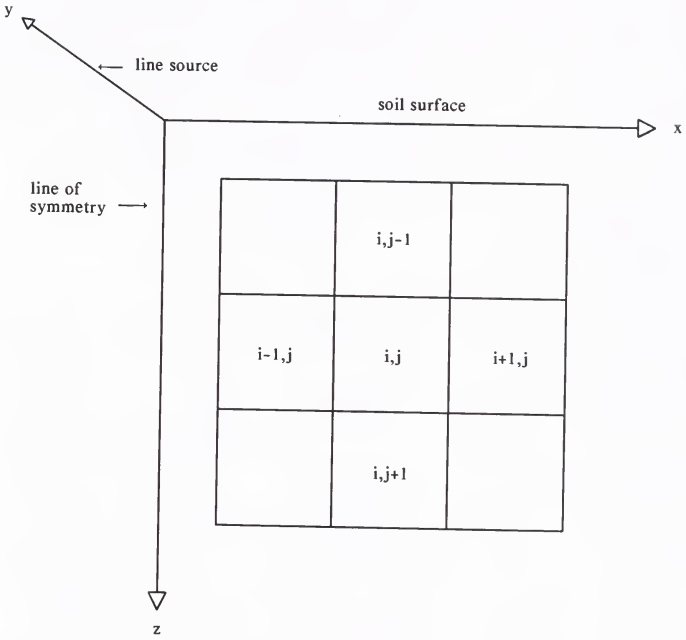

Figure 5.7. Schematic diagram of the finite-difference grid system for the two-dimensional model of water movement and extraction.

$$\frac{1}{\Delta x}\left\{\left[K_{i+\frac{1}{2},j}\left(\frac{\partial \psi}{\partial x}\right)_{i+\frac{1}{2},j}\right] - \left[K_{i-\frac{1}{2},j}\left(\frac{\partial \psi}{\partial x}\right)_{i-\frac{1}{2},j}\right]\right\} \tag{5.40}$$

The derivatives of ψ with respect to x were approximated as

$$\left(\frac{\partial \psi}{\partial x}\right)_{i+\frac{1}{2},j} = \frac{\psi_{i+1,j} - \psi_{i,j}}{\Delta x} \tag{5.41}$$

$$\left(\frac{\partial \psi}{\partial x}\right)_{i-\frac{1}{2},j} = \frac{\psi_{i,j} - \psi_{i-1,j}}{\Delta x} \tag{5.42}$$

which when substituted back into equation (5.40) gave

$$\frac{1}{\Delta x}\left\{\left[K_{i+\frac{1}{2},j}\left(\frac{\psi_{i+1,j} - \psi_{i,j}}{\Delta x}\right)\right] - \left[K_{i-\frac{1}{2},j}\left(\frac{\psi_{i,j} - \psi_{i-1,j}}{\Delta x}\right)\right]\right\} \tag{5.43}$$

Equation (5.43) represents the finite difference approximation of horizontal flow through a porous medium. This equation was combined with the finite difference approximation of vertical flow previously derived for the one dimensional model (equation (5.7)) to produce the two-dimensional finite difference equation for flow through a porous medium.

$$\begin{aligned} C^n_{i,j}\frac{\psi^{n+1}_{i,j} - \psi^n_{i,j}}{\Delta t} = {} & \frac{1}{\Delta x}\left\{\left[K^n_{i+\frac{1}{2},j}\left(\frac{\psi^{n+1}_{i+1,j} - \psi^{n+1}_{i,j}}{\Delta x}\right)\right]\right. \\ & \left. - \left[K^n_{i-\frac{1}{2},j}\left(\frac{\psi^{n+1}_{i,j} - \psi^{n+1}_{i-1,j}}{\Delta x}\right)\right]\right\} \\ & + \frac{1}{\Delta z}\left\{\left[K^n_{i,j+\frac{1}{2}}\left(\frac{\psi^{n+1}_{i,j+1} - \psi^{n+1}_{i,j}}{\Delta z} - 1\right)\right]\right. \\ & \left. - \left[K^n_{i,j-\frac{1}{2}}\left(\frac{\psi^{n+1}_{i,j} - \psi^{n+1}_{i,j-1}}{\Delta z} - 1\right)\right]\right\} - S^n_{i,j} \end{aligned} \tag{5.44}$$

The equation was then rearranged so that the unknowns were on the left hand side and the knowns were on the right hand side.

$$
\begin{aligned}
&- \left[\frac{K^n_{i-\frac{1}{2},j}}{\Delta x^2}\right]\psi^{n+1}_{i-1,j} \; - \left[\frac{K^n_{i,j-\frac{1}{2}}}{\Delta z^2}\right]\psi^{n+1}_{i,j-1} \\
&+ \left[\frac{C^n_{i,j}}{\Delta t} + \frac{K^n_{i+\frac{1}{2},j} + K^n_{i-\frac{1}{2},j}}{\Delta x^2} \; + \frac{K^n_{i,j+\frac{1}{2}} + K^n_{i,j-\frac{1}{2}}}{\Delta z^2}\right]\psi^{n+1}_{i,j} \\
&- \left[\frac{K^n_{i+\frac{1}{2},j}}{\Delta x^2}\right]\psi^{n+1}_{i+1,j} \; - \left[\frac{K^n_{i,j+\frac{1}{2}}}{\Delta z^2}\right]\psi^{n+1}_{i,j+1} \\
&= \frac{C^n_{i,j}}{\Delta t}\psi^n_{i,j} \; + \frac{K^n_{i,j-\frac{1}{2}} - K^n_{i,j+\frac{1}{2}}}{\Delta z} \; - S^n_{i,j}
\end{aligned}
\tag{5.45}
$$

or in a more usable form

$$
A_{i,j}\psi^{n+1}_{i,j-1} + B_{i,j}\psi^{n+1}_{i-1,j} + D_{i,j}\psi^{n+1}_{i,j} + E_{i,j}\psi^{n+1}_{i+1,j} + F_{i,j}\psi^{n+1}_{i,j+1} = R_{i,j} \tag{5.46}
$$

where

$$
A_{i,j} = - \frac{K^n_{i,j-\frac{1}{2}}}{\Delta z^2} \tag{5.47}
$$

$$
B_{i,j} = - \frac{K^n_{i-\frac{1}{2},j}}{\Delta x^2} \tag{5.48}
$$

$$
D_{i,j} = \frac{C^n_{i,j}}{\Delta t} - A_{i,j} - B_{i,j} - E_{i,j} - F_{i,j} \tag{5.49}
$$

$$
E_{i,j} = - \frac{K^n_{i+\frac{1}{2},j}}{\Delta x^2} \tag{5.50}
$$

$$F_{i,j} = -\frac{K^n_{i,j+\frac{1}{2}}}{\Delta z^2} \tag{5.51}$$

$$R_{i,j} = \frac{C^n_{i,j}}{\Delta t}\psi^n_{i,j} + \frac{K^n_{i,j-\frac{1}{2}} - K^n_{i,j+\frac{1}{2}}}{\Delta z} - S^n_{i,j} \tag{5.52}$$

Equation (5.46) was written for each of the interior nodes $2 \leq i \leq I-1$ and $2 \leq j \leq J-1$ in the soil profile. The grids bordering the boundaries required equation (5.46) to be modified so that it would describe the boundary conditions.

Boundary Conditions

The two-dimensional solution dictated that four separate boundary conditions be specified. In addition, the four cells at the corners of the flow domain were affected by a vertical and a horizontal boundary condition and had to be treated accordingly.

Top boundary. A flux boundary condition was employed for the surface grids. The surface flux, $q_{i,s}$, was equal to 0 at all times except during irrigation. During irrigation, the surface grids closest to the line source were assigned a flux proportional to the application rate. The number of grids through which infiltration occurred depended on the grid size and the soil type.

To describe the surface boundary condition for the nodes $2 \leq i \leq I-1$ at $j=1$, equation (5.46) was modified to

$$B_{i,1}\psi^{n+1}_{i-1,1} + D_{i,1}\psi^{n+1}_{i,1} + E_{i,1}\psi^{n+1}_{i+1,1} + F_{i,1}\psi^{n+1}_{i,2} = R_{i,1} \tag{5.53}$$

where

$$D_{i,1} = \frac{C^n_{i,1}}{\Delta t} - B_{i,1} - E_{i,1} - F_{i,1} \tag{5.54}$$

$$R_{i,1} = \frac{C^n_{i,1}}{\Delta t}\psi^n_{i,1} + \frac{q_{i,s} - K^n_{i,3/2}}{\Delta z} - S^n_{i,1} \tag{5.55}$$

and $B_{i,1}$, $E_{i,1}$, and $F_{i,1}$ are as previously defined.

Bottom boundary. A constant potential boundary condition was again used to model the water table. The modification of equation (5.46) to describe the lower boundary for the nodes $2 \leq i \leq I\text{-}1$ at j=J, was

$$A_{i,J}\psi_{i,J-1}^{n+1} + B_{i,J}\psi_{i-1,J}^{n+1} + D_{i,J}\psi_{i,J}^{n+1} + E_{i,J}\psi_{i+1,J}^{n+1} = R_{i,J} \tag{5.56}$$

where

$$D_{i,J} = \frac{C_{i,J}^{n}}{\Delta t} - A_{i,J} - B_{i,J} - E_{i,J} + \frac{K_{i,J+\frac{1}{2}}^{n}}{\Delta z^2} \tag{5.57}$$

$$R_{i,J} = \frac{C_{i,J}^{n}}{\Delta t}\psi_{i,J}^{n} + \frac{K_{i,J-\frac{1}{2}}^{n} - K_{i,J+\frac{1}{2}}^{n}}{\Delta z} + \frac{K_{i,J+\frac{1}{2}}^{n}}{\Delta z^2}\psi_{bottom} - S_{i,J}^{n} \tag{5.58}$$

and $A_{i,J}$, $B_{i,J}$, and $E_{i,J}$ are as previously defined. An equation for a flux bottom boundary condition was also developed to give the model greater versatility.

Left boundary. The left boundary of the model was defined as the plane of symmetry that passed through the center of the bed. Because by definition there is no flow across a line of symmetry, this boundary was simulated with a no flux boundary condition ($q_{L,j}$=0).

Flux across a boundary in the horizontal direction is described by the partial differential equation

$$q = -K(\psi)\left[\frac{\partial\psi}{\partial x}\right] \tag{5.59}$$

When equation (5.59) was discretized around i it became

$$q_{L,j} = -K_{i,j}\left[\frac{\psi_{i+\frac{1}{2},j} - \psi_{i-\frac{1}{2},j}}{\Delta x}\right] \tag{5.60}$$

which when evaluated at $i = \frac{1}{2}$, the axis of symmetry and the left boundary , gave

$$q_{\frac{1}{2},j} = -K_{\frac{1}{2},j}\left[\frac{\psi_{1,j} - \psi_{0,j}}{\Delta z}\right] = q_{L,j} \tag{5.61}$$

When equation (5.44) was evaluated at the nodes $2 \leq j \leq J-1$ at the first column of nodes, $i=1$, it became

$$C^n_{1,j}\frac{\psi^{n+1}_{1,j} - \psi^n_{1,j}}{\Delta t} = \frac{1}{\Delta x}\left\{\left[K^n_{3/2,j}\left(\frac{\psi^{n+1}_{2,j} - \psi^{n+1}_{1,j}}{\Delta x}\right)\right] - \left[K^n_{1/2,j}\left(\frac{\psi^{n+1}_{1,j} - \psi^{n+1}_{0,j}}{\Delta x}\right)\right]\right\} + \frac{1}{\Delta z}\left\{\left[K^n_{1,j+\frac{1}{2}}\left(\frac{\psi^{n+1}_{1,j+1} - \psi^{n+1}_{1,j}}{\Delta z} - 1\right)\right] - \left[K^n_{1,j-\frac{1}{2}}\left(\frac{\psi^{n+1}_{1,j} - \psi^{n+1}_{1,j-1}}{\Delta z} - 1\right)\right]\right\} - S^n_{1,j} \tag{5.62}$$

The $K^n_{1/2,j}$ term is equal to $q_{L,j}$ with which it can be replaced to give

$$C^n_{1,j}\frac{\psi^{n+1}_{1,j} - \psi^n_{1,j}}{\Delta t} = \frac{1}{\Delta x}\left\{\left[K^n_{3/2,j}\left(\frac{\psi^{n+1}_{2,j} - \psi^{n+1}_{1,j}}{\Delta x}\right)\right] + q_{L,j}\right\} + \frac{1}{\Delta z}\left\{\left[K^n_{1,j+\frac{1}{2}}\left(\frac{\psi^{n+1}_{1,j+1} - \psi^{n+1}_{1,j}}{\Delta z} - 1\right)\right] - \left[K^n_{1,j-\frac{1}{2}}\left(\frac{\psi^{n+1}_{1,j} - \psi^{n+1}_{1,j-1}}{\Delta z} - 1\right)\right]\right\} - S^n_{1,j} \tag{5.63}$$

When equation (5.63) was rearranged so that unknowns were on the left and knowns on the right it became

$$-\left[\frac{K^n_{1,j-\frac{1}{2}}}{\Delta z^2}\right]\psi^{n+1}_{1,j-1} + \left[\frac{C^n_{1,j}}{\Delta t} + \frac{K^n_{3/2,j}}{\Delta x^2} + \frac{K^n_{1,j+\frac{1}{2}} + K^n_{1,j-\frac{1}{2}}}{\Delta z^2}\right]\psi^{n+1}_{1,j}$$

$$- \left[\frac{K^n_{3/2,j}}{\Delta x^2}\right]\psi^{n+1}_{2,j} - \left[\frac{K^n_{1,j+\frac{1}{2}}}{\Delta z^2}\right]\psi^{n+1}_{1,j+1}$$

$$= \frac{C^n_{1,j}}{\Delta t}\psi^n_{1,j} + \frac{q_{L,j}}{\Delta x} + \frac{K^n_{1,j-\frac{1}{2}} - K^n_{1,j+\frac{1}{2}}}{\Delta z} - S^n_{1,j} \tag{5.64}$$

or in a more usable form

$$A_{1,j}\psi^{n+1}_{1,j-1} + D_{1,j}\psi^{n+1}_{1,j} + E_{1,j}\psi^{n+1}_{2,j} + F_{1,j}\psi^{n+1}_{1,j+1} = R_{1,j} \tag{5.65}$$

where

$$A_{1,j} = -\frac{K^n_{1,j-\frac{1}{2}}}{\Delta z^2} \tag{5.66}$$

$$D_{1,j} = \frac{C^n_{1,j}}{\Delta t} - A_{1,j} - B_{1,j} - F_{1,j} \tag{5.67}$$

$$E_{1,j} = -\frac{K^n_{3/2,j}}{\Delta x^2} \tag{5.68}$$

$$F_{1,j} = -\frac{K^n_{1,j+\frac{1}{2}}}{\Delta z^2} \tag{5.69}$$

$$R_{1,j} = \frac{C^n_{1,j}}{\Delta t}\psi^n_{1,j} + \frac{q_{L,j}}{\Delta x} + \frac{K^n_{1,j-\frac{1}{2}} - K^n_{1,j+\frac{1}{2}}}{\Delta z} - S^n_{1,j} \tag{5.70}$$

Right boundary. The right boundary represented the wall of the lysimeter and was also simulated as a no flux boundary ($q_{R,j}$=0). The finite difference equation was derived by evaluating equation (5.60) at i=I+½ and following the steps described in the previous section. The equation for the column of nodes at i=I and $2 \leq j \leq$ J-1 was then

$$A_{I,j}\psi^{n+1}_{I,j-1} + B_{I,j}\psi^{n+1}_{I-1,j} + D_{I,j}\psi^{n+1}_{I,j} + F_{I,j}\psi^{n+1}_{I,j+1} = R_{I,j} \tag{5.71}$$

where

$$D_{I,j} = \frac{C^n_{I,j}}{\Delta t} - A_{I,j} - B_{I,j} - F_{I,j} \tag{5.72}$$

$$R_{I,j} = \frac{C^n_{I,j}}{\Delta t}\psi^n_{I,j} - \frac{q_{R,j}}{\Delta x} + \frac{K^n_{I,j-\frac{1}{2}} - K^n_{I,j+\frac{1}{2}}}{\Delta z} - S^n_{I,j} \tag{5.73}$$

and $A_{I,j}$, $B_{I,j}$, and $F_{I,j}$ are as previously defined.

Corner cells. Because the four cells found in each of the corners of the two-dimensional mesh were influenced by two boundaries, special equations had to be written for them. They were derived by evaluating equation (5.44) at the appropriate four nodes (1,1), (I,1), (1,J), and (I,J).

Solution

Updating of the soil parameters, surface infiltration, mass balance, and time steps were implemented as described for the one-dimensional model. The system of equations for the two-dimensional model produced a banded matrix equation with 5 nonzero diagonals of the form shown in equation (5.74).

$$\begin{vmatrix}
D_{1,1} & E_{1,1} & & F_{1,1} & & & & & & \\
B_{2,1} & D_{2,1} & E_{2,1} & & F_{2,1} & & & & & \\
 & B_{3,1} & D_{3,1} & 0 & & F_{3,1} & & & & \\
A_{1,2} & & 0 & D_{1,2} & E_{1,2} & & F_{1,2} & & & \\
 & A_{2,2} & & B_{2,2} & D_{2,2} & E_{2,2} & & F_{2,2} & & \\
 & & A_{3,2} & & B_{3,2} & D_{3,2} & 0 & & F_{3,2} & \\
 & & & A_{1,3} & & 0 & D_{1,3} & E_{1,3} & & \\
 & & & & A_{2,3} & & B_{2,3} & D_{2,3} & E_{2,3} & \\
 & & & & & A_{3,3} & & B_{3,3} & D_{3,3}
\end{vmatrix}
\begin{vmatrix} \psi_{1,1} \\ \psi_{2,1} \\ \psi_{3,1} \\ \psi_{1,2} \\ \psi_{2,2} \\ \psi_{3,2} \\ \psi_{1,3} \\ \psi_{2,3} \\ \psi_{3,3} \end{vmatrix}
= \begin{vmatrix} R_{1,1} \\ R_{2,1} \\ R_{3,1} \\ R_{1,2} \\ R_{2,2} \\ R_{3,2} \\ R_{1,3} \\ R_{2,3} \\ R_{3,3} \end{vmatrix} \tag{5.74}$$

Equation (5.74) is an example of the matrix equation for a 3 x 3 mesh. The number of diagonals (NBAND) enclosed by the A and F terms, including the empty diagonals, varies with respect to the number of cells in the x-direction and is given by

$$NBAND = 2I + 1 \tag{5.75}$$

which for the above example would be 7.

Thurnau (1963) developed the algorithm BANDSOLVE to solve a large, sparse matrix with a narrow band centered on the main diagonal. The algorithm operates only on the banded part of the matrix (NBAND diagonals) and does not require computer storage for the elements above or below the band. An appropriate choice of the grid numbering system can reduce the total width of the band. Reddell and Sunada (1970) and Stone (1987) used BANDSOLVE to solve two-dimensional water flow models. The BANDSOLVE algorithm was incorporated into a subroutine and used to solve the system of equations in this work as well. This subroutine is given in Appendix B as part of the two-dimensional program.

Water Extraction by Plant Roots

A macroscopic extraction function modeled after the one used by Smajstrla (1982) was used. The function was modified to include a root distribution term that permitted root water uptake from each grid to be estimated. It was further modified to calculate the soil water extraction rate as a function of the actual evapotranspiration rate as suggested by Stone (1987). The extraction function was

$$S_{i,j} = \frac{ET_r \, A_{total} \, RDT_{i,j}}{A_{i,j}} \, R_{i,j}^{(ET_r/R_{i,j}C)} \tag{5.76}$$

where

$S_{i,j}$ = the soil water extraction rate (mm/hr),

ET_r = the predetermined evapotranspiration rate (mm/hr),

$RDT_{i,j}$ = the root distribution term or the percentage of water extraction for the soil cell when water was not limiting,

A_{total} = total surface area of the lysimeter (mm^2),

$A_{i,j}$ = surface area of the individual cell (mm^2), and

C = a calibration constant.

$R_{i,j}$ was defined as the relative available soil water content given mathematically by

$$R_{i,j} = \frac{\theta_{i,j} - \theta_{wp}}{\theta_{fc} - \theta_{wp}} \tag{5.77}$$

where

$\theta_{i,j}$ = soil water content,

θ_{wp} = soil water content at the wilting point, and

θ_{fc} = soil water content at field capacity.

The function permitted rapid soil water extraction when water was readily available and forced a logarithmic decrease in the extraction rate as the water was depleted. The function also limited extraction during periods of high potential evapotranspiration and allowed it to recover to near potential rates during periods of low potential evapotranspiration. The function prevented the wilting point from being reached in any grid by limiting extraction to very low rates as the wilting point was approached.

The extraction function was not used to estimate the evapotranspiration losses from the soil profile. Instead it was used to repartition those losses within the profile. The ET_r values required by the extraction function were predetermined and could be either the experimentally measured evapotranspiration, or values computed by multiplying potential evapotranspiration by a crop coefficient.

Figure 5.8 shows the shape of equation (5.76) for four different daily evapotranspiration rates (ET). The figure is in dimensionless form and plots relative available soil water content (R) versus the relative soil water extraction rate (S/ET) for C = 10. It illustrates how the extraction function repartitions ET with respect to available soil moisture in order to meet the daily evapotranspiration requirement.

Equation (5.76) was used to calculate a water extraction rate from each grid at every time step. The calculated extraction rates of the grids were summed and compared to the actual ET_r. If the calculated total water extraction rate was not equal to the actual ET_r, the extraction rate of each grid was linearly adjusted so that the calculated and actual ET_r were equal. Linear adjustment was performed by equation (5.78).

$$S_{i,j} = S_{i,j} \frac{ET_r}{\sum S_{i,j}} \tag{5.78}$$

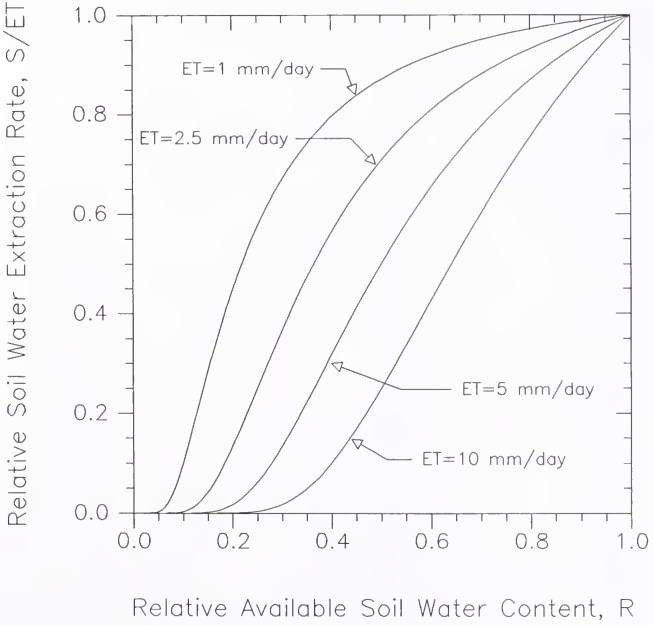

Figure 5.8. Effect of the relative available soil water and four ET rates on the predicted soil water exctraction rate.

The evapotranspiration rate, ET_r, in equation (5.76) was calculated by distributing the daily predetermined ET (mm/day) over a 24-hr period. A sinusoidal type distribution given by

$$ET_r = \frac{2\ ET}{t_{cycle}} \sin\left[\frac{2\pi\, t_{day}}{t_{cycle}} - \frac{\pi}{2}\right] + \frac{2\ ET}{t_{cycle}} \tag{5.79}$$

was selected where

ET_r = the predicted evapotranspiration rate (mm/hr)

ET = the predetermined daily evapotranspiration (mm/day)

t_{cycle} = the period of the cycle, (hr), in this case 24 hr, and

t_{day} = the current time on the 24-hr clock minus t_{start}, the beginning time of the cycle, (hr).

Figure 5.9 presents the shape of equation (5.79) for a hypothetical ET = 12 mm/day, t_{cycle} = 24 hr, and t_{start} = 3:00. The maximum ET_r occurs at $t_{cycle}/2$ or for this example at 15:00. This type of distribution most accurately simulated the ET rates observed in the lysimeters.

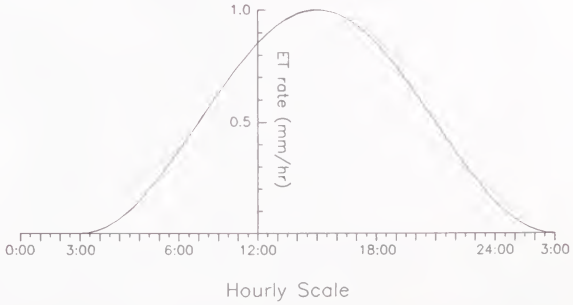

Figure 5.9. Simulated distribution of the daily ET over a 24-hr period.

Two-Dimensional Model Verification

Before the two-dimensional model was compared to solutions found in the literature, the model was tested to verify that it was fully functional. The first series of tests simulated equilibrium conditions in a soil profile with no flux boundaries and initially uniform pressure heads. Equilibrium conditions for such profiles depend on the profile depth and are easily predetermined. The profiles were simulated using both an analytical expression and the tabulated data search to update soil parameters. Because there were no fluxes into or out of the system, this permitted the mass balance errors resulting from roundoff (0.05%) and the table search procedure (0.45%) to be determined. The profiles were also simulated using constant and variable grid sizes. Both strategies produced excellent results but the variable grid sizes yielded considerable time savings.

The second series of tests were identical to the first with the exception that a constant potential surface was used to simulate a water table at the lower boundary. It was found that time steps on the order of 0.0001 hr were initially required to minimize the mass balance error if the pressure head difference between adjoining cells at the boundaries was greater than 1000 mm (as occurs with an initially very dry uniform soil profile above a water table). Once a more gradual gradient was established, the time step could be rapidly increased as prescribed by equation (5.33) without increasing mass balance errors. Overall, the mass balance errors were minimal (less than 1%) in these tests.

The accuracy of the two-dimensional model was determined by comparing it to analytical and numerical solutions found in the literature. The comparisons were selected to test the applicability and accuracy of the model with soils that had widely varying hydraulic properties.

The two-dimensional model was compared to the one-dimensional model of Rubin and Steinhardt (1963) discussed earlier. This was done by setting the surface boundary condition of the two-dimensional model to a uniform flux for each surface cell. The fluxes

represented rainfall intensities of 12.7 and 47 mm/hr on a Rehevot sand semi-infinite profile with a uniform initial soil water content of 0.005.

Nonuniform cell sizes, which varied from 10 mm to 100 mm at increasing distances from the origin, were used in both the x and z-directions to reduce execution time and test the stability of the numerical scheme. The model accurately predicted that water contents did not vary in the x-direction and the vertical water contents were in excellent agreement with those of Rubin and Steinhardt (1963). The results are shown in Figures 5.10 and 5.11.

Thomas et al. (1976) conducted an experimental study to model subsurface irrigation from line sources. Their experiment was conducted in a soil bin containing a clay loam soil with hydraulic conductivity exponentially related to pressure head as in equation (5.35), $K_s = 40.32$ mm/hr, and $\alpha = 0.01258$ mm^{-1}. The line sources, of strength $Q = 378$ mm^2/hr, were buried 150 mm below the surface and 1220 mm apart. A water table at 6.1 m below the surface was simulated by using ceramic candles to maintain a constant suction of 4880 mm at a depth of 1220 mm. The top of the soil bin was covered with plastic to prevent evaporation. Pressure heads were measured under steady-state conditions.

Thomas et al. (1976) also developed an analytical series solution for steady-state infiltration from parallel buried line sources with an underlying constant potential surface. They then compared their analytical solutions to the experimental data with some success.

Equation (5.35) and a linear soil-moisture release function were incorporated into the two-dimensional model developed in this study to allow comparison with the analytical solution. Steady-state infiltration from a buried line source was simulated for similar boundary conditions. No flow conditions were used to simulate the line of symmetry at the right boundary and zero evaporation at the soil surface. The left boundary was also simulated as a no flow boundary with the exception of the cell which contained the source. The source cell's left boundary was simulated with a constant flux proportional to the strength, Q. The source was centered at $(x,z) = (0,150)$ mm and the right boundary was located at $(610,z)$ mm, respectively. Constant potential grids were used to simulate a water table at a depth of 6.1 m.

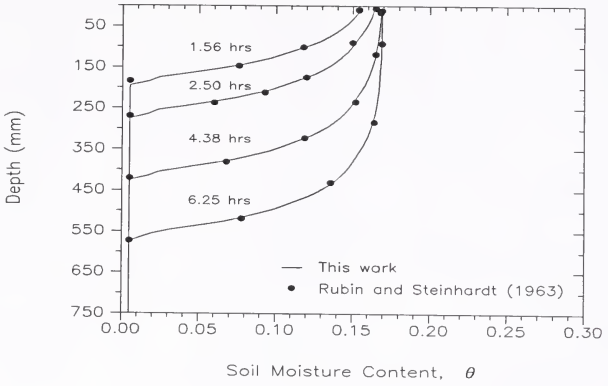

Figure 5.10. Two-dimensional model simulated results of soil water content profiles for infiltration into Rehevot sand under constant rain intensity of 12.7 mm/hr.

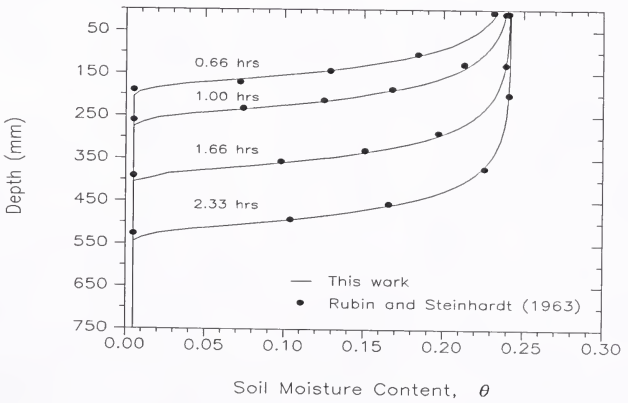

Figure 5.11. Two-dimensional model simulated results of soil water content profiles for infiltration into Rehevot sand under constant rain intensity of 47 mm/hr.

Figure 5.12 shows the analytical solutions and the simulation results as lines of constant pressure head. In general, they were in good agreement especially at the shallower depths. The divergence between the analytical and simulated curves that is observed at depths greater than 450 mm can be attributed to the effects of the lower boundary. The analytical solution does not contain a variable that specifies the depth of the underlying constant potential surface. Consequently, the analytical solution will be the same for any deep constant potential surface while the numerical simulation will not.

Warrick and Lomen (1977) developed an analytical solution for a buried line source above a shallow water table based on the steady-state linear moisture flow equation proposed by Raats (1972). Their solution was also a series type solution which, however, included the depth to the constant potential surface. They used the same clay loam soil as Thomas et al. (1976) to present a numerical example of a single buried line source of strength $Q = 378$ mm/hr at (0,150) mm above a water table at (x,300) mm.

The two-dimensional model was used to simulate infiltration and redistribution for the boundary conditions used by Warrick and Lomen (1977). The source was simulated as the flux across the left boundary of a single cell, while the water table was simulated as a constant potential surface with $\psi = 0$. Figure 5.13 compares lines of constant pressure head from this work and the analytical solution. Agreement between the two solutions was very good. The lines of constant $\psi = -100$ and $\psi = -200$ mm produced by the numerical model were slightly more elevated near the source because in the numerical model the source was approximated as a flux across a cell boundary of finite length. In contrast, the analytical solution treats the source as a point along the z-axis. Consequently, the saturated zone around the source was larger in the numerical solution and the constant pressure head lines were shifted upwards.

Ragab et al. (1984) used a simulation model based on the matrix flux potential concept to describe two-dimensional infiltration from a surface line source. They modeled a semi-infinite profile of experimental sand whose hydraulic conductivity-water content relationship was approximated by

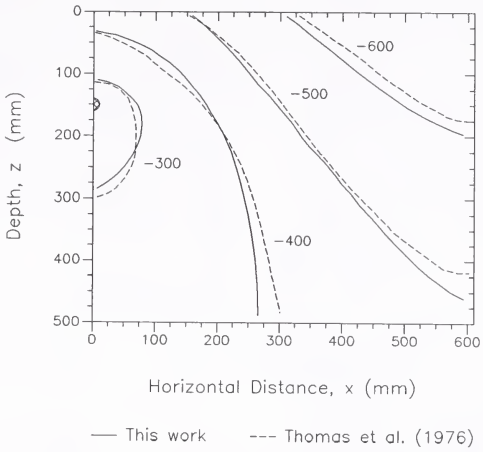

Figure 5.12. Lines of constant pressure head, ψ (mm), for parallel buried line sources 1220 mm apart.

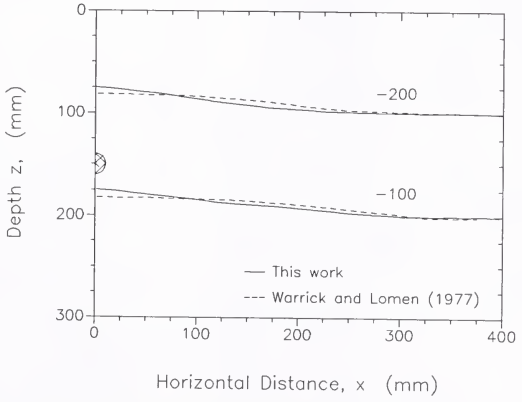

Figure 5.13. Lines of constant pressure head, ψ (mm), for a buried line source with a water table 300 mm below the soil surface.

$$K(\theta) = 22.51\,\theta^{3.49} \tag{5.80}$$

They presented results for 0.40 hr of infiltration from a source of strength $Q = 11442$ mm^2/hr on a profile with an initial soil moisture content of 0.01.

Because Ragab et al. (1984) did not give an analytical expression for the soil moisture retention curve that they presented, it was necessary to fit an empirical function to the curve. The empirical function and equation (5.80) were incorporated into this work's two-dimensional model which was then used to simulate infiltration and redistribution under identical initial and boundary conditions. Results were in good agreement with those presented by Ragab et al. (1984) and are shown in Figures 5.14 and 5.15.

Figure 5.14 shows the vertical water content distribution under the line source after 0.40 hr of infiltration. Figure 5.15 presents the horizontal water content distribution at a depth of 210 mm after the same time period. Differences between the two solutions were small and were attributed to errors arising from the translation of pressure head to water content with the empirically fitted function.

Simulation of the Lysimeter Study

To check the ability of the two-dimensional model to predict changes in soil water status under field conditions, the model was used to simulate infiltration, redistribution, and extraction for the conditions encountered in the lysimeters. Because the geometry of the problem was unique, a special finite difference mesh was developed (Figure 5.16). Cell sizes varied from 20 mm to 100 mm at increasing distances from the origin in both the x and z-directions. The smallest grids were concentrated near the source (top left corner) where the most rapid changes in water content took place. Small grid sizes were also used immediately above the water table. The largest grids were used in those sections of the soil profile where changes in water content were very small.

Constant potential grids were used to simulate the water table at a depth of 720 mm by assigning a constant pressure head value to the nodes of the last row of cells in

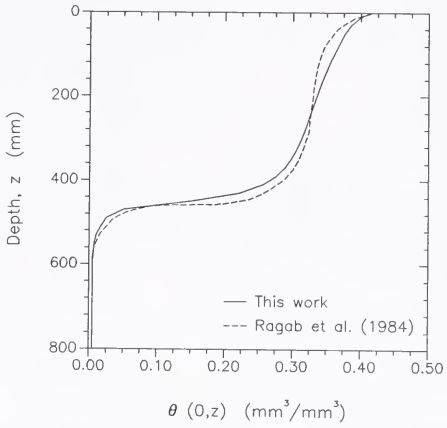

Figure 5.14. The vertical water content distribution at (0,z) for a line source discharge of 11442 mm^2/hr after 0.40 hrs.

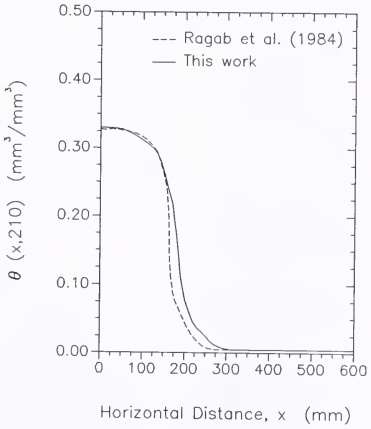

Figure 5.15. The horizontal water content distribution at (x,210) for a line source discharge of 11442 mm^2/hr after 0.40 hrs.

Figure 5.16. These nodes were located at j = J+1 in the finite difference mesh and the cell size in the vertical direction was Δz = 30 mm. Hence, ψ_{bottom} = 15 mm.

The trapezoidal bed shape meant that in a rectangular mesh, the upper right hand portion (represented by the cells with the dotted lines in Figure 5.16) corresponded to the atmosphere above the furrow. To isolate the "atmosphere" cells and prevent interaction between them and the cells in the soil profile, the conductivities at the boundaries of each "atmosphere" cell ($K_{i+\frac{1}{2},j}$, $K_{i-\frac{1}{2},j}$, $K_{i,j+\frac{1}{2}}$, $K_{i,j-\frac{1}{2}}$) were forced to equal zero. This created a no flow boundary condition along the edge of the bed and furrow.

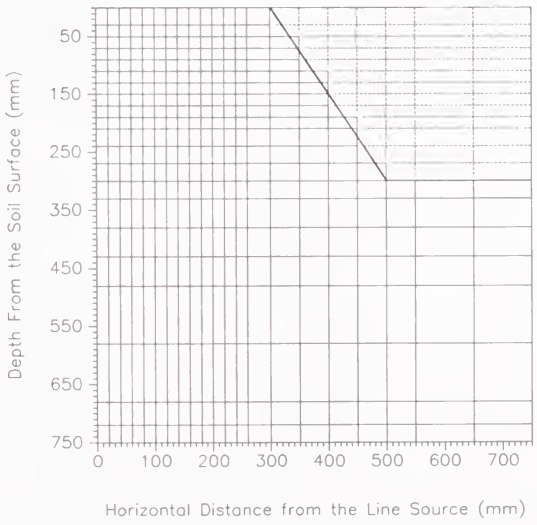

Figure 5.16. Finite difference mesh for the lysimeter problem.

Estimated Daily ET

Daily ET was a component of the extraction function and was estimated independently. As discussed in Chapter 4, weekly ET values were easily and accurately obtained from the field data. The resolution of the drainage lysimeters, however, did not permit daily ET to be measured directly. Instead, daily ET for each of the soils was estimated by multiplying daily Penman ET values by appropriate crop coefficients. Crop coefficients were developed by dividing observed weekly ET of each soil by the corresponding weekly Penman ET. Figure 5.17 presents estimated daily ET from the lysimeters for each of the three soils.

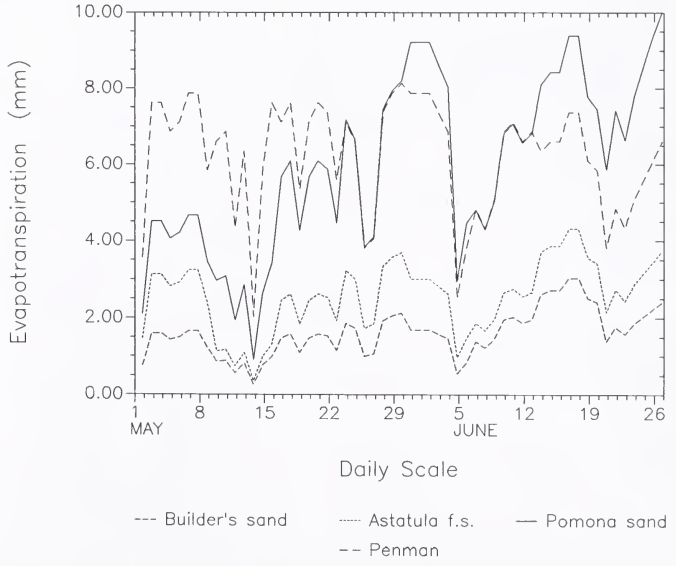

Figure 5.17. Comparison of Penman ET and estimated daily ET from the lysimeters during the final two months of the growing season.

In general, the weekly crop coefficients progressively increased during the growing season. The coefficients ranged from 0.21-0.41 in builder's sand, 0.34-0.58 in Astatula f.s., and 0.59-1.54 in Pomona sand. The magnitudes of the final two Pomona sand crop coefficients (1.27 and 1.54) were larger than the conventionally accepted maximum crop coefficient for the subtropical zone ($\approx$ 1.2). Two explanations for such high values are the tremendous size of the tomato plants in the Pomona sand lysimeters during the final weeks of the growing season (Table 4.1) and the oasis effect that may have been created because the lysimeters were buffered by grass and not by an extensive tomato field crop.

The Root Distribution Term, RDT.

The purpose of the root distribution term was to determine the fraction of the total water use extracted from each cell in the finite difference mesh. The term was a function of soil type and plant growth stage and was determined empirically from the field data.

Because the resolution of the field data did not permit the RDT of each cell to be individually determined, the finite difference mesh of Figure 5.16 was divided into 12 compartments with each being comprised of three to 87 cells as shown in Figure 5.18. Ten of the 12 compartments contained the locations of the tensiometers used to monitor soil water potential in the lysimeters. The transpiration fraction of ET was extracted from these compartments. The evaporation fraction of ET was extracted from the three-celled compartment at the surface of the furrow (There was no evaporation from the bed because of the plastic mulch.). Finally, no extraction or evaporation was permitted from the largest compartment which contained 87 cells.

The fraction of daily ET extracted from each compartment was ascertained from the field data. The fraction removed from the three-celled compatrment responsible for evaporation was easily computed by dividing daily evaporation (Figure 4.23) by daily ET (Figure 5.17). The procedure for determining the extraction fraction from the 10 compartments responsible for the transpiration component, however, was more complex.

Volumes of water extracted during a given time period from the compartment containing a given tensiometer were extrapolated from the soil water potential data collected with the tensiometers. This volume was divided by the total volume of water extracted from the lysimeter over the same time period to give the contribution of that compartment. Because there was considerable scatter in the daily RDT terms of each compartment, weekly averages were calculated for use in the simulation model. The root distribution term of each cell in a given compartment was then computed by dividing the compartment RDT by the number of cells in that compartment.

Figures 5.19 and 5.20 present the distribution of extraction from Astatula f.s. during the week of May 2 and Pomona sand during the week of June 6, respectively. As expected, during the earlier growth stages of the plants, most of the roots were concentrated immediately below the irrigation source. It was somewhat surprising, however, that even during the twelfth week of the growing season, 50% of the extraction occurred in the immediate vicinity of the trickle source.

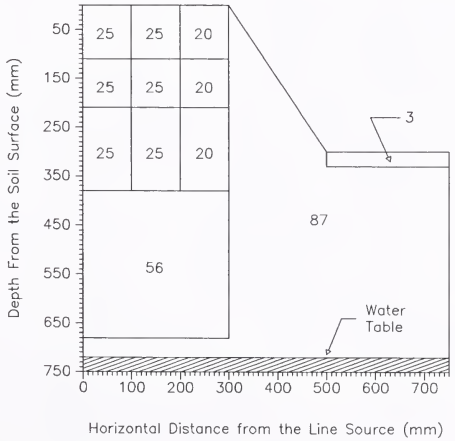

Figure 5.18. The number of cells contained by each soil compartment.

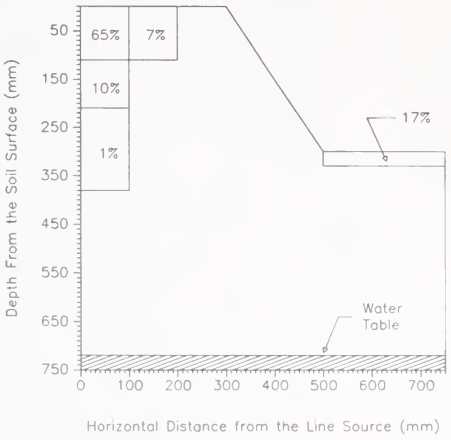

Figure 5.19. Distribution of extraction in Astatula f.s. for the week of May 2.

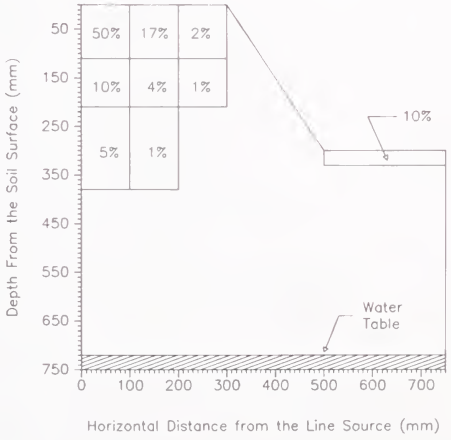

Figure 5.20. Distribution of extraction in Pomona sand for the week of June 6.

Simulation Results

The two-dimensional model was used to simulate infiltration, redistribution, and extraction in Astatula f.s. and Pomona sand for one week of the growing season. Model outputs were compared to field data collected with the microcomputer based data acquisition system. The initial conditions for the model were determined directly from the observed soil water potentials. The estimated daily ET rates, the root distribution terms, and the irrigation times, durations, and application rates were inputs to the model. The daily ET was distributed over the day as computed by equation (5.79) with a 24-hour cycle and a lag time of three hours as shown in Figure 5.9.

The field data used for evaluation of the model were taken from the weeks of May 2 and June 6 for the Astatula f.s. and the Pomona sand, respectively. These two weeks were selected because they presented extremes in the plant growth stages while also including several irrigation-extraction cycles. Because of the hydraulic characteristics of builder's sand, only three of the nine tensiometers in the bedded portion of the soil profile were located in the wetted zone. Therefore, there was little change in the soil water potential data from the instruments and the data base generated for this soil was not adequate for verification of the simulation model.

During the simulation process it was determined that the hydraulic conductivity values that were being predicted by equation (2.9) were too large. Capillary rise from the water table was greater and drainage from irrigation occurred more rapidly in Astatula f.s. and Pomona sand than observed in the field. The saturated hydraulic conductivity of the soils, which is the scaling factor in equation (2.9), was therefore modified to reduce the hydraulic conductivity function. The measured and modified saturated hydraulic conductivities are given in Table 5.1. The modification required by the Astatula f.s. was small while that required by the Pomona sand was quite large. The modifications were justified because considerable error may have been introduced while packing the soil columns during the experimental determination of saturated hydraulic conductivity. The soil columns in the laboratory were packed with soil that had been air dried. In contrast, wet soils were used

when the soil profiles were reconstructed in the lysimeters at the beginning of the field study. The Pomona sand, when wet and packed, adopted clay-like properties and became soft and malleable. This was attributed to the high organic matter content of the soil. Apparently, this process also affected the bulk density and saturated hydraulic conductivity of the soil. The modified hydraulic conductivities produced simulated results that were in good agreement with the field data.

Table 5.1. Measured and Modified Saturated Hydraulic Conductivity.

Soil Type	Saturated Hydraulic Conductivity K_s (mm/hr)	
	Measured	Modified
Builder's sand	536.07	536.07
Astatula f.s.	428.35	400.00
Pomona sand	169.77	100.00

Comparisons between the simulated results and the field data are presented for 9 of the 10 sites in the soil profile which were monitored by the data acquisition system. The results are presented for each of the three radial distances at depths of 100, 200, and 300 mm. The results for the final site which was located at a depth of 500 mm are not presented because they were dominated by the water table and showed very little variation. Figures 21-23 and 24-26 present simulated and measured pressure heads in Astatula f.s. and Pomona sand, respectively.

Simulated pressure heads were in good agreement with observed field pressure heads for all of the sites during the week of May 2 in Astatula f.s. and the week of June 6 in Pomona sand. However, there were two consistent discrepancies between the simulated and observed data.

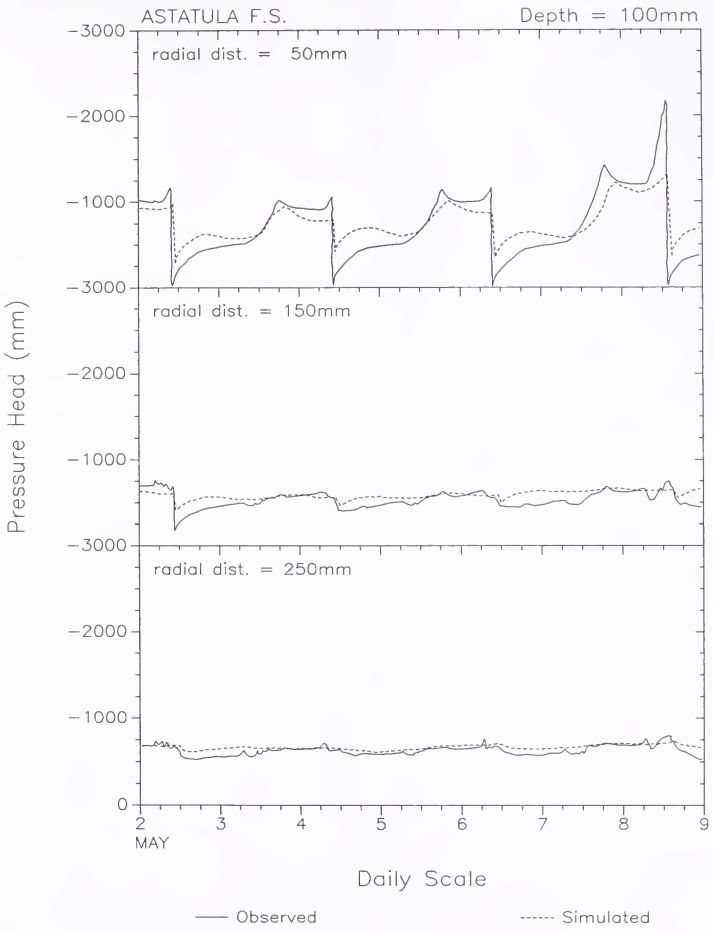

Figure 5.21. Comparison of simulated and observed pressure heads at a depth of 100 mm in Astatula f.s. for the week of May 2.

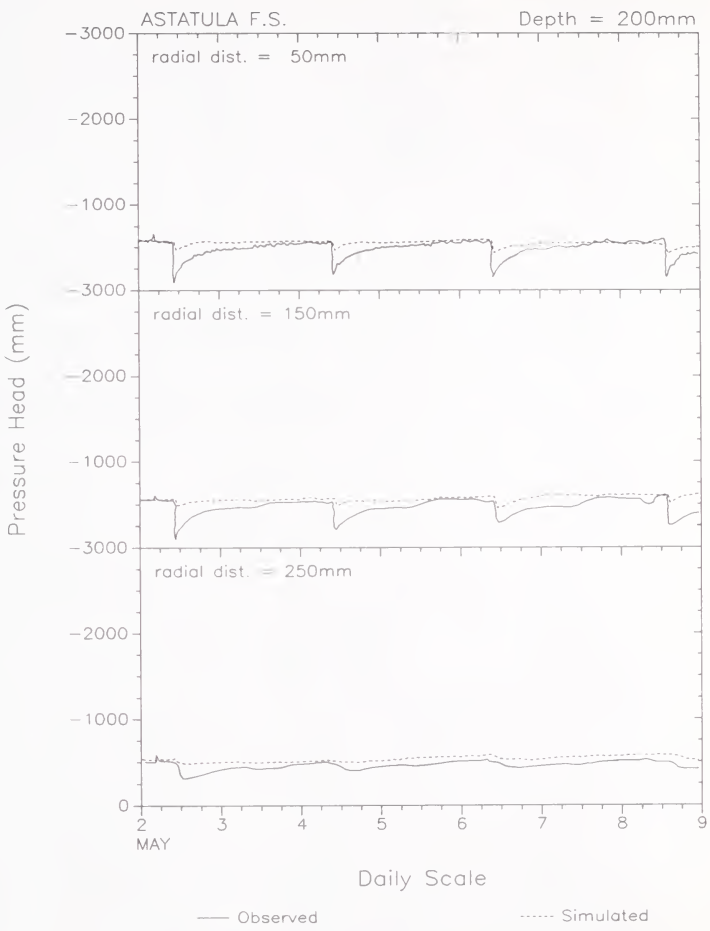

Figure 5.22. Comparison of simulated and observed pressure heads at a depth of 200 mm in Astatula f.s. for the week of May 2.

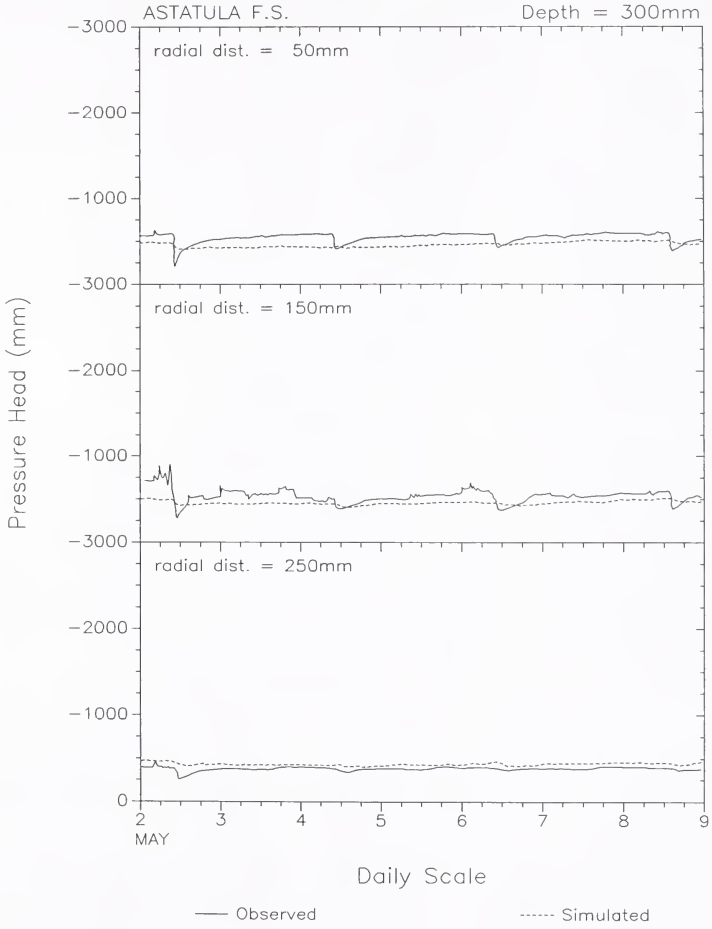

Figure 5.23. Comparison of simulated and observed pressure heads at a depth of 300 mm in Astatula f.s. for the week of May 2.

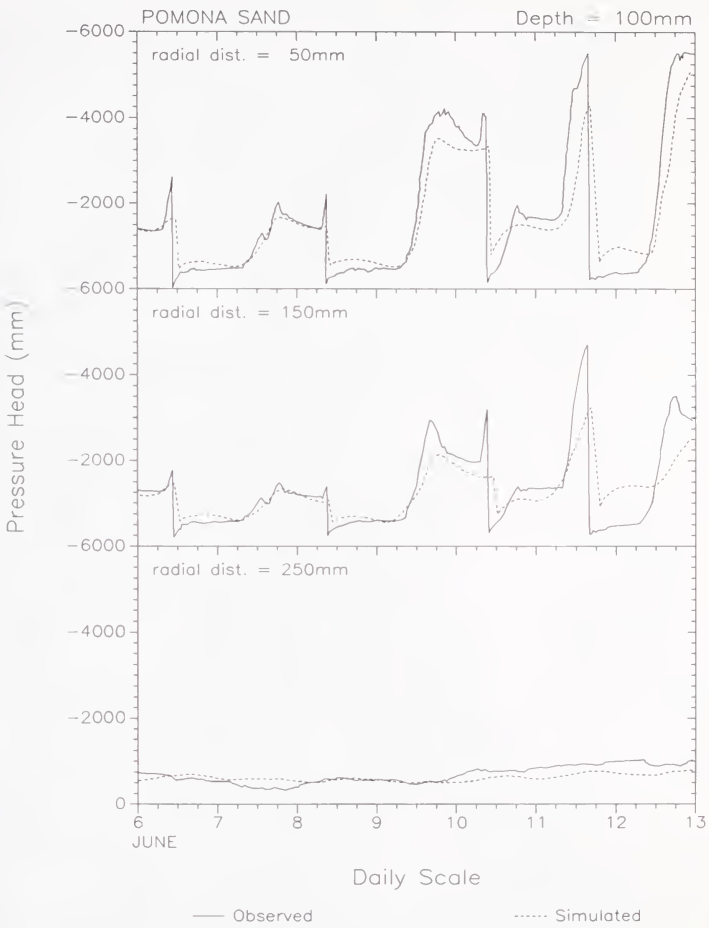

Figure 5.24. Comparison of simulated and observed pressure heads at a depth of 100 mm in Pomona sand for the week of June 6.

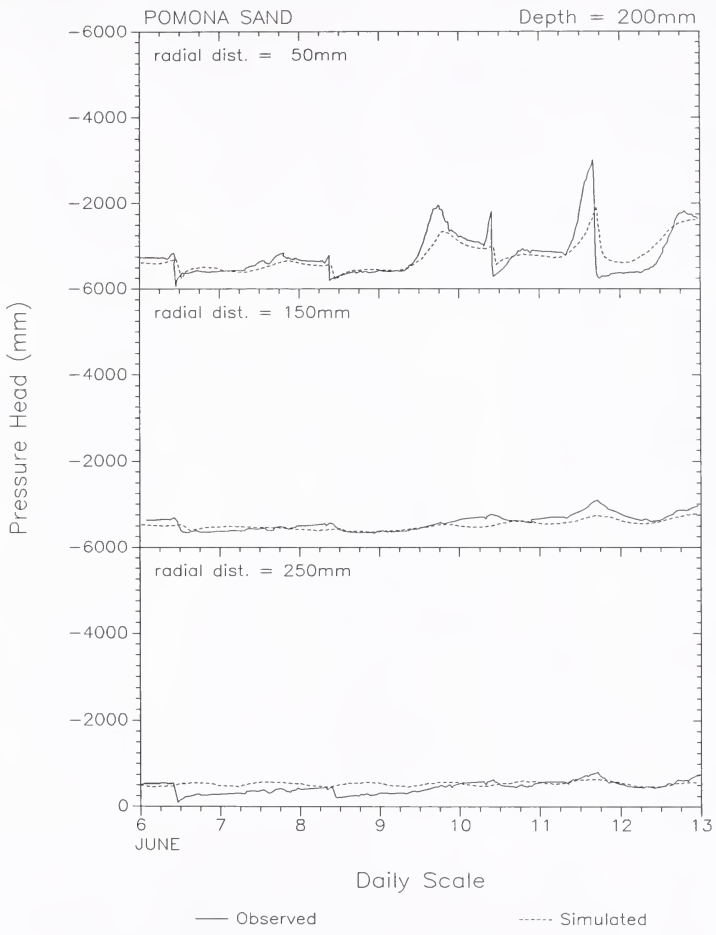

Figure 5.25. Comparison of simulated and observed pressure heads at a depth of 200 mm in Pomona sand for the week of June 6.

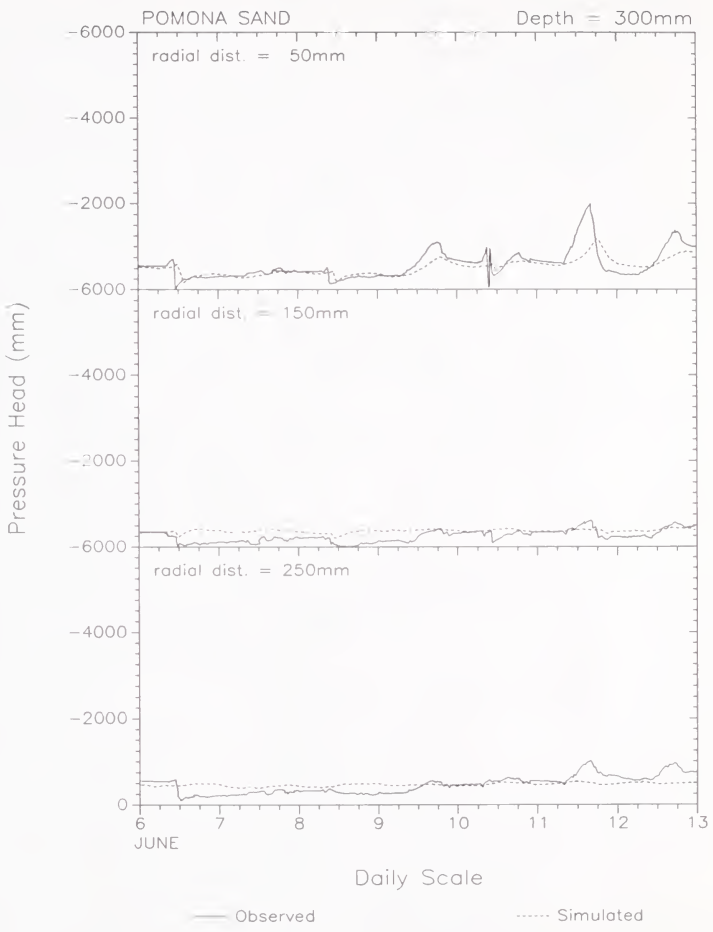

Figure 5.26. Comparison of simulated and observed pressure heads at a depth of 300 mm in Pomona sand for the week of June 6.

The first discrepancy occurred between the predicted response to an irrigation and the magnitude of the instrument response, even at the sites farthest from the line source. One possible explanation is instrumentation error. Originally, if one of the tensiometers in a lysimeter produced a dramatic change in output voltage, a slight incompatibility between the impedance of the transducers and the A/D board of the data acquisition device caused the other nine instruments in the lysimeter to respond in the same way. To dampen this undesirable response, a reference voltage was read before each data channel was monitored. This strategy permitted accurate measurement of soil water status under most conditions encountered in the lysimeters. However, if a given instrument produced a very large and sudden change in output voltage, the channels that were read immediately afterwards were still slightly affected.

The second discrepancy is apparent in the model's failure to predict the sudden extraction peaks that concurred with sunrise. These peaks indicate a sudden extraction at daybreak which the sinusoidal curve that was used to distribute daily ET over a 24-hour period failed to predict. Attempts to reproduce the peaks by shortening the period of the sinusoidal curve and concentrating higher ET rates during the daylight periods met with limited success. Errors may also have been introduced by using the relatively large soil compartments to estimate the root distribution term. Root extraction may have been more concentrated near the surface.

Additionally, differences between the simulated results and field data may be attributed to the assumptions made to simplify the mathematical solution of the problem such as homogeneous, isotropic and nonhysteretic soils, uniform application of irrigation water, and a true two-dimensional soil profile with uniform plant growth and root extraction. Overall, agreement between simulated results and field data was good and the performance of the two-dimensional model was satisfactory.

Model Applications

The numerical model developed in this work provides a tool for the study of soil water movement under the unique conditions that occur in Florida without the cost normally associated with field experiments. The model may be used to determine optimum irrigation scheduling and wetting front movement for a wide variety of soils and atmospheric conditions.

An application that could have an immediate effect on the vegetable industry is to use the model to investigate the horizontal movement of the wetting front as a function of soil hydraulic characteristics and irrigation system properties. The results would allow growers to optimize the placement of fertilizer bands. Placement should allow the wetting fronts to reach the fertilizer bands so that plants can access the nutrients. If the results indicate that fertilizer bands must be positioned too close to the plants, it may be desirable to eliminate the bands completely and use fertigation to provide the necessary nutrients.

The model may also be used to optimize the duration, frequency, and application rate of irrigations as a function of soil type and water table depth in order to maintain a desired soil water potential in the soil profile.

A third application is to use the model in the design of irrigation systems in order to optimize emitter spacing. This application may be particularly effective when trying to determine the maximum distance individual emitters may be spaced along a lateral and still simulate a line source, as well as determining the effects of individually clogged or partially clogged emitters on the soil water status.

CHAPTER 6
SUMMARY AND CONCLUSIONS

In Florida, vegetables are often grown on mulched beds in sandy soils that commonly require irrigation even if they are subject to naturally occurring high water tables. Increasingly, these crops are being irrigated with line source trickle irrigation systems. A set of six rain-sheltered field lysimeters were developed to simulate these production systems.

Experiments were conducted in the lysimeters to measure crop water use and redistribution and extraction patterns of a tomato crop. A two-dimensional finite difference model was developed to simulate water infiltration, redistribution, and extraction under the above conditions. The model may be used to evaluate and recommend irrigation strategies.

The Lysimeter System

Three different Florida sandy soils were used to fill the lysimeters, with each of the soils occupying a pair of lysimeters. The soils were selected to provide a wide range of water holding capacities. One mulched bed was reconstructed in each lysimeter. Each drainage lysimeter contained a water table regulation device and was irrigated with a line source drip irrigation system. Water table levels could be adjusted and maintained to within 3 mm of the desired depth setting. Irrigation laterals were installed along the centerline of each bed.

A microcomputer-based data acquisition system for continuous soil water potential measurements was developed. The system consisted of tensiometer-mounted pressure transducers, a work station data acquisition and control device, and a portable microcomputer. Three of the six lysimeters were instrumented with 10 tensiometers per lysimeter. In order to provide a complete description of the soil profile in the lysimeter, the 10 tensiometers were installed at different depths and radial distances from the irrigation lateral. The

instrumentation error was on the order of 0.2 kPa which was significant only when the soil water potentials measured were near saturation.

Field Data

Experiments were conducted in the lysimeters to measure crop water use and redistribution and extraction patterns of a tomato crop. Inherent limitations of the instrumentation and of drainage type lysimeters prevented accurate measurements of daily water use, although wetting and drying patterns could still be determined. As the measurement period increased, the relative size of the error diminished. Thus, weekly water use was accurately determined, especially during high water use periods.

The design of the lysimeters permitted crop water use to be partitioned into irrigation and water table recharge components. The water use data indicate that crop water use was a function of plant size and the plants' source of water (irrigation versus water table) was a function of soil type. Results also demonstrated that a significant portion of daily plant water use was provided by the water table. This indicates that naturally occurring high water tables may significantly alter irrigation requirements. However, the contribution of the water table to crop water use is also a function of water table depth. Redistribution and extraction patterns calculated from the soil water potential measurements showed that very little change in soil water status took place at horizontal distances of more than 200 mm from the irrigation lateral and at depths greater than 300 mm.

From the field data, it can be concluded that the largest portion of extraction occurred within 100 mm horizontally and 150 mm vertically of the irrigation source. The soil water potential data indicated that during the early morning, prior to irrigation, and again in the late afternoon, several hours after an irrigation, the plants may have begun to experience short term water stresses (up to -50 kPa). Other recent research (Clark, 1989) has indicated that even soil water potentials of -15 kPa may reduce the size of the fruit and the yield. It appears, therefore, that frequent irrigations that would bring the region of the soil profile

nearest the irrigation source back to field capacity may be an appropriate irrigation management strategy.

Numerical Simulation

A one-dimensional simulation model was developed as the precursor of a two-dimensional model. Its purpose was to verify that the finite difference equations closely approximated the governing partial differential equation. The one-dimensional model was in excellent agreement with several numerical and steady-state analytical solutions.

The two-dimensional model was developed to simulate soil water infiltration, redistribution, and extraction in a soil profile overlaying a shallow water table and irrigated by a line source drip irrigation system. The model was compared to numerical and steady-state analytical solutions from the literature with success. It was then used to simulate two-dimensional soil water movement in the lysimeters. The model results were in good agreement with the field data collected using the microcomputer based data acquisition system.

Model Applications

The two-dimensional model can be used to investigate many different irrigation strategies under the unique conditions encountered in Florida without the cost normally associated with field experiments. Applications of the model include using it to optimize the placement of fertilizer bands in a mulched bed so that the wetting fronts may reach the nutrients and make them readily available to the plant roots, using it to optimize the duration, frequency, and application rate of irrigations as a function of soil type and water table depth in order to maintain a desired soil water potential in the soil profile, and using it to design irrigation systems with optimal emitter spacings.

APPENDIX A
SOIL TEST REPORTS

Three samples of each soil were taken from various depths in the lysimeters and submitted for analysis to the University of Florida's IFAS Soil Testing Laboratory. Analyses were done on pH, percent organic matter, macro and micro nutrient concentrations, copper toxicity, and soluble salts. Standard fertilization recommendations for a tomato crop were also provided.

Tables A.1-A.3, A.4-A.6, and A.7-A.9 present the concentrations of P, K, Mg, and Ca for the three soil samples of builder's sand, Astatula f.s., and Pomona sand, respectively. They also give fertilizer recommendations. The footnotes mentioned at the bottom of each table are found on page 132. Table A.10 presents the results from the micronutrient, organic matter, copper toxicity, and soluble salts tests. Kidder (1983) was used to interpret the micronutrient soil test results.

Table A.1. Routine Test Report and Standard Fertilization Recommendations: Builder's sand sample 1.

SAMPLE INFORMATION

client's identification: BUIDLERS 1 lab number: 12757

crop: TOMATO soil texture: SAND

Both interpretations and recommendations are based upon the soil test results and research/experience with the specified crop under Florida's growing conditions.

SOIL TEST RESULTS AND THEIR INTERPRETATIONS

pH (1:2 S:W) 6.7 A-E BUFFER VALUE:

MECHLICH I EXTRACTABLE			v. low	low	medium	high	v. high	off scale
PHOSPHORUS	(ppm P)	0	*					
POTASSIUM	(ppm K)	20	*****					
MAGNESIUM	(ppm Mg)	4	******	**				
CALCIUM	(ppm Ca)	24						

LIME AND FERTILIZER RECOMMENDATIONS

For TOMATO: apply 0.0 tons lime per acre
120 pounds N per acre
160 pounds P_2O_5 per acre
160 pounds K_2O per acre

These footnotes are an integral part of the fertilization recommendation. PLEASE READ THEM CAREFULLY. They are unique for each soil/crop situation.

SEE FOOTNOTE(S): 201 202 203 204 205 207 211 767

Table A.2. Routine Test Report and Standard Fertilization Recommendations: Builder's sand sample 2.

SAMPLE INFORMATION

client's identification: BUIDLERS 2 lab number: 12758

crop: TOMATO soil texture: SAND

Both interpretations and recommendations are based upon the soil test results and research/experience with the specified crop under Florida's growing conditions.

SOIL TEST RESULTS AND THEIR INTERPRETATIONS

pH (1:2 S:W) 7.2 A-E BUFFER VALUE:

MECHLICH I EXTRACTABLE			v. low	low	medium	high	v. high	off scale
PHOSPHORUS	(ppm P)	0	*					
POTASSIUM	(ppm K)	16	****					
MAGNESIUM	(ppm Mg)	8	******	****				
CALCIUM	(ppm Ca)	36						

LIME AND FERTILIZER RECOMMENDATIONS

For TOMATO: apply 0.0 tons lime per acre
120 pounds N per acre
160 pounds P_2O_5 per acre
160 pounds K_2O per acre

These footnotes are an integral part of the fertilization recommendation. PLEASE READ THEM CAREFULLY. They are unique for each soil/crop situation.

SEE FOOTNOTE(S): 201 202 203 204 205 207 211 767

Table A.3. Routine Test Report and Standard Fertilization Recommendations: Builder's sand sample 3.

SAMPLE INFORMATION

client's identification: BUIDLERS 3 lab number: 12759

crop: TOMATO soil texture: SAND

Both interpretations and recommendations are based upon the soil test results and research/experience with the specified crop under Florida's growing conditions.

SOIL TEST RESULTS AND THEIR INTERPRETATIONS

pH (1:2 S:W) 6.5 A-E BUFFER VALUE:

MECHLICH I EXTRACTABLE			v. low	low	medium	high	v. high	off scale
PHOSPHORUS	(ppm P)	0	*					
POTASSIUM	(ppm K)	136	******	******	*******	**		
MAGNESIUM	(ppm Mg)	12	******	*****				
CALCIUM	(ppm Ca)	32						

LIME AND FERTILIZER RECOMMENDATIONS

For TOMATO: apply 0.0 tons lime per acre
120 pounds N per acre
160 pounds P_2O_5 per acre
55 pounds K_2O per acre

These footnotes are an integral part of the fertilization recommendation. PLEASE READ THEM CAREFULLY. They are unique for each soil/crop situation.

SEE FOOTNOTE(S): 201 202 203 204 205 207 211 767

Table A.4. Routine Test Report and Standard Fertilization Recommendations: Astatula f.s. sample 1.

SAMPLE INFORMATION

client's identification: ASTATULA 1 lab number: 12760

crop: TOMATO soil texture: SAND

Both interpretations and recommendations are based upon the soil test results and research/experience with the specified crop under Florida's growing conditions.

SOIL TEST RESULTS AND THEIR INTERPRETATIONS

pH (1:2 S:W) 6.4 A-E BUFFER VALUE:

MECHLICH I EXTRACTABLE			v. low	low	medium	high	v. high	off scale
PHOSPHORUS	(ppm P)	140	******	******	*******	******	*	
POTASSIUM	(ppm K)	104	******	******	*******	*		
MAGNESIUM	(ppm Mg)	88	******	******	*******	******	***	
CALCIUM	(ppm Ca)	700						

LIME AND FERTILIZER RECOMMENDATIONS

For TOMATO: apply 0.0 tons lime per acre
120 pounds N per acre
55 pounds P_2O_5 per acre
55 pounds K_2O per acre

These footnotes are an integral part of the fertilization recommendation. PLEASE READ THEM CAREFULLY. They are unique for each soil/crop situation.

SEE FOOTNOTE(S): 201 202 203 204 205 207 211

Table A.5. Routine Test Report and Standard Fertilization Recommendations: Astatula f.s. sample 2.

SAMPLE INFORMATION

client's identification: ASTATULA 2 lab number: 12761

crop: TOMATO soil texture: SAND

Both interpretations and recommendations are based upon the soil test results and research/experience with the specified crop under Florida's growing conditions.

SOIL TEST RESULTS AND THEIR INTERPRETATIONS

pH (1:2 S:W) 7.4 A-E BUFFER VALUE:

MECHLICH I EXTRACTABLE			v. low	low	medium	high	v. high	off scale
PHOSPHORUS	(ppm P)	120	******	******	*******	*****		
POTASSIUM	(ppm K)	20	******					
MAGNESIUM	(ppm Mg)	72	******	******	*******	******	*	
CALCIUM	(ppm Ca)	596						

LIME AND FERTILIZER RECOMMENDATIONS

For TOMATO: apply 0.0 tons lime per acre
120 pounds N per acre
55 pounds P_2O_5 per acre
160 pounds K_2O per acre

These footnotes are an integral part of the fertilization recommendation. PLEASE READ THEM CAREFULLY. They are unique for each soil/crop situation.

SEE FOOTNOTE(S): 201 202 203 204 205 207 211

Table A.6. Routine Test Report and Standard Fertilization Recommendations: Astatula f.s. sample 3.

SAMPLE INFORMATION

client's identification: ASTATULA 3 lab number: 12762

crop: TOMATO soil texture: SAND

Both interpretations and recommendations are based upon the soil test results and research/experience with the specified crop under Florida's growing conditions.

SOIL TEST RESULTS AND THEIR INTERPRETATIONS

pH (1:2 S:W) 7.6 A-E BUFFER VALUE:

MECHLICH I EXTRACTABLE			v. low	low	medium	high	v. high	off scale
PHOSPHORUS	(ppm P)	164	******	******	*******	******	***	
POTASSIUM	(ppm K)	16	*****					
MAGNESIUM	(ppm Mg)	76	******	******	*******	******	**	
CALCIUM	(ppm Ca)	816						

LIME AND FERTILIZER RECOMMENDATIONS

For TOMATO: apply 0.0 tons lime per acre
120 pounds N per acre
55 pounds P_2O_5 per acre
160 pounds K_2O per acre

These footnotes are an integral part of the fertilization recommendation. PLEASE READ THEM CAREFULLY. They are unique for each soil/crop situation.

SEE FOOTNOTE(S): 201 202 203 204 205 207 211

Table A.7. Routine Test Report and Standard Fertilization Recommendations: Pomona sand sample 1.

SAMPLE INFORMATION

client's identification: POMONA 1 lab number: 12763

crop: TOMATO soil texture: SAND

Both interpretations and recommendations are based upon the soil test results and research/experience with the specified crop under Florida's growing conditions.

SOIL TEST RESULTS AND THEIR INTERPRETATIONS

pH (1:2 S:W) 4.4 A-E BUFFER VALUE: 7.24

MECHLICH I EXTRACTABLE			v. low	low	medium	high	v. high	off scale
PHOSPHORUS	(ppm P)	16	******					
POTASSIUM	(ppm K)	156	******	******	*******	****		
MAGNESIUM	(ppm Mg)	100	******	******	*******	******	*****	
CALCIUM	(ppm Ca)	420						

LIME AND FERTILIZER RECOMMENDATIONS

For TOMATO: apply 3.5 tons lime per acre
120 pounds N per acre
160 pounds P_2O_5 per acre
55 pounds K_2O per acre

These footnotes are an integral part of the fertilization recommendation. PLEASE READ THEM CAREFULLY. They are unique for each soil/crop situation.

SEE FOOTNOTE(S): 201 202 203 204 205 207 211 761 762

Table A.8. Routine Test Report and Standard Fertilization Recommendations: Pomona sand sample 2.

SAMPLE INFORMATION

client's identification: POMONA 2 lab number: 12764

crop: TOMATO soil texture: SAND

Both interpretations and recommendations are based upon the soil test results and research/experience with the specified crop under Florida's growing conditions.

SOIL TEST RESULTS AND THEIR INTERPRETATIONS

pH (1:2 S:W) 4.6 A-E BUFFER VALUE: 7.22

MECHLICH I EXTRACTABLE			v. low	low	medium	high	v. high	off scale
PHOSPHORUS	(ppm P)	12	*****					
POTASSIUM	(ppm K)	44	******	*****				
MAGNESIUM	(ppm Mg)	72	******	******	*******	******	*	
CALCIUM	(ppm Ca)	232						

LIME AND FERTILIZER RECOMMENDATIONS

For TOMATO: apply 3.5 tons lime per acre
120 pounds N per acre
160 pounds P_2O_5 per acre
160 pounds K_2O per acre

These footnotes are an integral part of the fertilization recommendation. PLEASE READ THEM CAREFULLY. They are unique for each soil/crop situation.

SEE FOOTNOTE(S): 201 202 203 204 205 207 211 761 762

Table A.9. Routine Test Report and Standard Fertilization Recommendations: Pomona sand sample 3.

SAMPLE INFORMATION

client's identification: POMONA 3 lab number: 12765

crop: TOMATO soil texture: SAND

Both interpretations and recommendations are based upon the soil test results and research/experience with the specified crop under Florida's growing conditions.

SOIL TEST RESULTS AND THEIR INTERPRETATIONS

pH (1:2 S:W) 4.7 A-E BUFFER VALUE: 7.18

MECHLICH I EXTRACTABLE			v. low	low	medium	high	v. high	off scale
PHOSPHORUS	(ppm P)	8	***					
POTASSIUM	(ppm K)	32	******	**				
MAGNESIUM	(ppm Mg)	56	******	******	*******	*****		
CALCIUM	(ppm Ca)	156						

LIME AND FERTILIZER RECOMMENDATIONS

For TOMATO: apply 3.5 tons lime per acre
120 pounds N per acre
160 pounds P_2O_5 per acre
160 pounds K_2O per acre

These footnotes are an integral part of the fertilization recommendation. PLEASE READ THEM CAREFULLY. They are unique for each soil/crop situation.

SEE FOOTNOTE(S): 201 202 203 204 205 207 211 761 762

Footnotes for Lime and Fertilizer Recommendations in Tables A.1-A.9.

201. Use low-salt index fertilizer sources where soluble salt injury is a problem.

202. Fertilizer may be applied in split applications, part broadcast and part banded to reduce leaching losses and lessen danger of fertilizer burn.

203. on new soils or where micronutrients are known to be deficient, apply 5 lbs of Mn, 3 lbs of Zn, 4 lbs of Fe, 3 lbs Cu, and 1.5 lbs of B per acre.

204. In cold soil or following fumigation, apply 20 to 25% of the recommended N in Nitrate form.

205. If supplemental irrigation is not available, reduce the amounts suggested by 25%.

207. Sidedress with 20 to 30 lbs N plus 40 to 60 lbs K_2O per acre 1 to 5 times depending on number of leaching rains and length of harvest season.

211. On graywall susceptible varieties increase K_2O by 20 to 25%.

761. Either calcitic or dolomitic limestone may be used.

762. Lime recommendations are based on the Adams-Evans lime requirement test which is run on all mineral soils having a pH below 6.0. When, the recommended amount of lime is incorporated in the surface 6 inches of soil, the soil pH level should adjust to a pH level beyond which additional liming benefit is not expected.

763. Apply the equivalent of 35 lbs elemental Mg per acre in a soluble form, such as magnesium sulfate or sulfate of potash magnesia.

Table A.10. Micronutrients, Organic Matter, Copper Toxicity Test, and Soluble Salts.

Lab No.	Sample ID	Percent Organic Matter	Total PPM			pH
			Sol. Salts	Zn	Cu	Mn	
12757	Sand 1	0.00	112	0.32	0.16	0.36	6.7
12758	Sand 2	0.03	84	0.36	0.16	0.32	7.2
12759	Sand 3	0.00	322	3.28	0.16	0.32	6.5
12760	Astatula 1	0.49	476	19.60	16.00	16.00	6.4
12761	Astatula 2	0.62	112	15.20	16.00	13.20	7.4
12762	Astatula 3	0.62	84	16.80	16.80	34.00	7.6
12763	Pomona 1	4.29	770	3.76	0.20	1.20	4.4
12764	Pomona 2	5.08	252	3.84	0.20	1.96	4.6
12765	Pomona 3	6.64	154	13.60	0.16	1.16	4.7

APPENDIX B
NUMERICAL MODEL PROGRAM LISTING

```
*
*   VARIABLE LIST OF THE TWO-DIMENSIONAL MODEL
*
*
*   A          - subdiagonal values of cofficient matrix (1/mm-hr)
*   ALPHA      - the alpha parameter in van Genuchten's equation
*
*   B          - subdiagonal values of cofficient matrix (1/mm-hr)
*   BOTTOM     - depth of simulated soil profile (mm)
*
*   C          - array which contains only elements enclosed by the outer
*                outer bands or diagonals of the solution matrix.  This
*                array is NMAX*MBAND
*   CF         - correction factor used for linear adjustment of the
*                extraction term
*   COND       - hydraulic conductivity (mm/hr)
*   CONDS      - saturated hydraulic conductivity (cm/hr)
*   CONTAB     - tabulated hydraulic conductivity (mm/hr)
*   C1         - specific water capacity (1/mm)
*
*   D          - diagonal values of coefficient matrix (1/mm-hr)
*   DAYLITE    - length of the extraction cycle (hr)
*   DAYTIME    - the number of hours into the extraction cycle (hr)
*   DELTA      - sum of flows into and out of the profile since start (mm)
*   DEPTH      - the vertical dist. from the origin of the cell nodes (mm)
*   DRAIN      - total drainage from the profile (mm)
*   DT         - time increment as determined by subroutine TSTEP (hr)
*   DTMAX      - maximum size of the time increment (hr)
*   DTMIN      - minimum size of the time increment (hr)
*   DZ         - grid size in the z-direction (mm)
*   DZINIT     - used to read grid size from file INITIAL.DAT (mm)
*   D1         - distance between the nodes at (J,I) and (J-1,I) (mm)
*   D2         - distance between the nodes at (J,I) and (J+1,I) (mm)
*   D3         - distance between the nodes at (J,I) and (J,I-1) (mm)
*   D4         - distance between the nodes at (J,I) and (J,I+1) (mm)
*
*   E          - superdiagonal values of cofficient matrix (1/mm-hr)
*   ERRMASS    - mass balance error (mm)
```

```
*   ET        = daily predetermined evapotranspiration (mm/day)
*   ETP       = daily predetermined evapotranspiration (mm/day)
*   ETRATE    = hourly evapotranspiration rate (mm/hr)
*   EXTRACT   = total extraction from the soil profile (mm)
*
*   F         = superdiagonal values of cofficient matrix (1/mm-hr)
*   FA        = parameter in the tabulated search routine
*   FB        = parameter in the tabulated search routine
*   FLOWIN    = total flux into the soil profile from the top and
*               bottom boundaries (mm)
*   FLUX      = flux into the soil profile from the top and bottom
*               boundaries at each iteration (mm)
*
*   H         = soil moisture pressure head (mm)
*   HBOT      = bottom boundary pressure head (mm)
*   HINIT     = initial pressure head for uniform initial cond. (mm)
*   HTAB      = tabulated pressure heads (mm)
*
*   I         = counter in the x-direction
*   ICOUNT    = counter used to determine the number of iterations
*               before the output was printed
*   IDAY      = counter of simulated days
*   INDEX     = index in the routing technique of subroutine UPDAT1
*   IOPTION   = used to select what type of initial conditions will
*               be used; uniform or nonuniform
*   ISOIL     = the soil type for the simulation
*   ITERMAX   = maximum number of iterations permitted in the simulation
*   IX        = number of internal nodes in the x-direction
*   I1 - I6   = horizontal node numbers used to determine the boundary
*               between the soil profile and atmosphere soils
*
*   J         = counter in the z-direction
*   JX2       = number of internal nodes in the z-direction
*   J1 - J6   = vertical node numbers used to determine the boundary
*               between the soil profile and atmosphere soils
*
*   K1        = hydraulic cond. at the top surface of a cell (mm/hr)
*   K2        = hydraulic cond. at the bottom surface of a cell (mm/hr)
*   K3        = hydraulic cond. at the left surface of a cell (mm/hr)
*   K4        = hydraulic cond. at the right surface of a cell (mm/hr)
*
*   LENGTH    = the length of the soil profile in the y-direction (mm)
*   LOWBC     = type of bottom boundary condition
*
*   MBAND     = number of diagonals in the banded solution matrix, C,
*               including the zero diagonals enclosed by the outlying
*               diagonals
*   MID       = the subscript of the main diagonal term in array C
*   MONTH     = month of the year (5 or 6 during the growing season)
*
```

```
*   NDATA     = size of the tabulated soil characteristic data files
*   NITER     = iteration counter
*   NMAX      = the number of cells in the profile
*
*   Q         = net flux of grid (mm/hr)
*   QB        = flux across the bottom boundary (mm/hr)
*   QBINIT    = initial flux across the bottom boundary (mm/hr)
*   QL        = flux across the left boundary (mm/hr)
*   QLINIT    = initial flux across the left boundary (mm/hr)
*   QLIRR     = application rate at the left boundary (mm/hr)
*   QMAX      = variable to which the largest of the flux, net flux, or
*             = extraction rate is assigned (mm/hr)
*   QR        = flux across the right boundary (mm/hr)
*   QRINIT    = initial flux across the right boundary (mm/hr)
*   QS        = flux across the surface boundary (mm/hr)
*   QSINIT    = initial flux across the top boundary (mm/hr)
*   QSIRR     = application rate at the soil surface (mm/hr)
*   Q1        = flux across the top surface of a cell (mm/hr)
*   Q2        = flux across the bottom surface of a cell (mm/hr)
*   Q3        = flux across the left surface of a cell (mm/hr)
*   Q4        = flux across the right surface of a cell (mm/hr)
*
*   R         = solution vector of the tridiagonal matrix (1/hr)
*   RADIUS    = the horizontal dist. from the origin of the cell nodes (mm)
*   RDT       = the fraction of total extraction removed from each cell
*   RWC       = relative available soil water content
*
*   S         = soil water extraction (1/hr)
*   SINIT     = used to read initial constant soil water extraction
*               from the data file INITIAL.DAT (1/hr)
*   SOILTP    = character variable used to read the soil name
*   STORAGE   = soil water storage in the soil profile (mm)
*   STORCHK   = initial storage plus sum of flows in and flows out (mm)
*   STORDEL   = change in storage between initial and current (mm)
*   STRINIT   = initial storage of the soil profile (mm)
*   SUMOFS    = the sum of the extraction before linear adjustment (mm3/hr)
*   SUNRISE   = time (0-24) that the extraction cycle begins (hr)
*   SUNSET    = time (0-24) that the extraction cycle ends (hr)
*   SWC       = array holding specific water capacity (1/mm)
*   SWCTAB    = tabulate specific water capacity (1/mm)
*
*   TAREA     = the total surface area of the soil profile (mm2)
*   TIME      = current time (hr)
*   TIME24    = 24 hr time counter (hr)
*   TIMEND    = end time of the simulation in hours from start (hr)
*
*   VN        = the n parameter in van Genuchten's equation
*
```

```
*   WC        = water content of a grid (mm/mm)
*   WCFC      = water content at field capacity (mm/mm)
*   WCR       = residual water content (mm/mm)
*   WCS       = saturated water content (mm/mm)
*   WCWP      = water content at wilting point (mm/mm)
*   WCTAB     = tabulated water contents (mm/mm)
*   WIDTH     = the width of the soil profile in the x-direction
*
*   ZETA      = maximum allowable change in water content in any grid
*
```

```
C TWO-DIMENSIONAL MODEL TO SIMULATE SOIL WATER INFILTRATION,
C REDISTRIBUTION, AND EXTRACTION.
C Written in Micrsoft FORTRAN for PC-compatible machines

C
      PARAMETER (IS=21, JS=21)
      IMPLICIT REAL (K)
      REAL LENGTH
C
      COMMON /DIMEN/  BOTTOM,DEPTH(JS),LENGTH,RADIUS(IS),TAREA,WIDTH
      COMMON /EXTRCT/ DRAIN,EXTRACT,S(JS,IS)
      COMMON /FLOW/   FLOWIN,Q(JS,IS),QB(IS),QL(JS),QR(JS),QS(IS)
      COMMON /GRID/   DX(IS),DZ(JS),IX,JZ
      COMMON /HEADS/  H(JS,IS),HBOT,LOWBC
      COMMON /HYDROL/ K1(JS,IS),K2(JS,IS),K3(JS,IS),K4(JS,IS)
      COMMON /MASSBL/ DELTA,ERRMASS,STORAGE,STORCHK,STORDEL,STRINIT
      COMMON /PARAMS/ COND(JS,IS),SWC(JS,IS),WC(JS,IS)
      COMMON /SOILS1/ FA,FB,ISOIL,NDATA
      COMMON /SOILS2/ ALPHA,VN,CONDS,WCR,WCS
      COMMON /SRATE/  ETP(60),RDT(JS,IS),SUNRISE,SUNSET,WCFC,WCWP
      COMMON /TABLES/ HTAB(120),WCTAB(120),SWCTAB(120),CONTAB(120)
      COMMON /TIME/   IDAY,DT,DTMAX,DTMIN,MONTH,TIME,TIME24,TIMEND
C
      NITER  = 0
      ICOUNT = 0
C
      OPEN (UNIT=7, FILE='twodim.out')
      OPEN (UNIT=8, FILE='heads.out')
C
C UPDAT1 is used to update the soil properties of the lysimeter soils.
C UPDAT2 is used to update the soil properties of the other soils.
C
      CALL INPUT(ITERMAX)
      IF(ISOIL .LE. 3) THEN
         CALL UPDAT1
      ELSE
         CALL UPDAT2
      END IF
      CALL CONDUC(0)
      CALL MASBAL(0)
      CALL ROOT
C
C -----------------------------------------------------------------------
C Beginning of simulation loop
C -----------------------------------------------------------------------
C
C
98    CONTINUE
C
```

```
C ---------------------------------------------------------------------
C Write the soil profile summary.  Initial set of output will
C give the initial conditions.
C
      IF (TIME.GE.TIMEND) GOTO 599
C
C     This GO TO statement is used to print out the output of
C     every iteration.
C     GO TO 599
C
C Output is printed every ICOUNT number of iterations.
C
      IF (ICOUNT .EQ. 100 .OR. ICOUNT .EQ. 0) THEN
         ICOUNT = 0
         GO TO 599
      END IF
C
      GO TO 699
C
C
599   WRITE(*,11) TIME,DT,NITER
11    FORMAT(' TIME = ',F12.7,'   DT = ',F10.7,'   ITERATION = ',I5)
C
      WRITE(7,600) TIME24,IDAY,TIME,DT,NITER
600   FORMAT('Time =',4X,F11.7,' hr',2x,'Day =',I2,7X,
     &       'Cumulative Time =',F12.7,' hrs',/,
     &       'Time Step =',F10.7,' hr',16X,'Iteration = ',I5,/)
C
      WRITE(7,610)STRINIT,STORAGE,STORDEL,FLOWIN,EXTRACT,DRAIN
610   FORMAT('Initial Storage',20X,E13.7,' mm3',/,
     &       'Current Storage',20X,E13.7,' mm3',/,
     &       'Change in Storage',18X,E13.7,' mm3',/,
     &       'Sum of Surface Fluxes',14X,E13.7,' mm3',/,
     &       'Sum of Root Extractions',12X,E13.7,' mm3',/,
     &       'Sum of Drainage Extractions',8X,E13.7,' mm3')
C
      WRITE(7,620)DELTA,STORCHK,ERRMASS
620   FORMAT('Sum of Surface Fluxes - Extractions',E13.7,' mm3',/,
     &       'Initial Storage + Sum',14X,E13.7,' mm3',/,
     &       'Mass Balance Error',17X,E13.7,' mm3',/)
C
      WRITE(7,630) QS(1),QB(1)
630   FORMAT('Inflow Rate at Upper Surface  =',E13.7,' mm/hr',/
     &       'Outflow Rate at Lower Surface =',E13.7,' mm/hr',//)
C
         WRITE(7,645) (RADIUS(I), I=1,IX)
645      FORMAT(6X,25F9.2)
C
      DO 10 J=1,JZ
         WRITE(7,650) DEPTH(J), (H(J,I), I=1,IX)
650      FORMAT(F6.1,25F9.2)
10    CONTINUE
```

```
C     ---------------------------------------------------------------
C     This section outputs the heads of 10 cells that correspond to the

C     10 tensiometer locations
C
      H50  = (H(13,3)  + H(14,3)) / 2
      H150 = (H(13,8)  + H(14,8)) / 2
      H250 = (H(13,13) + H(14,13)) / 2
      WRITE(8,655) MONTH,IDAY,TIME24;H(5,3), H(5,8), H(5,13),
     &             H(10,3),H(10,8),H(10,13),H50,H150,H250,H(18,8)
655   FORMAT(2I4,F9.4,10F9.1)
C     ---------------------------------------------------------------
C
C
      IF (LOWBC.EQ.1) GO TO 97
C
         WRITE(7,660) DEPTH(JZ+1), (H(JZ+1,I), I=1,IX)
660      FORMAT(F6.1,25F9.2)
C
97    WRITE(7,670)
670   FORMAT(///)
C
699   IF (TIME.GE.TIMEND) GOTO 99
C
C
      IF (NITER.GE.ITERMAX) THEN
         WRITE(*,*) '  The maximum number of iterations is exceeded.',
     &              '  The program is terminated !'
         GO TO 99
      END IF
C
      CALL ETDIST
      CALL TSTEP
      CALL REDIST
      IF(ISOIL .LE. 3) THEN
         CALL UPDAT1
      ELSE
         CALL UPDAT2
      END IF
      CALL CONDUC(1)
      CALL MASBAL(1)
C
C Count the number of iterations
C
      NITER = NITER + 1
      ICOUNT = ICOUNT + 1
C
      GO TO 98
C
99    STOP
      END
```

```
C ***********************************************************************
C
      SUBROUTINE INPUT(ITERMAX)
C
C This subroutine reads in the input and initial values of the
C variables from the files INITIAL.DAT and INITHEAD.DAT.
C     INITIAL.DAT contains inital values for variables such as
C     the depth of the soil profile (BOTTOM), the width of the
C     profile (WIDTH), and the surface flux (QS).
C     INITHEAD.DAT is used to input initial pressure heads (H)
C     when a nonuniform initial conditions are desired.
C
C ***********************************************************************
C
C
      PARAMETER (IS=21, JS=21)
      REAL LENGTH
      CHARACTER*15 SOILTP
C
      COMMON /DIMEN/  BOTTOM,DEPTH(JS),LENGTH,RADIUS(IS),TAREA,WIDTH
      COMMON /EXTRCT/ DRAIN,EXTRACT,S(JS,IS)
      COMMON /FLOW/   FLOWIN,Q(JS,IS),QB(IS),QL(JS),QR(JS),QS(IS)
      COMMON /GRID/   DX(IS),DZ(JS),IX,JZ
      COMMON /HEADS/  H(JS,IS),HBOT,LOWBC
      COMMON /MASSBL/ DELTA,ERRMASS,STORAGE,STORCHK,STORDEL,STRINIT
      COMMON /PARAMS/ COND(JS,IS),SWC(JS,IS),WC(JS,IS)
      COMMON /SOILS1/ FA,FB,ISOIL,NDATA
      COMMON /SOILS2/ ALPHA,VN,CONDS,WCR,WCS
      COMMON /SRATE/  ETP(60),RDT(JS,IS),SUNRISE,SUNSET,WCFC,WCWP
      COMMON /TABLES/ HTAB(120),WCTAB(120),SWCTAB(120),CONTAB(120)
      COMMON /TIME/   IDAY,DT,DTMAX,DTMIN,MONTH,TIME,TIME24,TIMEND
C
C -----------------------------------------------------------------------
C Input the soil type and then open the appropriate soils' data
C file and read the soil hydraulic properties.
C -----------------------------------------------------------------------
C
C     This GO TO is used to bypass soil selection
C     GO TO 911
C
      WRITE(*,110)
110   FORMAT(1X,'The eight soils listed below are available',/1x,
     &          'for the simulation.  Enter your selection',/1x,
     &          'below and press <ENTER>.',2(/))
C
      WRITE(*,120)
120   FORMAT(1X,'1.  Astatula f.s.',/1x,'2.  Builders sand',/1x,
     &          '3.  Pomona sand',/1x,'4.  Arredondo f.s.',/1x,
     &          '5.  Rehevot sand',/1x,'6.  Adelanto loam',/1x,
     &          '7.  Pachappa loam',/1x,'8.  Yolo light clay',2(/))
C
      READ(*,*) ISOIL
```

```
C
C  Open the corresponding soils data file
C
      GO TO (901,902,903,904,905,906,907,908), ISOIL
C
901       VN    = 3.52816
          ALPHA = 0.03265
          CONDS = 42.835
          WCR   = 0.030
          WCS   = 0.412
          WCFC  = 0.095
          WCWP  = 0.030
          SOILTP = 'ASTATULA F.S.'
          GO TO 911
C
902       VN    = 6.58530
          ALPHA = 0.03166
          CONDS = 53.607
          WCR   = 0.010
          WCS   = 0.348
          WCFC  = 0.034
          WCWP  = 0.010
          SOILTP = 'BUILDERS SAND'
          GO TO 911
C
903       VN    = 3.00943
          ALPHA = 0.02946
          CONDS = 12.977
          WCR   = 0.100
          WCS   = 0.538
          WCFC  = 0.149
          WCWP  = 0.100
          SOILTP = 'POMONA SAND'
          GO TO 911
C
904       OPEN (UNIT=1, FILE='arredond.dat', STATUS='OLD')
          NDATA = 118
          FA = 4.
          FB = 8.1
          WCFC  = 0.084
          WCWP  = 0.030
          SOILTP = 'ARREDONDO F.S.'
          GO TO 910
C
905       OPEN (UNIT=1, FILE='rehevot.dat', STATUS='OLD')
          NDATA = 59
          FA = 1.
          FB = 1.1
          WCFC  = 0.036
          WCWP  = 0.004
          SOILTP = 'REHEVOT SAND'
          GO TO 910
```

```
C
906       OPEN (UNIT=1, FILE='adelanto.dat', STATUS='OLD')
          NDATA = 49
          FA = 1.
          FB = 2.0
          WCFC  = 0.095
          WCWP  = 0.030
          SOILTP = 'ADELANTO LOAM'
          GO TO 910
C
907       OPEN (UNIT=1, FILE='pachappa.dat', STATUS='OLD')
          NDATA = 49
          FA = 1.
          FB = 2.
          WCFC  = 0.095
          WCWP  = 0.030
          SOILTP = 'PACHAPPA LOAM'
          GO TO 910
C
908       OPEN (UNIT=1, FILE='yoloclay.dat', STATUS='OLD')
          NDATA = 49
          FA = 1.
          FB = 1.1
          WCFC  = 0.340
          WCWP  = 0.070
          SOILTP = 'YOLO LIGHT CLAY'
C
C
C Read the soil parameters for the selected soil from the appropriate
C data file.  These parameters will be used for the table search in
C subroutine UPDAT2
C
910    READ(1,140)
140    FORMAT(5(/))
       READ(1,150) (HTAB(J),WCTAB(J),SWCTAB(J),CONTAB(J),J=1,NDATA)
150    FORMAT(4(3X,E12.5))
C
C
C ---------------------------------------------------------------------
C Interactive input of model parameters
C
911    WRITE(*,160)
160    FORMAT(//1X,'Enter the number of iterations and press <ENTER>.',/)

C
       READ(*,*)ITERMAX
C
C
```

```
      WRITE(*,180)
180   FORMAT(/,' Enter the simulation beginning day and press <ENTER>.',

     &       /,' The day must be an integer greater than 0 with',
     &         ' day=1 corresponding to',
     &       /,' May 01 and day=32 corresponding to June 01, etc.',/)
C
      READ(*,*)IDAY
C
      WRITE(*,200)
200   FORMAT(/,' Enter the simulation beginning time and press <ENTER>.'

     &      ,/,' Time must be given as a number from 0 to 24.',/)
C
      READ(*,*) TIME
C
      WRITE(*,220)
220   FORMAT(/,' Enter the simulation ending time in number of hours sin

     &ce the beginning time',/' and press <ENTER>.',/)
C
      READ(*,*)TIMEND
C
C
      TIME24 = TIME
      MONTH = 5 + IDAY / 32
C
C
C ---------------------------------------------------------------------
C
C Open data file containing initial information
C
      OPEN (UNIT=2, FILE='init2-d.dat', STATUS='OLD')
C
C
C Read in the minimum and maximum allowable timesteps, DTMIN and
C DTMAX.
C
      READ(2,250) DTMIN, DTMAX
250   FORMAT(5(/),2(2X,F9.2))
C
C Read in the Upper Boundary condition, QSINIT, and the application
C rate, QSIRR.
C
      READ(2,260) QSINIT,QSIRR
260   FORMAT(7(/),2(2X,F9.2))
C
C Read in the the type of lower boundary condition, LOWBC, where
C LOWBC=0 means a constant potential B.C. and
C LOWBC=1 means a constant flux B.C.
C and the flux, QBINIT, across the bottom boundary.
C If LOWBC=0, QBINIT should also be 0.
```

```
C
      READ(2,285) LOWBC,QBINIT
285   FORMAT(9(/),2X,I9,2X,F9.2)
C
C Read in the left, QLINIT, and the right, QRINIT, boundary conditions.

C Also read QLIRR, the application rate of a buried line source.
C
      READ(2,265) QLINIT,QRINIT,QLIRR
265   FORMAT(7(/),3(2X,F9.2))
C
C Read in the constant extraction rate, SINIT, in units of 1/hr.
C Extraction is not permitted in the grid immediately above the
C water table.
C
      READ(2,280) SINIT
280   FORMAT(7(/),2X,F9.2)
C
C Read the desired profile depth, BOTTOM (z-dimension),
C the profile width, WIDTH (x-dimension), and the
C length (y-dimension usually taken as 1).
C
      READ(2,270) BOTTOM,WIDTH,LENGTH
270   FORMAT(11(/),3(2X,F9.2))
C
C TAREA = the total surface area of the profile
C
      TAREA = WIDTH * LENGTH
C
C  Read the number of cells in the z (vertical) and x (horizontal)
C  directions.
C
      READ(2,275) JZ,IX
275   FORMAT(6(/),2(2X,I9))
C
C Initialize various variables.
C
      DO 40 J=1,JZ-1
      DO 40 I=1,IX
          S(J,I) = SINIT
40    CONTINUE
C
C Assign DZ to each cell.  Because nonuniform cell sizes are used,
C the grid sizes can not be directly computed.
C
      DO 10 J=1,10
         DZ(J) = 20.0
         QL(J) = QLINIT
         QR(J) = QRINIT
10    CONTINUE
         DZ(1) = 30.0
C
```

```
      DO 11 J=11,14
         DZ(J) = 30.0
         QL(J) = QLINIT
         QR(J) = QRINIT
11    CONTINUE
C
      DO 12 J=15,17
         DZ(J) = 50.0
         QL(J) = QLINIT
         QR(J) = QRINIT
12    CONTINUE
C

      DO 13 J=18,20
         DZ(J) = 100.0
         QL(J) = QLINIT
         QR(J) = QRINIT
13    CONTINUE
         DZ(JZ) = 40.0
         DZ(JZ+1) = 30.0
C
C Depth calculations
C
      DEPTH(1) = DZ(1) / 2
      DO 20 J=2,JZ+1
         DEPTH(J) = DEPTH(J-1) + ( DZ(J-1) + DZ(J) ) / 2
20    CONTINUE
C
C Assign DX to each cell
C
      DO 15 I=1,14
         DX(I) = 20.0
         QS(I) = QSINIT
         QB(I) = QBINIT
         S(JZ,I) = 0.0
15    CONTINUE
         DX(14) = 40.0
         QS(1) = QSIRR
C
      DO 16 I=15,19
         DX(I) = 50.0
         QS(I) = QSINIT
         QB(I) = QBINIT
         S(JZ,I) = 0.0
16    CONTINUE
C
      DO 17 I=20,21
         DX(I) = 100.0
         QS(I) = QSINIT
         QB(I) = QBINIT
         S(JZ,I) = 0.0
17    CONTINUE
```

```
C
C Calculation of horizotal distance from the origin (line source)
C
      RADIUS(1) = DX(1) / 2
      DO 25 I=2,IX
         RADIUS(I) = RADIUS(I-1) + ( DX(I-1) + DX(I) ) / 2
25    CONTINUE
C
C ---------------------------------------------------------------------
C
C Ask what type of Initial Conditions will be used.
C        1. Uniform Initial Conditions with user specified HINIT.
C        2. Nonuniform Initial Conditions read from a data file.
C
      WRITE(*,230)
230   FORMAT(/,' What type of Initial Conditions will be used?',//7x,
     & ' 1.  Uniform Initial Conditions with user specified HINIT.',/7X,

     & ' 2.  Nonuniform Initial Conditions read from a data file.',//,
     & ' Choose the number of your option and press <ENTER>.',/)
C
      READ(*,*) IOPTION
C
C If IOPTION=1, uniform initial conditions will be used and the
C pressure head of the bottom boundary, HBOT, is read from the
C file INITIAL.DAT.  In the case of a flux bottom B.C., HBOT is
C still read, but is not used again.
C
C If IOPTION=2, nonuniform initial conditions are read from
C INITHEAD.DAT including HBOT. A minimum of JZ and a maximum of
C JZ+1 initial pressure heads are read.
C If a flux bottom B.C.condition is used, only JZ initial
C pressure heads are read ending with the node above the boundary.
C
      GO TO (921,922) IOPTION
C
C ---------------------------------------------------------------------
C
C Read in the Lower Boundary Condition, HBOT.
C
921   READ(2,290) HBOT
290   FORMAT(6(/),2X,F9.2)
C
C Input the Initial Conditions (Pressure Heads), HINIT, in mm,
C to be used in the simulation.
C
      WRITE(*,240)
240   FORMAT(/,' Enter the Initial Condition in terms of a pressure head

     &, H, in mm,',/' and press <ENTER>.',/)
C
      READ(*,*) HINIT
```

```
C
      DO 30 I=1,IX
         H(JZ+1,I) = HBOT
      DO 30 J=1,JZ
          H(J,I) = HINIT
30    CONTINUE
C
      GO TO 923
C
C ---------------------------------------------------------------------
C

922   OPEN (UNIT=3, FILE='inithead.dat', STATUS='OLD')
C
      READ(3,300)
300   FORMAT(31(/))
C
      DO 50 J=1,JZ
         READ(3,310) (H(J,I), I=1,IX)
310      FORMAT(6X,25F9.2)
50    CONTINUE
C
      IF (LOWBC.EQ.1) GO TO 923
C
      READ(3,320) HBOT
320   FORMAT(6X,F9.2)
C
      DO 60 I=1,IX
         H(JZ+1,I) = HBOT
60    CONTINUE
C
C ---------------------------------------------------------------------
C Read in the weather data, i.e. ETP, SUNRISE, SUNSET
C
923   OPEN (UNIT=4, FILE='weather.dat', STATUS='OLD')
C
      READ(4,1110) SUNRISE,SUNSET
1110  FORMAT(2(/),8X,F7.3,/8X,F7.3,6(/))
C
      IF(ISOIL .EQ. 1 .OR. ISOIL .EQ. 4 .OR. ISOIL .EQ. 5) THEN
         DO 1120 I=1,57
            READ(4,1130) ETP(I)
1130        FORMAT(18X,F15.2)
1120     CONTINUE
         GO TO 926
      END IF
C
      IF(ISOIL .EQ. 2) THEN
         DO 1140 I=1,57
            READ(4,1150) ETP(I)
1150        FORMAT(36X,F15.2)
1140     CONTINUE
```

```
         GO TO 926
      END IF
C
      IF(ISOIL.EQ.3 .OR.ISOIL.EQ.6 .OR.ISOIL.EQ.7 .OR.ISOIL.EQ.8) THEN
         DO 1160 I=1,57
            READ(4,1170) ETP(I)
1170        FORMAT(54X,F15.2)
1160     CONTINUE
      END IF
C
C -----------------------------------------------------------------------
C
C Write the initial parameters for the simulation.
C
926   WRITE(7,600) SOILTP,QSINIT
600   FORMAT('TWO-DIMENSIONAL SIMULATION OF A SOIL PROFILE',//,
     &       'Soil:  ',A,//,
     &       'Upper Boundary condition at Soil Surface:  Flux Density ='

     &       ,F10.4,' mm/hr')
C
      IF (LOWBC.EQ.1) GO TO 604
C
      WRITE(7,603) DEPTH(JZ+1),HBOT,QLINIT,QRINIT
603   FORMAT('Lower Boundary condition at Depth of ',F6.1,' mm:  ',
     &       'Matric Potential =',F7.1,' mm',/,
     &       'Left  Boundary condition at I = 1/2:      Flux Density =',

     &        F10.4,' mm/hr',/,
     &       'Right Boundary condition at I = IX+1/2:  Flux Density =',

     &        F10.4,' mm/hr',/)
C
      WRITE(7,610)JZ,BOTTOM,IX
610   FORMAT('The Number Of Vertical Increments = ',I3,/,
     &       'Depth To Water Table = ',F6.1,' mm',/,
     &       'The Number Of Radial Increments   = ',I3,/)
C
      GO TO 619
C
604   WRITE(7,605) BOTTOM,QBINIT,QLINIT,QRINIT
605   FORMAT('Lower Boundary condition at Depth of ',F6.1,' mm:  ',
     &       'Flux Density =',F6.1,' mm/hr',/,
     &       'Left  Boundary condition at I = 1/2:      Flux Density =',

     &        F10.4,' mm/hr',/,
     &       'Right Boundary condition at I = IX+1/2:  Flux Density =',

     &        F10.4,' mm/hr',/)
C
```

```
611   WRITE(7,612)JZ,IX
612   FORMAT('The Number Of Vertical Increments = ',I3,/,
     &       'The Number Of Radial Increments   = ',I3,/)
C
619   WRITE(7,620) TIME,TIMEND
620   FORMAT('Begin Time =',F9.4,' hr',16x,'End Time =',7X,F12.7,' hrs')


      RETURN
      END
```

```
C ***********************************************************************
C
      SUBROUTINE ROOT
C
C This subroutine computes the root distributin term, RDT,
C for each cell in the profile.  The RDT corresponds to the
C fraction of the evapotranspiration rate, ETRATE, extracted
C from each cell.
C
C ***********************************************************************
C
C
      PARAMETER (IS=21, JS=21)
C
      COMMON /EXTRCT/ DRAIN,EXTRACT,S(JS,IS)
      COMMON /GRID/   DX(IS),DZ(JS),IX,JZ
      COMMON /PARAMS/ COND(JS,IS),SWC(JS,IS),WC(JS,IS)
      COMMON /SRATE/  ETP(60),RDT(JS,IS),SUNRISE,SUNSET,WCFC,WCWP
      COMMON /TIME/   IDAY,DT,DTMAX,DTMIN,MONTH,TIME,TIME24,TIMEND
C
C ---------------------------------------------------------------------
C
      DO 10 J=1,JZ
      DO 10 I=1,IX
         RDT(J,I) = 0.0
10    CONTINUE
C
C ---------------------------------------------------------------------
C
      DO 20 J=1,5
C
         DO 30 I=1,5
            RDT(J,I) = 0.50 / 25
30       CONTINUE
C
         DO 40 I=6,10
            RDT(J,I) = 0.17 / 25
40       CONTINUE
C
         DO 50 I=11,14
            RDT(J,I) = 0.02 / 25
50       CONTINUE
C
20    CONTINUE
C
      DO 70 J=6,10
C
         DO 80 I=1,5
            RDT(J,I) = 0.10 / 25
80       CONTINUE
C
```

```
          DO 90 I=6,10
             RDT(J,I) = 0.04 / 25
90        CONTINUE
C
          DO 100 I=11,14
             RDT(J,I) = 0.01 / 25
100       CONTINUE
C
70     CONTINUE
C
       DO 120 J=11,15
C
          DO 130 I=1,5
             RDT(J,I) = 0.05 / 25
130       CONTINUE
C
          DO 140 I=6,10
             RDT(J,I) = 0.01 / 25
140       CONTINUE
C
          DO 150 I=11,14
             RDT(J,I) = 0.00 / 20
150       CONTINUE
C
120    CONTINUE
C
       DO 170 J=16,19
       DO 170 I=1,14
          RDT(J,I) = 0.00 / 56
170    CONTINUE
C
       J = 14
       DO 190 I=19,21
          RDT(J,I) = 0.10 / 3
190    CONTINUE
C
       RETURN
       END
```

```
C ***********************************************************************
C
      SUBROUTINE ETDIST
C
C This subroutine uses daily potential evapotranspiration to
C compute an evapotranspiration rate for the soil profile.
C that is distributed over the day with a sinusoidal function.
C From that, the extraction rate of each cell is computed and
C linearly adjusted to meet the daily evapotranspiration rate.
C
C ***********************************************************************
C
      PARAMETER (IS=21, JS=21)
      REAL LENGTH
C
      COMMON /DIMEN/  BOTTOM,DEPTH(JS),LENGTH,RADIUS(IS),TAREA,WIDTH
      COMMON /EXTRCT/ DRAIN,EXTRACT,S(JS,IS)
      COMMON /GRID/   DX(IS),DZ(JS),IX,JZ
      COMMON /TIME/   IDAY,DT,DTMAX,DTMIN,MONTH,TIME,TIME24,TIMEND
      COMMON /SRATE/  ETP(60),RDT(JS,IS),SUNRISE,SUNSET,WCFC,WCWP
      COMMON /PARAMS/ COND(JS,IS),SWC(JS,IS),WC(JS,IS)
C
C -----------------------------------------------------------------------
C Computation of total profile evapotranspiration rate, ETRATE, at
C a given time with a sinusoidal distribution of daily potential
C evapotranspiration, ETP.
C -----------------------------------------------------------------------
C
      PI = 3.141592654
      DAYLITE = SUNSET - SUNRISE
      OMEGA   = 2 * PI / DAYLITE
      DAYTIME = TIME24 - SUNRISE
C
      IF(TIME24 .LT. SUNRISE .AND. IDAY .GT. 1) THEN
         ET = ETP(IDAY-1)
      ELSE
         ET = ETP(IDAY)
      END IF
      ETMAX   = 2 * ET / DAYLITE
C
      ETRATE = (ETMAX / 2) * SIN( OMEGA*DAYTIME - PI/2 ) + ETMAX/2
C
C -----------------------------------------------------------------------
C Computation of soil water extraction rate, S(J,I), and linear
C adjustment of the sum of S(J,I) over all cells, SUMOFS, to make
C sure that the total evapotranspiration rate, ETRATE, is met.
C -----------------------------------------------------------------------
C
      IF(ETRATE .EQ. 0.0) THEN
         DO 10 J=1,JZ-1
         DO 10 I=1,IX
            S(J,I) = 0.0
```

```
10        CONTINUE
          RETURN
       END IF
C
       CC      = 10.0
       SUMOFS =  0.0
C
       DO 20 J=1,JZ-1
       DO 20 I=1,IX
C
          RWC = (WC(J,I) - WCWP) / (WCFC - WCWP)
          IF(RWC .GT. 1.0) RWC = 1.0
C
          IF(RWC .LE. 0.0) THEN
             S(J,I) = 0.0
             GO TO 20
          END IF
C
C Compute the fraction of the ETrate to be extracted at each cell
C in terms of mm3/hr -- a function of the root distribution term, RDT.
C
          FRACTN = ETRATE * TAREA * RDT(J,I)
C
C Compute the extraction of each cell in terms of mm3/hr as modified by

C the relative available soil water content term.
C
          S(J,I) = FRACTN * RWC**(ETRATE / RWC / CC)
          SUMOFS = SUMOFS + S(J,I)
C
20     CONTINUE
C
C Linear adjustment -- CF is the correction factor that forces the
C computed total profile extraction rate to equal the predetermined
C ETrate.
C
       IF(SUMOFS .EQ. 0.0) THEN
          CF = 1.0
       ELSE
          CF = ETRATE * TAREA / SUMOFS
       END IF
C
C Computation of the corrected cell extraction rate and conversion to
C units of mm/(mm-hr).
C
       DO 30 J=1,JZ-1
       DO 30 I=1,IX
          S(J,I) = S(J,I) * CF / DZ(J) / (DX(I) * LENGTH)
30     CONTINUE
C
       RETURN
       END
```

```
C ***********************************************************************
C
      SUBROUTINE MASBAL(NPASS)
C
C This subroutine computes the mass balance of the soil profile
C two different ways to check the stability of the model.
C Method one sums the water contents of each grid in the soil profile.
C Method two adds the sum (DELTA) of total inflows, drainage, and root
C extractions to the inital storage, STRINIT,
C ERRMASS, the mass balance error, is the difference between the two.
C
C ***********************************************************************
C
      PARAMETER (IS=21, JS=21)
      REAL LENGTH
C
      COMMON /DIMEN/  BOTTOM,DEPTH(JS),LENGTH,RADIUS(IS),TAREA,WIDTH
      COMMON /EXTRCT/ DRAIN,EXTRACT,S(JS,IS)
      COMMON /FLOW/   FLOWIN,Q(JS,IS),QB(IS),QL(JS),QR(JS),QS(IS)
      COMMON /GRID/   DX(IS),DZ(JS),IX,JZ
      COMMON /HEADS/  H(JS,IS),HBOT,LOWBC
      COMMON /MASSBL/ DELTA,ERRMASS,STORAGE,STORCHK,STORDEL,STRINIT
      COMMON /PARAMS/ COND(JS,IS),SWC(JS,IS),WC(JS,IS)
      COMMON /TIME/   IDAY,DT,DTMAX,DTMIN,MONTH,TIME,TIME24,TIMEND
C
C Initialize the cumulative infiltration and extraction
C
C
C
      IF(NPASS.EQ.0) THEN
         FLOWIN  = 0.0
         EXTRACT = 0.0
         DRAIN   = 0.0
         STORAGE = 0.0
         DELTA   = 0.0
         STORCHK = 0.0
C
         DO 10 J=1, JZ
         DO 10 I=1, IX
            STORAGE = STORAGE + WC(J,I) * DZ(J) * DX(I) * LENGTH
10       CONTINUE
C
         STRINIT = STORAGE
         STOROLD  = STORAGE
         RETURN
      ENDIF
C
C Compute cumulative infiltration and extraction
C
      FLUX    = 0.0
      STORAGE = 0.0
      UPTAKE  = 0.0
```

```
C
      DO 20 J=1, JZ-1
      DO 20 I=1, IX
         STORAGE = STORAGE + WC(J,I) * DZ(J) * DX(I) * LENGTH
         UPTAKE  = UPTAKE + S(J,I) * DT * DZ(J) * DX(I) * LENGTH
         FLUX = FLUX + ( QL(J) - QR(I) ) * DZ(J) * DT * LENGTH
20    CONTINUE
C
      DO 30 I=1, IX
         STORAGE = STORAGE + WC(JZ,I) * DZ(JZ) * DX(I) * LENGTH
         FLUX = FLUX + ( QS(I) - QB(I) ) * DX(I) * DT * LENGTH
         DRAIN   = DRAIN + S(JZ,I) * DZ(JZ) * DX(I) * DT * LENGTH
30    CONTINUE
C
      FLOWIN = FLOWIN + FLUX
      EXTRACT = EXTRACT + UPTAKE
      DELTA =  FLOWIN - EXTRACT - DRAIN
      STORCHK = STRINIT + DELTA
      STORDEL = STORAGE - STRINIT
      ERRMASS = STORAGE - STORCHK
C
      STOROLD  = STORAGE
C
      RETURN
      END
C
```

```
C ***************************************************************************
C
      SUBROUTINE CONDUC(NPASS)
C
C This subroutine determines the conductivity at the four surfaces of
C each cell, K1, K2, K3, K4.  At the initial pass (NPASS=0) it will
C compute the initial K's for all cells and assign values of zero to
C the Ks of the cells above the furrow area (atmosphere cells).
C
C For the remaining passes, (NPASS=1), only the K's of the actual cells

C (cells in the soil profile) will be computed.
C
C ***************************************************************************
C
      PARAMETER (IS=21, JS=21)
      IMPLICIT REAL (K)
C
      COMMON /GRID/   DX(IS),DZ(JS),IX,JZ
      COMMON /HEADS/  H(JS,IS),HBOT,LOWBC
      COMMON /HYDROL/ K1(JS,IS),K2(JS,IS),K3(JS,IS),K4(JS,IS)
      COMMON /PARAMS/ COND(JS,IS),SWC(JS,IS),WC(JS,IS)
C
      I1 = 14
      J1 = 2
      J2 = 5
      J3 = 9
      J4 = 12
      J5 = 13
      J6 = 14
C
C ---------------------------------------------------------------------
C Initial computation of hydraulic conductivities at cell boundaries.
C Zero assigned to Ks of non soil profile cells.
C ---------------------------------------------------------------------
C
C
      IF(NPASS.EQ.0) THEN
C
         DO 10 J=1,J1
            DO 20 I=2,I1
               IF(J .EQ. 1) THEN
                  K1(J,I) = 0.0
               ELSE
                  K1(J,I) = (COND(J,I) + COND(J-1,I))/2
               END IF
               K2(J,I) = (COND(J,I) + COND(J+1,I))/2
               K3(J,I) = (COND(J,I) + COND(J,I-1))/2
               K4(J,I) = (COND(J,I) + COND(J,I+1))/2
20          CONTINUE
            K4(J,I1) = 0.0
C
```

```
            DO 30 I=I1+1,IX
               K1(J,I) = 0.0
               K2(J,I) = 0.0
               K3(J,I) = 0.0
               K4(J,I) = 0.0
30          CONTINUE
10       CONTINUE
C
         K1(1,1) = 0.0
         K2(1,1) = (COND(1,1) + COND(2,1))/2
         K3(1,1) = 0.0
         K4(1,1) = (COND(1,1) + COND(1,2))/2
C
         I2 = I1 + 1
         JB = J1 + 1
         DO 40 J=JB,J2
            DO 50 I=2,I2
               K1(J,I) = (COND(J,I) + COND(J-1,I))/2
               K2(J,I) = (COND(J,I) + COND(J+1,I))/2
               K3(J,I) = (COND(J,I) + COND(J,I-1))/2
               K4(J,I) = (COND(J,I) + COND(J,I+1))/2
50          CONTINUE
            K4(J,I2) = 0.0
C
            DO 60 I=I2+1,IX
               K1(J,I) = 0.0
               K2(J,I) = 0.0
               K3(J,I) = 0.0
               K4(J,I) = 0.0
60          CONTINUE
C
40       CONTINUE
            K1(JB,I2) = 0.0
C
         I3 = I2 + 1
         JB = J2 + 1
         DO 70 J=JB,J3
            DO 80 I=2,I3
               K1(J,I) = (COND(J,I) + COND(J-1,I))/2
               K2(J,I) = (COND(J,I) + COND(J+1,I))/2
               K3(J,I) = (COND(J,I) + COND(J,I-1))/2
               K4(J,I) = (COND(J,I) + COND(J,I+1))/2
80          CONTINUE
            K4(J,I3) = 0.0
C
            DO 90 I=I3+1,IX
               K1(J,I) = 0.0
               K2(J,I) = 0.0
               K3(J,I) = 0.0
               K4(J,I) = 0.0
90          CONTINUE
C
```

```
70      CONTINUE
           K1(JB,I3) = 0.0
C
        I4 = I3 + 1
        JB = J3 + 1
        DO 100 J=JB,J4
           DO 110 I=2,I4
              K1(J,I) = (COND(J,I) + COND(J-1,I))/2
              K2(J,I) = (COND(J,I) + COND(J+1,I))/2
              K3(J,I) = (COND(J,I) + COND(J,I-1))/2
              K4(J,I) = (COND(J,I) + COND(J,I+1))/2
110        CONTINUE
           K4(J,I4) = 0.0
C
           DO 120 I=I4+1,IX
              K1(J,I) = 0.0
              K2(J,I) = 0.0
              K3(J,I) = 0.0
              K4(J,I) = 0.0
120        CONTINUE
C
100     CONTINUE
           K1(JB,I4) = 0.0
C
        I5 = I4 + 1
        JB = J4 + 1
        J = JB
           DO 140 I=2,I5
              K1(J,I) = (COND(J,I) + COND(J-1,I))/2
              K2(J,I) = (COND(J,I) + COND(J+1,I))/2
              K3(J,I) = (COND(J,I) + COND(J,I-1))/2
              K4(J,I) = (COND(J,I) + COND(J,I+1))/2
140        CONTINUE
           K4(J,I5) = 0.0
C
           DO 150 I=I5+1,IX
              K1(J,I) = 0.0
              K2(J,I) = 0.0
              K3(J,I) = 0.0
              K4(J,I) = 0.0
150        CONTINUE
              K1(JB,I5) = 0.0
C
        I6 = I5 + 1
        JB = J5 + 1
        DO 160 J=JB,JZ-1
        DO 160 I=2,IX-1
           K1(J,I) = (COND(J,I) + COND(J-1,I))/2
           K2(J,I) = (COND(J,I) + COND(J+1,I))/2
           K3(J,I) = (COND(J,I) + COND(J,I-1))/2
           K4(J,I) = (COND(J,I) + COND(J,I+1))/2
160     CONTINUE
```

```
C
         DO 180 I=I6,IX-1
            K1(JB,I) = 0.0
180      CONTINUE
C
         J = JZ
         IF (LOWBC.EQ.1) GO TO 69
C
C ---------------------------------------------------------------------
C Constant potential lower b.c. (HBOT=constant) at J=JZ+1/2
C ---------------------------------------------------------------------
C
         DO 190 I=1,IX
C
            IF(I .EQ. 1 ) THEN
               K1(J,I) = (COND(J,I) + COND(J-1,I))/2
               K2(J,I) = (COND(J,I) + COND(J+1,I))/2
               K3(J,I) = 0.0
               K4(J,I) = (COND(J,I) + COND(J,I+1))/2
               GO TO 190
            END IF
C
            IF(I .EQ. IX) THEN
               K1(J,I) = (COND(J,I) + COND(J-1,I))/2
               K2(J,I) = (COND(J,I) + COND(J+1,I))/2
               K3(J,I) = (COND(J,I) + COND(J,I-1))/2
               K4(J,I) = 0.0
               GO TO 190
            END IF
C
            K1(J,I) = (COND(J,I) + COND(J-1,I))/2
            K2(J,I) = (COND(J,I) + COND(J+1,I))/2
            K3(J,I) = (COND(J,I) + COND(J,I-1))/2
            K4(J,I) = (COND(J,I) + COND(J,I+1))/2
C
190      CONTINUE
C
         GO TO 200
C
C ---------------------------------------------------------------------
C Constant flux lower boundary condition (QB=constant) at J=JZ+1/2
C ---------------------------------------------------------------------
C
69       DO 210 I=1,IX
C
            IF(I .EQ. 1 ) THEN
               K1(J,I) = (COND(J,I) + COND(J-1,I))/2
               K2(J,I) = 0.0
               K3(J,I) = 0.0
               K4(J,I) = (COND(J,I) + COND(J,I+1))/2
               GO TO 210
            END IF
```

```
C
            IF(I .EQ. IX) THEN
               K1(J,I) = (COND(J,I) + COND(J-1,I))/2
               K2(J,I) = 0.0
               K3(J,I) = (COND(J,I) + COND(J,I-1))/2
               K4(J,I) = 0.0
               GO TO 210
            END IF
C
            K1(J,I) = (COND(J,I) + COND(J-1,I))/2
            K2(J,I) = 0.0
            K3(J,I) = (COND(J,I) + COND(J,I-1))/2
            K4(J,I) = (COND(J,I) + COND(J,I+1))/2
C
210      CONTINUE
C
C ---------------------------------------------------------------------
C  Constant flux boundary condition at the line of symmetry (I=1)
C ---------------------------------------------------------------------
C
200      I = 1
         DO 220 J=2,JZ-1
            K1(J,I) = (COND(J,I) + COND(J-1,I))/2
            K2(J,I) = (COND(J,I) + COND(J+1,I))/2
            K3(J,I) = 0.0
            K4(J,I) = (COND(J,I) + COND(J,I+1))/2
220      CONTINUE
C
C ---------------------------------------------------------------------
C  Constant flux b.c. at the right end of the lysimeter (I=IX)
C ---------------------------------------------------------------------
C
         I = IX
         DO 230 J=J6,JZ-1
            K1(J,I) = (COND(J,I) + COND(J-1,I))/2
            K2(J,I) = (COND(J,I) + COND(J+1,I))/2
            K3(J,I) = (COND(J,I) + COND(J,I-1))/2
            K4(J,I) = 0.0
230      CONTINUE
            K1(J6,I) = 0.0
C
         RETURN
      END IF
C
```

```
C ---------------------------------------------------------------------
C Computation of hydraulic conductivities at cell boundaries for each
C succeeding iteration.
C ---------------------------------------------------------------------
C
      DO 310 J=1,J1
         DO 320 I=2,I1
            IF(J .EQ. 1) THEN
               K1(J,I) = 0.0
            ELSE
               K1(J,I) = (COND(J,I) + COND(J-1,I))/2
            END IF
            K2(J,I) = (COND(J,I) + COND(J+1,I))/2
            K3(J,I) = (COND(J,I) + COND(J,I-1))/2
            K4(J,I) = (COND(J,I) + COND(J,I+1))/2
320      CONTINUE
         K4(J,I1) = 0.0
310   CONTINUE
C
      K2(1,1) = (COND(1,1) + COND(2,1))/2
      K4(1,1) = (COND(1,1) + COND(1,2))/2
C
      I2 = I1 + 1
      JB = J1 + 1
      DO 340 J=JB,J2
         DO 350 I=2,I2
            K1(J,I) = (COND(J,I) + COND(J-1,I))/2
            K2(J,I) = (COND(J,I) + COND(J+1,I))/2
            K3(J,I) = (COND(J,I) + COND(J,I-1))/2
            K4(J,I) = (COND(J,I) + COND(J,I+1))/2
350      CONTINUE
         K4(J,I2) = 0.0
340   CONTINUE
      K1(JB,I2) = 0.0
C
      I3 = I2 + 1
      JB = J2 + 1
      DO 370 J=JB,J3
         DO 380 I=2,I3
            K1(J,I) = (COND(J,I) + COND(J-1,I))/2
            K2(J,I) = (COND(J,I) + COND(J+1,I))/2
            K3(J,I) = (COND(J,I) + COND(J,I-1))/2
            K4(J,I) = (COND(J,I) + COND(J,I+1))/2
380      CONTINUE
         K4(J,I3) = 0.0
370   CONTINUE
      K1(JB,I3) = 0.0
C
```

```
      I4 = I3 + 1
      JB = J3 + 1
      DO 400 J=JB,J4
         DO 410 I=2,I4
            K1(J,I) = (COND(J,I) + COND(J-1,I))/2
            K2(J,I) = (COND(J,I) + COND(J+1,I))/2
            K3(J,I) = (COND(J,I) + COND(J,I-1))/2
            K4(J,I) = (COND(J,I) + COND(J,I+1))/2
410      CONTINUE
         K4(J,I4) = 0.0
400   CONTINUE
      K1(JB,I4) = 0.0
C
      I5 = I4 + 1
      JB = J4 + 1
      J = JB
      DO 440 I=2,I5
         K1(J,I) = (COND(J,I) + COND(J-1,I))/2
         K2(J,I) = (COND(J,I) + COND(J+1,I))/2
         K3(J,I) = (COND(J,I) + COND(J,I-1))/2
         K4(J,I) = (COND(J,I) + COND(J,I+1))/2
440   CONTINUE
      K4(J,I5) = 0.0
      K1(JB,I5) = 0.0
C

      I6 = I5 + 1
      JB = J5 + 1
      DO 460 J=JB,JZ-1
      DO 460 I=2,IX-1
         K1(J,I) = (COND(J,I) + COND(J-1,I))/2
         K2(J,I) = (COND(J,I) + COND(J+1,I))/2
         K3(J,I) = (COND(J,I) + COND(J,I-1))/2
         K4(J,I) = (COND(J,I) + COND(J,I+1))/2
460   CONTINUE
C
      DO 480 I=I6,IX-1
         K1(JB,I) = 0.0
480   CONTINUE
C
C
      J = JZ
      IF (LOWBC.EQ.1) GO TO 469
C
```

```
C ---------------------------------------------------------------------
C Constant potential lower b.c. (HBOT=constant) at J=JZ+1/2
C ---------------------------------------------------------------------
C
      DO 490 I=1,IX
C
         IF(I .EQ. 1 ) THEN
            K1(J,I) = (COND(J,I) + COND(J-1,I))/2
            K2(J,I) = (COND(J,I) + COND(J+1,I))/2
            K4(J,I) = (COND(J,I) + COND(J,I+1))/2
            GO TO 490
         END IF
C
         IF(I .EQ. IX) THEN
            K1(J,I) = (COND(J,I) + COND(J-1,I))/2
            K2(J,I) = (COND(J,I) + COND(J+1,I))/2
            K3(J,I) = (COND(J,I) + COND(J,I-1))/2
            GO TO 490
         END IF
C
         K1(J,I) = (COND(J,I) + COND(J-1,I))/2
         K2(J,I) = (COND(J,I) + COND(J+1,I))/2
         K3(J,I) = (COND(J,I) + COND(J,I-1))/2
         K4(J,I) = (COND(J,I) + COND(J,I+1))/2
C
490   CONTINUE
C
      GO TO 500
C
C ---------------------------------------------------------------------
C Constant flux lower boundary condition (QB=constant) at J=JZ+1/2
C ---------------------------------------------------------------------
C
469   DO 510 I=1,IX
C
         IF(I .EQ. 1 ) THEN
            K1(J,I) = (COND(J,I) + COND(J-1,I))/2
            K4(J,I) = (COND(J,I) + COND(J,I+1))/2
            GO TO 510
         END IF
C
         IF(I .EQ. IX) THEN
            K1(J,I) = (COND(J,I) + COND(J-1,I))/2
            K3(J,I) = (COND(J,I) + COND(J,I-1))/2
            GO TO 510
         END IF
C
         K1(J,I) = (COND(J,I) + COND(J-1,I))/2
         K3(J,I) = (COND(J,I) + COND(J,I-1))/2
         K4(J,I) = (COND(J,I) + COND(J,I+1))/2
C
510   CONTINUE
```

```
C
C ---------------------------------------------------------------------
C  Constant flux boundary condition at the line of symmetry (I=1)
C ---------------------------------------------------------------------
C
500   I = 1
      DO 520 J=2,JZ-1
         K1(J,I) = (COND(J,I) + COND(J-1,I))/2
         K2(J,I) = (COND(J,I) + COND(J+1,I))/2
         K4(J,I) = (COND(J,I) + COND(J,I+1))/2
520   CONTINUE
C
C ---------------------------------------------------------------------
C  Constant flux b.c. at the right end of the lysimeter (I=IX)
C ---------------------------------------------------------------------
C
      I = IX
      DO 530 J=J6,JZ-1
         K1(J,I) = (COND(J,I) + COND(J-1,I))/2
         K2(J,I) = (COND(J,I) + COND(J+1,I))/2
         K3(J,I) = (COND(J,I) + COND(J,I-1))/2
530   CONTINUE
      K1(J6,I) = 0.0
C
C
      RETURN
      END
```

```
C ***********************************************************************
C
      SUBROUTINE TSTEP
C
C This subroutine determines the time step with the expression given by
C Zaradny (1978)
C
C                 DT = ZETA*DZ/QMAX
C
C where QMAX is the maximum change in flux occurring for any grid
C and 0.015<ZETA<0.035.  The lower limit of ZETA limits DT during
C times of high infiltration or redistribution, or rapid variation
C in boundary conditions.  Higher values of ZETA can be used if
C there is slow change in soil water movement i.e. during extraction.
C
C ***********************************************************************
C
      PARAMETER (IS=21, JS=21)
      IMPLICIT REAL (K)
C
      COMMON /EXTRCT/ DRAIN,EXTRACT,S(JS,IS)
      COMMON /FLOW/   FLOWIN,Q(JS,IS),QB(IS),QL(JS),QR(JS),QS(IS)
      COMMON /GRID/   DX(IS),DZ(JS),IX,JZ
      COMMON /HEADS/  H(JS,IS),HBOT,LOWBC
      COMMON /HYDROL/ K1(JS,IS),K2(JS,IS),K3(JS,IS),K4(JS,IS)
      COMMON /PARAMS/ COND(JS,IS),SWC(JS,IS),WC(JS,IS)
      COMMON /TIME/   IDAY,DT,DTMAX,DTMIN,MONTH,TIME,TIME24,TIMEND
C
      QMAX = 0.0
      EXT  = 0.0
C
C ---------------------------------------------------------------------
C Finding the magnitude of largest extraction rate in the mesh
C ---------------------------------------------------------------------
C
      DO 10 J=1,JZ
      DO 10 I=1,IX
         IF( EXT.LT.ABS(S(J,I)) )  EXT = ABS(S(J,I))
10    CONTINUE
C
C ---------------------------------------------------------------------
C Compare surface flux to extraction rate and choose the largest
C magnitude to be assigned to QMAX
C ---------------------------------------------------------------------
C
      IF( QMAX .LT. EXT ) QMAX = EXT
C
```

```
C ----------------------------------------------------------------------
C Loop to compute flux, Q, at each surface in the profile and compare
C it to QMAX.
C               Q1 = Flux at the top surface of a cell
C               Q2 = Flux at the bottom surface of a cell
C               Q3 = Flux at the left surface of a cell
C               Q4 = Flux at the right surface of a cell
C ----------------------------------------------------------------------
C
      DO 40 J=1,JZ
         DO 50 I=1,IX
C
            IF (J .EQ. 1) THEN
               Q1 = QS(I)
            ELSE
               D1 = (DZ(J) + DZ(J-1)) / 2.0
               Q1 = -1.0 * K1(J,I) * ((H(J,I) - H(J-1,I) ) / D1 - 1.0)
            END IF
C
            IF (J .EQ. JZ) THEN
C
               IF (LOWBC.EQ.0) THEN
C
C                 If the flux across the top surface (I=IX-1/2) of
C                 the last row of grids (I=IX) is in the downwards
C                 (positive) direction it is extracted as drainage.
                  S(J,I) = 0.0
                  IF (Q1 .GT. 0.0) S(J,I) = Q1 / DZ(I)
C
                  D2 = (DZ(J) + DZ(J+1)) / 2.0
                  Q2 = -1.0 * K2(J,I) * ((HBOT - H(J,I) ) / D2 - 1.0)
                  QB(I) = Q2
               ELSE
                   Q2 = QB(I)
               END IF
C
            ELSE
               D2 = (DZ(J) + DZ(J+1)) / 2.0
               Q2 = -1.0 * K2(J,I) * ((H(J+1,I) - H(J,I) ) / D2 - 1.0)
            END IF
C
            IF(I .EQ. 1) THEN
               Q3 = QL(J)
            ELSE
               D3 = (DX(I) + DX(I-1)) / 2.0
               Q3 = -1.0 * K3(J,I) * ((H(J,I) - H(J,I-1) ) / D3)
            END IF
C
            IF(I .EQ. IX) THEN
               Q4 = QR(J)
            ELSE
               D4 = (DX(I) + DX(I+1)) / 2.0
```

```
               Q4 = -1.0 * K4(J,I) * ((H(J,I+1) - H(J,I) ) / D4)
            END IF
C
            FLXNET = (Q1 - Q2) + (Q3 - Q4)
            IF ( ABS(FLXNET) .GT. QMAX ) QMAX = ABS(FLXNET)
C
50       CONTINUE
40    CONTINUE
C
C -----------------------------------------------------------------------
C Determining the time step and the cumulative time.
C -----------------------------------------------------------------------
C
      IF (QMAX.EQ.0.0) THEN
         DT = DTMAX
         GO TO 60
      END IF
C
      ZETA = 0.025
      IF (QMAX.LE.1.0) ZETA = 0.035
      IF (QMAX.GE.10.00) ZETA = 0.015
C
      DT = ZETA * DZ(1) / QMAX
C
      IF (DT.GT.DTMAX) DT = DTMAX
      IF (DT.LT.DTMIN) DT = DTMIN
C
60    TIME = TIME + DT
      TIME24 = TIME24 + DT
      IF (TIME24.GT.24.0000) THEN
         TIME24 = TIME24 - 24.0000
         IDAY = IDAY + 1
      END IF
C
      RETURN
      END
```

```
C ***********************************************************************
C
      SUBROUTINE REDIST
C
C  This subroutine evaluates the coefficients of the banded matrix
C  equation AH = R where A has MBAND = IX*2+1 bands (including
C  the zero bands enclosed between the A and B and E and F terms
C  -- see equation (5.74) and is of the order of NMAX = IX*JZ.  The
C  subroutine stores the coefficients in the array C(NMAX,MBAND).
C
C ***********************************************************************
C
      PARAMETER (IS=21, JS=21)
      IMPLICIT REAL (K)
      DIMENSION C(JS*IS,IS*2+1), R(IS*JS)
C
      COMMON /EXTRCT/ DRAIN,EXTRACT,S(JS,IS)
      COMMON /FLOW/   FLOWIN,Q(JS,IS),QB(IS),QL(JS),QR(JS),QS(IS)
      COMMON /GRID/   DX(IS),DZ(JS),IX,JZ
      COMMON /HEADS/  H(JS,IS),HBOT,LOWBC
      COMMON /HYDROL/ K1(JS,IS),K2(JS,IS),K3(JS,IS),K4(JS,IS)
      COMMON /PARAMS/ COND(JS,IS),SWC(JS,IS),WC(JS,IS)
      COMMON /TIME/   IDAY,DT,DTMAX,DTMIN,MONTH,TIME,TIME24,TIMEND
C
C Compute the number of diagonals, MBAND, in the solution matrix.
C Compute the i-index of the array C(NMAX,MBAND) that the
C coefficients of the main diagonal terms will occupy.
C
      NMAX  = IX * JZ
      MBAND = IX * 2 + 1
      MID   = ( MBAND + 1 ) / 2
C
C Intialize the array C(N,MBAND), which contains only elements
C enclosed by the outer bands of the matrix
C
      DO 10 N=1,NMAX
      DO 10 M=1,MBAND
         C(N,M) = 0.0
10    CONTINUE
C
C -----------------------------------------------------------------------
C                    SET UP THE INTERIOR GRID POINTS
C -----------------------------------------------------------------------
C
      DO 30 J=2,JZ-1
         NN = IX * (J-1)
         DO 40 I=2,IX-1
            N  = NN + I
            C1 = SWC(J,I)
C
```

```
            D1 = (DZ(J) + DZ(J-1))/2
            D2 = (DZ(J) + DZ(J+1))/2
            D3 = (DX(I) + DX(I-1))/2
            D4 = (DX(I) + DX(I+1))/2
C
            C(N,1)     = -K1(J,I) / D1**2
            C(N,MID-1) = -K3(J,I) / D3**2
            C(N,MID+1) = -K4(J,I) / D4**2
            C(N,MBAND) = -K2(J,I) / D2**2
            C(N,MID)   =  C1/DT - C(N,1) - C(N,MID-1) - C(N,MID+1)
     &                    - C(N,MBAND)
            R(N)       =  C1*H(J,I)/DT + (K1(J,I)/D1 - K2(J,I)/D2)
     &                    - S(J,I)
40       CONTINUE
30     CONTINUE
C
C ---------------------------------------------------------------------
C                    SET UP THE BOUNDARY CONDITIONS
C ---------------------------------------------------------------------
C  Constant flux boundary condition at the surface (J=1)
C ---------------------------------------------------------------------
C
      J = 1
      DO 50 I=1,IX
         N  = I
         C1 = SWC(J,I)
C
         IF(I .EQ. 1) THEN
            D2 = (DZ(J) + DZ(J+1))/2
            D4 = (DX(I) + DX(I+1))/2
            C(N,MID+1) = -K4(J,I) / D4**2
            C(N,MBAND) = -K2(J,I) / D2**2
            C(N,MID)   =  C1/DT - C(N,MID+1) - C(N,MBAND)
            R(N)       =  C1*H(J,I)/DT + QL(J)/DX(I) +
     &                    (QS(I)/DZ(J) - K2(J,I)/D2) - S(J,I)
            GO TO 50
         END IF
C
         IF(I .EQ. IX) THEN
            D2 = (DZ(J) + DZ(J+1))/2
            D3 = (DX(I) + DX(I-1))/2
            C(N,MID-1) = -K3(J,I) / D3**2
            C(N,MBAND) = -K2(J,I) / D2**2
            C(N,MID)   =  C1/DT - C(N,MID-1) - C(N,MBAND)
            R(N)       =  C1*H(J,I)/DT - QR(J)/DX(I) +
     &                    (QS(I)/DZ(J) - K2(J,I)/D2) - S(J,I)
            GO TO 50
         END IF
C
         D2 = (DZ(J) + DZ(J+1))/2
         D3 = (DX(I) + DX(I-1))/2
         D4 = (DX(I) + DX(I+1))/2
```

```
C
        C(N,MID-1) = -K3(J,I) / D3**2
        C(N,MID+1) = -K4(J,I) / D4**2
        C(N,MBAND) = -K2(J,I) / D2**2
        C(N,MID)   =  C1/DT - C(N,MID-1) - C(N,MID+1) - C(N,MBAND)
        R(N)       =  C1*H(J,I)/DT + (QS(I)/DZ(J) - K2(J,I)/D2)
     &                - S(J,I)
50    CONTINUE
C -----------------------------------------------------------------------
C Set up boundary conditions for the last row, J=JZ and select type
C of boundary:   LOWBC = 0 means constant potential
C                LOWBC = 1 means constant flux
C -----------------------------------------------------------------------
C
      J = JZ
      IF (LOWBC.EQ.1) GO TO 69
C
C -----------------------------------------------------------------------
C Constant potential lower b.c. (HBOT=constant) at J=JZ+1/2
C -----------------------------------------------------------------------
C
      NN = IX * (JZ-1)
      DO 60 I=1,IX
         N  = NN + I
         C1 = SWC(J,I)
C
         IF(I .EQ. 1 ) THEN
            D1 = (DZ(J) + DZ(J-1))/2
            D2 = (DZ(J) + DZ(J+1))/2
            D4 = (DX(I) + DX(I+1))/2
            C(N,1)     = -K1(J,I) / D1**2
            C(N,MID+1) = -K4(J,I) / D4**2
            C(N,MID)   =  C1/DT - C(N,1) - C(N,MID+1) + K2(J,I)/D2**2
            R(N)       =  C1*H(J,I)/DT + QL(J)/DX(I) + (K1(J,I)/D1
     &                    - K2(J,I)/D2) + HBOT*K2(J,I)/D2**2 - S(J,I)
            GO TO 60
         END IF
C
         IF(I .EQ. IX) THEN
            D1 = (DZ(J) + DZ(J-1))/2
            D2 = (DZ(J) + DZ(J+1))/2
            D3 = (DX(I) + DX(I-1))/2
            C(N,1)     = -K1(J,I) / D1**2
            C(N,MID-1) = -K3(J,I) / D3**2
            C(N,MID)   =  C1/DT - C(N,1) - C(N,MID-1) + K2(J,I)/D2**2
            R(N)       =  C1*H(J,I)/DT - QR(J)/DX(I) + (K1(J,I)/D1
     &                    - K2(J,I)/D2) + HBOT*K2(J,I)/D2**2 - S(J,I)
            GO TO 60
         END IF
C
```

```
          D1 = (DZ(J) + DZ(J-1))/2
          D2 = (DZ(J) + DZ(J+1))/2
          D3 = (DX(I) + DX(I-1))/2
          D4 = (DX(I) + DX(I+1))/2
C
          C(N,1)      = -K1(J,I) / D1**2
          C(N,MID-1) = -K3(J,I) / D3**2
          C(N,MID+1) = -K4(J,I) / D4**2
          C(N,MID)    =  C1/DT - C(N,1) - C(N,MID-1) - C(N,MID+1)
     &                   + K2(J,I)/D2**2
          R(N)        =  C1*H(J,I)/DT + (K1(J,I)/D1 - K2(J,I)/D2)
     &                   + HBOT*K2(J,I)/D2**2 - S(J,I)
60     CONTINUE
C
       GO TO 80
C
C ---------------------------------------------------------------------
C Constant flux lower boundary condition (QB=constant) at J=JZ+1/2
C ---------------------------------------------------------------------
C
69     NN = IX * (JZ-1)
       DO 70 I=1,IX
          N  = NN + I
          C1 = SWC(J,I)
C
          IF(I .EQ. 1 ) THEN
             D1 = (DZ(J) + DZ(J-1))/2
             D4 = (DX(I) + DX(I+1))/2
             C(N,1)      = -K1(J,I) / D1**2
             C(N,MID+1) = -K4(J,I) / D4**2
             C(N,MID)    =  C1/DT - C(N,1) - C(N,MID+1)
             R(N)        =  C1*H(J,I)/DT + QL(J)/DX(I) +
     &                      (K1(J,I)/D1 - QB(I)/DZ(J)) - S(J,I)
             GO TO 70
          END IF
C
          IF(I .EQ. IX) THEN
             D1 = (DZ(J) + DZ(J-1))/2
             D3 = (DX(I) + DX(I-1))/2
             C(N,1)      = -K1(J,I) / D1**2
             C(N,MID-1) = -K3(J,I) / D3**2
             C(N,MID)    =  C1/DT - C(N,1) - C(N,MID-1)
             R(N)        =  C1*H(J,I)/DT - QR(J)/DX(I) +
     &                      (K1(J,I)/D1 - QB(I)/DZ(J)) - S(J,I)
             GO TO 70
          END IF
C
          D1 = (DZ(J) + DZ(J-1))/2
          D3 = (DX(I) + DX(I-1))/2
          D4 = (DX(I) + DX(I+1))/2
C
```

```
         C(N,1)     = -K1(J,I) / D1**2
         C(N,MID-1) = -K3(J,I) / D3**2
         C(N,MID+1) = -K4(J,I) / D4**2
         C(N,MID)   =  C1/DT - C(N,1) - C(N,MID-1) - C(N,MID+1)
         R(N)       =  C1*H(J,I)/DT + (K1(J,I)/D1 - QB(I)/DZ(J))
     &                 - S(J,I)
70    CONTINUE
C
C ---------------------------------------------------------------------
C  Constant flux boundary condition at the line of symmetry (I=1)
C ---------------------------------------------------------------------
C
80    I = 1
      N = 1
      DO 90 J=2,JZ-1
         N = N + IX
C
         D1 = (DZ(J) + DZ(J-1))/2
         D2 = (DZ(J) + DZ(J+1))/2
         D4 = (DX(I) + DX(I+1))/2
         C1 = SWC(J,I)
C
         C(N,1)     = -K1(J,I) / D1**2
         C(N,MID+1) = -K4(J,I) / D4**2
         C(N,MBAND) = -K2(J,I) / D2**2
         C(N,MID)   =  C1/DT - C(N,1) - C(N,MID+1) - C(N,MBAND)
         R(N) = C1*H(J,I)/DT + QL(J)/DX(I) + (K1(J,I)/D1 - K2(J,I)/D2)
     &          - S(J,I)
C
90    CONTINUE
C
C ---------------------------------------------------------------------
C  Constant flux b.c. at the right end of the lysimeter (I=IX)
C ---------------------------------------------------------------------
C
      I = IX
      DO 100 J=2,JZ-1
         N = IX * J
C
         D1 = (DZ(J) + DZ(J-1))/2
         D2 = (DZ(J) + DZ(J+1))/2
         D3 = (DX(I) + DX(I-1))/2
         C1 = SWC(J,I)
C
         C(N,1)     = -K1(J,I) / D1**2
         C(N,MID-1) = -K3(J,I) / D3**2
         C(N,MBAND) = -K2(J,I) / D2**2
         C(N,MID)   =  C1/DT - C(N,1) - C(N,MID-1) - C(N,MBAND)
         R(N) = C1*H(J,I)/DT - QR(J)/DX(I) + (K1(J,I)/D1 - K2(J,I)/D2)
     &          - S(J,I)
C
100   CONTINUE
```

```
C
      CALL BSOLVE(C, NMAX, MBAND, R)
C
      L = 0
      DO 110 J=1,JZ
      DO 110 I=1,IX
         L = L + 1
         H(J,I) = R(L)
110   CONTINUE
C
      RETURN
      END
```

```
C ***************************************************************************
C
      SUBROUTINE BSOLVE(C, N, M, V)
C
C  BANDSOLVE is an algorithm developed by D.H. Thurnau (1963) to
C  solve the matrix equations AX = B when the matrix A is of large
C  order and sparse such that a narrow band centered on the main
C  diagonal includes all the non-zero elements.  Parameter N is
C  the order of A, and M is the width of the band (total number of
C  diagonals enclosed by the two outermost bands), necessarily an
C  odd number of elements.  BANDSOLVE is very efficient because it
C  operates only on the banded portion of the matrix A, given in the
C  N by M array C.  The band elements of a given row of A appear in
C  the same row of C but shifted such that element A(i,j) becomes
C  C(i,j-1+(M+1)/2).  All band elements whether zero or nonzero must
C  given.  The values of undefined elements of C, such as C(1,1) or
C  C(N,M) are irrelevant.  The array V initially contains the vector
C  B.  After solution, the array V contains the answer vector X.  The
C  contents of array C are destroyed during solution which is done by
C  Gauss elimantion with row interchanges, followed by back
C  substituiton.  The array C in subroutine REDIST is already in the
C  N by M form and does not need further conversion to go into BANDSOLVE
C
C ***************************************************************************
C
      PARAMETER (IS=21, JS=21)
      DIMENSION C(JS*IS,IS*2+1), V(IS*JS)
      INTEGER PIV, R
C
C      DO 990 J=1,N
C         WRITE(9,991)J, (C(J,I), I=1,M)
C991      FORMAT(I3,9F8.5)
C990    CONTINUE
C
C ---------------- ROW SHIFTING AND ZERO PLACEMENT ---------------------
C
      LR = (M + 1) / 2
C
      DO 10 R=1,LR-1
      DO 10 I=1,LR-R
         DO 20 J=2,M
            C(R,J-1) = C(R,J)
20       CONTINUE
         C(R,M) = 0.0
         C(N+1-R,M+1-I) = 0.0
10    CONTINUE
C
C ---------------- ROW INTERCHANGE -------------------------------------
C
      DO 30 I=1,N-1
         PIV = I
C
```

```
         DO 40 R=I+1,LR
            IF(ABS(C(R,1)).GT.ABS(C(PIV,1))) PIV = R
40       CONTINUE
C
         IF(PIV .NE. I) THEN
            DO 50 J=1,M
                TEMP     = C(I,J)
                C(I,J)   = C(PIV,J)
                C(PIV,J) = TEMP
50          CONTINUE
            TEMP   = V(I)
            V(I)   = V(PIV)
            V(PIV) = TEMP
         END IF
C
C ---------------- TRIANGULARIZATION -----------------------------------
C
         V(I) = V(I) / C(I,1)
C
         DO 60 J=2,M
            C(I,J) = C(I,J) / C(I,1)
60       CONTINUE
C
         DO 70 R=I+1,LR
            TEMP = C(R,1)
            V(R) = V(R) - TEMP * V(I)
C
                DO 80 J=2,M
                   C(R,J-1) = C(R,J) - TEMP * C(I,J)
80              CONTINUE
C
            C(R,M) = 0.0
70       CONTINUE
C
         IF(LR .NE. N) LR = LR + 1
30    CONTINUE
C
C ---------------- BACK SOLUTION ---------------------------------------
C
      V(N) = V(N) / C(N,1)
      JM = 2
C
      DO 90 R=N-1,1,-1
         DO 100 J=2,JM
            V(R) = V(R) - C(R,J) * V(R-1+J)
100      CONTINUE
C
         IF(JM .NE. M) JM = JM + 1
90    CONTINUE
C
      RETURN
      END
```

```
C ***********************************************************************
C
      SUBROUTINE UPDAT1
C
C This subroutine uses van Genuchten's equations to compute
C values of water content, WC, specific water capacity, SWC,
C and hydraulic conductivity, COND, corresponding to a given
C pressure head, H.
C
C This routine is used for builder's sand, Astatula f.s., and
C Pomona sand.
C
C ***********************************************************************
C
      PARAMETER (IS=21, JS=21)
      REAL M, N
C
      COMMON /GRID/   DX(IS),DZ(JS),IX,JZ
      COMMON /HEADS/  H(JS,IS),HBOT,LOWBC
      COMMON /PARAMS/ COND(JS,IS),SWC(JS,IS),WC(JS,IS)
      COMMON /SOILS2/ ALPHA,VN,CONDS,WCR,WCS
C
      HLARGE = 0.0
      A = ALPHA
      N = VN
      M = 1.0 - 1.0 / N
C
      K = JZ
      IF(LOWBC .EQ. 0) K = JZ + 1
C
      DO 10 J=1,K
      DO 10 I=1,IX
C
         HEAD = ABS(H(J,I)) / 10.0
C
         IF (H(J,I).GE.HLARGE) THEN
            WC(J,I) = WCS
         ELSE
            WC(J,I) = WCR + (WCS - WCR) / (1.0 + (A * HEAD)**N )**M
         END IF
C
         IF (H(J,I).GE.HLARGE) THEN
            SWC(J,I) = 0.0
         ELSE
            SWC(J,I) =   (A * M * (WCS - WCR) / (1.0 - M))
     &                 * (1.0 / (1.0 + (A * HEAD)**N))
     &                 * (1.0 - (1.0 / (1.0 + (A * HEAD)**N)))**M
            SWC(J,I) = SWC(J,I) / 10.0
         END IF
C
```

```
          IF (H(J,I).GE.HLARGE) THEN
             COND(J,I) = CONDS * 10.00
          ELSE
             COND(J,I) = CONDS * ( (1.0 - (A * HEAD)**(N-1)
     &                  * (1.0 + (A * HEAD)**N)**(-M))**2
     &                  / (1.0 + (A * HEAD)**N)**(M/2) )
             COND(J,I) = COND(J,I) * 10.0
          END IF
C
C       WRITE(9,39)J,I,H(J,I),WC(J,I),COND(J,I),SWC(J,I)
C39     FORMAT(2I4,' H = ',F9.2,'  WC = ',F5.4,'  COND = ',E12.6,
C      &       '  C = ',E12.6)
10     CONTINUE
C
       RETURN
       END
```

```
C ***********************************************************************
C
      SUBROUTINE UPDAT2
C
C This subroutine uses an index routing technique with tabulated
C data to find the values of water content, WC, specific water
C capacity, SWC, and hydraulic conductivity, COND, corresponding
C to a given pressure head, H.
C
C  This routine is for Arredondo f.s., Rehevot sand, Adelanto loam,
C  Pachappa loam, and Yolo light clay.
C
C ***********************************************************************
C
      PARAMETER (IS=21, JS=21)
C
      COMMON /GRID/   DX(IS),DZ(JS),IX,JZ
      COMMON /HEADS/  H(JS,IS),HBOT,LOWBC
      COMMON /PARAMS/ COND(JS,IS),SWC(JS,IS),WC(JS,IS)
      COMMON /SOILS1/ FA,FB,ISOIL,NDATA
      COMMON /TABLES/ HTAB(120),WCTAB(120),SWCTAB(120),CONTAB(120)
C
      HLARGE = HTAB(1)
      HSMALL = HTAB(NDATA)
C
      N = JZ
      IF(LOWBC .EQ. 0 ) N = JZ + 1
C
      DO 10 J=1,N
      DO 10 I=1,IX
         HEAD = H(J,I)
         IF (HEAD .LE. HSMALL) HEAD = HSMALL
         IF (HEAD .GE. HLARGE) HEAD = HLARGE
C
         INDEX = ALOG10(-1.0 * HEAD) * (FA * 1.E01) - FB * 1.0E01
C
         IF (HEAD .LT. HTAB(INDEX+1)) INDEX = INDEX + 1
         IF (HEAD .GT. HTAB(INDEX)) INDEX = INDEX - 1
         IF (INDEX .GE. NDATA) INDEX = NDATA
         IF (INDEX .LE. 1)  INDEX = 1
C
         RATIO = ALOG10( HEAD / HTAB(INDEX) ) /
     &           ALOG10( HTAB(INDEX+1) / HTAB(INDEX) )
C
         WC(J,I) = WCTAB(INDEX) + RATIO * (WCTAB(INDEX+1) -WCTAB(INDEX))

C
```

```
          IF (H(J,I).GT.HLARGE) THEN
             SWC(J,I) = 0.0
          ELSE
             SWC(J,I) = SWCTAB(INDEX) * 1.E01**(RATIO *
     &                  ALOG10(SWCTAB(INDEX+1) / SWCTAB(INDEX)))
          END IF
C
          COND(J,I) = CONTAB(INDEX) * 1.E01**(RATIO *
     &                ALOG10(CONTAB(INDEX+1) / CONTAB(INDEX)))
C
10     CONTINUE
C
       RETURN
       END
```

APPENDIX C
TABULATED SOIL PARAMETERS

Table C.1. Hydraulic Properties of Arredondo Fine Sand.

Matric Potential (mm)	Water Content (mm/mm)	Specific Water Capacity (1/mm)	Hydraulic Conductivity (mm/hr)
-0.11220E 03	0.33450E 00	0.38710E-04	0.40497E 03
-0.11885E 03	0.33425E 00	0.36545E-04	0.40248E 03
-0.12589E 03	0.33400E 00	0.34497E-04	0.40000E 03
-0.13335E 03	0.33375E 00	0.32564E-04	0.39748E 03
-0.14125E 03	0.33350E 00	0.30742E-04	0.39497E 03
-0.14962E 03	0.33325E 00	0.29023E-04	0.39248E 03
-0.15849E 03	0.33300E 00	0.34249E-04	0.39000E 03
-0.16788E 03	0.33263E 00	0.38801E-04	0.38490E 03
-0.17783E 03	0.33225E 00	0.36631E-04	0.37987E 03
-0.18836E 03	0.33188E 00	0.34582E-04	0.37490E 03
-0.19953E 03	0.33150E 00	0.32649E-04	0.37000E 03
-0.21135E 03	0.33113E 00	0.30825E-04	0.36490E 03
-0.22387E 03	0.33075E 00	0.29101E-04	0.35986E 03
-0.23714E 03	0.33038E 00	0.27473E-04	0.35490E 03
-0.25119E 03	0.33000E 00	0.18585E-03	0.35000E 03
-0.26607E 03	0.32500E 00	0.32643E-03	0.30431E 03
-0.28184E 03	0.32000E 00	0.30818E-03	0.26458E 03
-0.29854E 03	0.31500E 00	0.29095E-03	0.23004E 03
-0.31623E 03	0.31000E 00	0.61797E-03	0.20000E 03
-0.33497E 03	0.29250E 00	0.90753E-03	0.15216E 03
-0.35481E 03	0.27500E 00	0.85681E-03	0.11576E 03
-0.37584E 03	0.25750E 00	0.80888E-03	0.88070E 02
-0.39811E 03	0.24000E 00	0.70909E-03	0.67002E 02
-0.42170E 03	0.22500E 00	0.61794E-03	0.46089E 02
-0.44668E 03	0.21000E 00	0.58336E-03	0.31703E 02
-0.47315E 03	0.19500E 00	0.55073E-03	0.21807E 02
-0.50119E 03	0.18000E 00	0.46793E-03	0.15001E 02
-0.53088E 03	0.16800E 00	0.39267E-03	0.88289E 01
-0.56234E 03	0.15600E 00	0.37070E-03	0.51964E 01
-0.59566E 03	0.14400E 00	0.34997E-03	0.30584E 01
-0.63096E 03	0.13200E 00	0.28221E-03	0.18001E 01
-0.66834E 03	0.12350E 00	0.22094E-03	0.10393E 01
-0.70795E 03	0.11500E 00	0.20858E-03	0.60002E 00
-0.74989E 03	0.10650E 00	0.19691E-03	0.34642E 00
-0.79433E 03	0.98000E-01	0.13122E-03	0.20000E 00

Table C.1. -- continued

Matric Potential (mm)	Water Content (mm/mm)	Specific Water Capacity (1/mm)	Hydraulic Conductivity (mm/hr)
-0.84140E 03	0.94500E-01	0.72265E-04	0.14483E 00
-0.89125E 03	0.91000E-01	0.68221E-04	0.10488E 00
-0.94406E 03	0.87500E-01	0.64405E-04	0.75951E-01
-0.10000E 04	0.84000E-01	0.52118E-04	0.55000E-01
-0.10593E 04	0.81500E-01	0.41004E-04	0.35913E-01
-0.11220E 04	0.79000E-01	0.38710E-04	0.23450E-01
-0.11885E 04	0.76499E-01	0.36542E-04	0.15312E-01
-0.12589E 04	0.73999E-01	0.27596E-04	0.99996E-02
-0.13335E 04	0.72500E-01	0.19538E-04	0.88008E-02
-0.14125E 04	0.71000E-01	0.18445E-04	0.77458E-02
-0.14962E 04	0.69500E-01	0.17414E-04	0.68173E-02
-0.15849E 04	0.68000E-01	0.13700E-04	0.60001E-02
-0.16788E 04	0.67000E-01	0.10347E-04	0.50455E-02
-0.17783E 04	0.66000E-01	0.97683E-05	0.42428E-02
-0.18836E 04	0.65000E-01	0.92218E-05	0.35678E-02
-0.19953E 04	0.64000E-01	0.87065E-05	0.30002E-02
-0.21135E 04	0.63000E-01	0.82200E-05	0.24342E-02
-0.22387E 04	0.62000E-01	0.77601E-05	0.19749E-02
-0.23714E 04	0.61000E-01	0.73261E-05	0.16023E-02
-0.25119E 04	0.60000E-01	0.43228E-05	0.13000E-02
-0.26607E 04	0.59750E-01	0.16325E-05	0.11858E-02
-0.28184E 04	0.59500E-01	0.15409E-05	0.10817E-02
-0.29854E 04	0.59250E-01	0.14547E-05	0.98667E-03
-0.31623E 04	0.59000E-01	0.20600E-05	0.90001E-03
-0.33497E 04	0.58500E-01	0.25930E-05	0.77702E-03
-0.35481E 04	0.58000E-01	0.24480E-05	0.67083E-03
-0.37584E 04	0.57500E-01	0.23111E-05	0.57916E-03
-0.39811E 04	0.57000E-01	0.16364E-05	0.50001E-03
-0.42170E 04	0.56750E-01	0.10299E-05	0.47287E-03
-0.44668E 04	0.56500E-01	0.97227E-06	0.44722E-03
-0.47315E 04	0.56250E-01	0.91788E-06	0.42295E-03
-0.50119E 04	0.56000E-01	0.86654E-06	0.40000E-03
-0.53088E 04	0.55750E-01	0.81806E-06	0.37224E-03
-0.56234E 04	0.55500E-01	0.77230E-06	0.34641E-03
-0.59566E 04	0.55250E-01	0.72910E-06	0.32237E-03
-0.63096E 04	0.55000E-01	0.68832E-06	0.30000E-03
-0.66834E 04	0.54750E-01	0.64981E-06	0.27108E-03
-0.70795E 04	0.54500E-01	0.61346E-06	0.24495E-03
-0.74989E 04	0.54250E-01	0.57915E-06	0.22134E-03
-0.79433E 04	0.54000E-01	0.54675E-06	0.20000E-03
-0.84140E 04	0.53750E-01	0.51617E-06	0.18915E-03
-0.89125E 04	0.53500E-01	0.48729E-06	0.17889E-03
-0.94406E 04	0.53200E-01	0.46003E-06	0.16918E-03
-0.10000E 05	0.53000E-01	0.32573E-06	0.16000E-03
-0.10593E 05	0.52875E-01	0.20502E-06	0.15475E-03

Table C.1. -- continued

Matric Potential (mm)	Water Content (mm/mm)	Specific Water Capacity (1/mm)	Hydraulic Conductivity (mm/hr)
-0.11220E 05	0.52750E-01	0.19355E-06	0.14967E-03
-0.11885E 05	0.52625E-01	0.18274E-06	0.14475E-03
-0.12589E 05	0.52500E-01	0.20699E-06	0.14000E-03
-0.13335E 05	0.52325E-01	0.22795E-06	0.13471E-03
-0.14125E 05	0.52150E-01	0.21520E-06	0.12961E-03
-0.14962E 05	0.51975E-01	0.20316E-06	0.12471E-03
-0.15849E 05	0.51800E-01	0.20550E-06	0.12000E-03
-0.16788E 05	0.51600E-01	0.20694E-06	0.11742E-03
-0.17783E 05	0.51400E-01	0.19537E-06	0.11489E-03
-0.18836E 05	0.51200E-01	0.18444E-06	0.11242E-03
-0.19953E 05	0.51000E-01	0.17413E-06	0.11000E-03
-0.21135E 05	0.50800E-01	0.16400E-06	0.10741E-03
-0.22387E 05	0.50600E-01	0.15520E-06	0.10488E-03
-0.23714E 05	0.50400E-01	0.14652E-06	0.10241E-03
-0.25119E 05	0.50200E-01	0.17290E-06	0.10000E-03
-0.26607E 05	0.49900E-01	0.19586E-06	0.84091E-04
-0.28184E 05	0.49600E-01	0.18491E-06	0.70712E-04
-0.29854E 05	0.49300E-01	0.17457E-06	0.59462E-04
-0.31623E 05	0.49000E-01	0.21973E-06	0.50001E-04
-0.33497E 05	0.48500E-01	0.25930E-06	0.42046E-04
-0.35481E 05	0.48000E-01	0.24480E-06	0.35356E-04
-0.37584E 05	0.47500E-01	0.23111E-06	0.29731E-04
-0.39811E 05	0.47000E-01	0.21818E-06	0.25001E-04
-0.42170E 05	0.46500E-01	0.20598E-06	0.22003E-04
-0.44668E 05	0.46000E-01	0.19445E-06	0.19365E-04
-0.47315E 05	0.45500E-01	0.18358E-06	0.17044E-04
-0.50119E 05	0.45000E-01	0.17331E-06	0.15000E-04
-0.53088E 05	0.44500E-01	0.16361E-06	0.12819E-04
-0.56234E 05	0.44000E-01	0.15446E-06	0.10955E-04
-0.59566E 05	0.43500E-01	0.14582E-06	0.93615E-05
-0.63096E 05	0.43000E-01	0.20649E-06	0.80001E-05
-0.66834E 05	0.42000E-01	0.25992E-06	0.56570E-05
-0.70795E 05	0.41000E-01	0.24539E-06	0.40001E-05
-0.74989E 05	0.40000E-01	0.23166E-06	0.28285E-05
-0.79433E 05	0.39000E-01	0.21870E-06	0.20000E-05
-0.84140E 05	0.38000E-01	0.20647E-06	0.94576E-06
-0.89125E 05	0.37000E-01	0.19492E-06	0.44722E-06
-0.94406E 05	0.36000E-01	0.18401E-06	0.21148E-06

From Clark (1982)

Table C.2. Hydraulic Properties of Rehevot Sand.

Matric Potential (mm)	Water Content (mm/mm)	Specific Water Capacity (1/mm)	Hydraulic Conductivity (mm/hr)
-0.15849E 02	0.39234E 00	0.50895E-03	0.48003E 03
-0.19953E 02	0.39048E 00	0.40995E-03	0.47998E 03
-0.25119E 02	0.38857E 00	0.37137E-03	0.47992E 03
-0.31623E 02	0.38618E 00	0.37822E-03	0.47976E 03
-0.39811E 02	0.38306E 00	0.39553E-03	0.47924E 03
-0.50119E 02	0.37893E 00	0.41914E-03	0.47760E 03
-0.63096E 02	0.37339E 00	0.45192E-03	0.47247E 03
-0.79433E 02	0.36580E 00	0.50029E-03	0.45703E 03
-0.10000E 03	0.35509E 00	0.57585E-03	0.41423E 03
-0.12589E 03	0.33928E 00	0.69998E-03	0.31956E 03
-0.15849E 03	0.31450E 00	0.90322E-03	0.18551E 03
-0.19953E 03	0.27334E 00	0.11122E-02	0.79740E 02
-0.25119E 03	0.21229E 00	0.10385E-02	0.28448E 02
-0.31623E 03	0.15321E 00	0.69659E-03	0.93759E 01
-0.39811E 03	0.11086E 00	0.38949E-03	0.30051E 01
-0.50119E 03	0.81818E-01	0.21416E-03	0.95437E 00
-0.63096E 03	0.61441E-01	0.12069E-03	0.30221E 00
-0.79433E 03	0.46753E-01	0.69733E-04	0.95608E-01
-0.10000E 04	0.35935E-01	0.40496E-04	0.30238E-01
-0.12589E 04	0.28106E-01	0.20847E-04	0.95625E-02
-0.15849E 04	0.23852E-01	0.85623E-05	0.30240E-02
-0.19953E 04	0.21859E-01	0.34862E-05	0.95627E-03
-0.25119E 04	0.20650E-01	0.18333E-05	0.30240E-03
-0.31623E 04	0.19738E-01	0.11472E-05	0.95627E-04
-0.39811E 04	0.18979E-01	0.75314E-06	0.30240E-04
-0.50119E 04	0.18358E-01	0.52248E-06	0.95627E-05
-0.63096E 04	0.17773E-01	0.38481E-06	0.30240E-05
-0.79433E 04	0.17240E-01	0.28380E-06	0.95627E-06
-0.10000E 05	0.16735E-01	0.21384E-06	0.30240E-06
-0.12589E 05	0.16255E-01	0.16312E-06	0.95627E-07
-0.15849E 05	0.15790E-01	0.12517E-06	0.30240E-07
-0.19953E 05	0.15341E-01	0.97071E-07	0.95627E-08
-0.25119E 05	0.14898E-01	0.75446E-07	0.30240E-08
-0.31623E 05	0.14469E-01	0.58922E-07	0.95627E-09
-0.39811E 05	0.14040E-01	0.46236E-07	0.30240E-09
-0.50119E 05	0.13621E-01	0.36229E-07	0.95627E-10
-0.63096E 05	0.13203E-01	0.28620E-07	0.30240E-10
-0.79433E 05	0.12789E-01	0.22547E-07	0.95627E-11
-0.10000E 06	0.12379E-01	0.17830E-07	0.30240E-11
-0.12589E 06	0.11968E-01	0.14093E-07	0.95627E-12
-0.15849E 06	0.11562E-01	0.11142E-07	0.30240E-12
-0.19953E 06	0.11155E-01	0.88344E-08	0.95627E-13
-0.25119E 06	0.10750E-01	0.69962E-08	0.30240E-13

Table C.2. -- continued

Matric Potential (mm)	Water Content (mm/mm)	Specific Water Capacity (1/mm)	Hydraulic Conductivity (mm/hr)
-0.31623E 06	0.10346E-01	0.55495E-08	0.95627E-14
-0.39811E 06	0.99418E-02	0.44001E-08	0.30240E-14
-0.50119E 06	0.95391E-02	0.34897E-08	0.95627E-15
-0.63096E 06	0.91364E-02	0.27699E-08	0.30240E-15
-0.79433E 06	0.87342E-02	0.21978E-08	0.95627E-16
-0.10000E 07	0.83324E-02	0.17449E-08	0.30240E-16
-0.12589E 07	0.79307E-02	0.13851E-08	0.95627E-17
-0.15849E 07	0.75294E-02	0.10997E-08	0.30240E-17
-0.19953E 07	0.71281E-02	0.87324E-09	0.95627E-18
-0.25119E 07	0.67270E-02	0.69336E-09	0.30240E-18
-0.31623E 07	0.63260E-02	0.55066E-09	0.95627E-19
-0.39811E 07	0.59251E-02	0.43729E-09	0.30240E-19
-0.50119E 07	0.55243E-02	0.34729E-09	0.95627E-20
-0.63096E 07	0.51235E-02	0.27583E-09	0.30240E-20
-0.79433E 07	0.47228E-02	0.21906E-09	0.95627E-21
-0.10000E 08	0.43222E-02	0.17400E-09	0.30240E-21

From Clark (1982)

Table C.3. Hydraulic Properties of Adelanto Loam.

Matric Potential (mm)	Water Content (mm/mm)	Specific Water Capacity (1/mm)	Hydraulic Conductivity (mm/hr)
-0.10000E 03	0.42500E 00	0.13799E-04	0.18900E 01
-0.12589E 03	0.42460E 00	0.13799E-04	0.18327E 01
-0.15849E 03	0.42420E 00	0.10961E-04	0.17771E 01
-0.19953E 03	0.42380E 00	0.87065E-05	0.17399E 01
-0.25119E 03	0.42340E 00	0.69158E-05	0.17198E 01
-0.31623E 03	0.42300E 00	0.82378E-05	0.17000E 01
-0.39811E 03	0.42220E 00	0.87272E-05	0.16170E 01
-0.50119E 03	0.42140E 00	0.77980E-05	0.15380E 01
-0.63096E 03	0.42040E 00	0.75710E-05	0.14687E 01
-0.79433E 03	0.41920E 00	0.65609E-05	0.14081E 01
-0.10000E 04	0.41800E 00	0.18232E-04	0.13500E 01
-0.12589E 04	0.41080E 00	0.24838E-04	0.11479E 01
-0.15849E 04	0.40360E 00	0.29038E-04	0.97602E 00
-0.19953E 04	0.38960E 00	0.37867E-04	0.68508E 00
-0.25119E 04	0.36880E 00	0.35962E-04	0.39695E 00
-0.31623E 04	0.34800E 00	0.33779E-04	0.23000E 00
-0.39811E 04	0.31960E 00	0.30982E-04	0.89951E-01
-0.50119E 04	0.29120E 00	0.22013E-04	0.35179E-01
-0.63096E 04	0.26880E 00	0.13356E-04	0.14241E-01
-0.79433E 04	0.25240E 00	0.89666E-05	0.59667E-02
-0.10000E 05	0.23600E 00	0.56474E-05	0.25000E-02
-0.12589E 05	0.22640E 00	0.33117E-05	0.14126E-02
-0.15849E 05	0.21680E 00	0.24116E-05	0.79820E-03
-0.19953E 05	0.20880E 00	0.15675E-05	0.49091E-03
-0.25119E 05	0.20240E 00	0.11065E-05	0.32864E-03
-0.31623E 05	0.19600E 00	0.93379E-06	0.22000E-03
-0.39811E 05	0.18880E 00	0.78545E-06	0.13509E-03
-0.50119E 05	0.18160E 00	0.62391E-06	0.82950E-04
-0.63096E 05	0.17440E 00	0.49558E-06	0.51350E-04
-0.79433E 05	0.16720E 00	0.39366E-06	0.32047E-04
-0.10000E 06	0.16000E 00	0.28667E-06	0.20000E-04
-0.12589E 06	0.15400E 00	0.20698E-06	0.13510E-04
-0.15849E 06	0.14800E 00	0.16989E-06	0.91255E-05
-0.19953E 06	0.14160E 00	0.14365E-06	0.60206E-05
-0.25119E 06	0.13480E 00	0.11757E-06	0.38796E-05
-0.31623E 06	0.12800E 00	0.93389E-07	0.25000E-05
-0.39811E 06	0.12120E 00	0.74182E-07	0.16238E-05
-0.50119E 06	0.11440E 00	0.58059E-07	0.10547E-05
-0.63096E 06	0.10780E 00	0.44741E-07	0.68072E-06
-0.79433E 06	0.10140E 00	0.34992E-07	0.43658E-06
-0.10000E 07	0.95000E-01	0.26928E-07	0.28000E-06
-0.12589E 07	0.89000E-01	0.20698E-07	0.19269E-06
-0.15849E 07	0.83000E-01	0.16989E-07	0.13260E-06

Table C.3. -- continued

Matric Potential (mm)	Water Content (mm/mm)	Specific Water Capacity (1/mm)	Hydraulic Conductivity (mm/hr)
-0.19953E 07	0.76600E-01	0.14365E-07	0.87484E-07
-0.25119E 07	0.69800E-01	0.11757E-07	0.55335E-07
-0.31623E 07	0.63000E-01	0.90648E-08	0.35000E-07
-0.39811E 07	0.56600E-01	0.69818E-08	0.22809E-07
-0.50119E 07	0.50200E-01	0.51998E-08	0.14865E-07

From Clark (1982)

Table C.4. Hydraulic Properties of Pachappa Loam.

Matric Potential (mm)	Water Content (mm/mm)	Specific Water Capacity (1/mm)	Hydraulic Conductivity (mm/hr)
-0.10000E 03	0.45520E 00	0.55196E-04	0.80000E 01
-0.12589E 03	0.45340E 00	0.55196E-04	0.77544E 01
-0.15849E 03	0.45180E 00	0.46582E-04	0.75163E 01
-0.19953E 03	0.45000E 00	0.41355E-04	0.72326E 01
-0.25119E 03	0.44800E 00	0.34579E-04	0.69091E 01
-0.31623E 03	0.44600E 00	0.41189E-04	0.66000E 01
-0.39811E 03	0.44200E 00	0.43636E-04	0.61802E 01
-0.50119E 03	0.43800E 00	0.57172E-04	0.57871E 01
-0.63096E 03	0.42880E 00	0.81209E-04	0.49094E 01
-0.79433E 03	0.41440E 00	0.78731E-04	0.37732E 01
-0.10000E 04	0.40000E 00	0.11809E-03	0.29000E 01
-0.12589E 04	0.36000E 00	0.13799E-03	0.12727E 01
-0.15849E 04	0.32000E 00	0.10413E-03	0.55852E 00
-0.19953E 04	0.28400E 00	0.74009E-04	0.23593E 00
-0.25119E 04	0.25200E 00	0.55327E-04	0.95922E-01
-0.31623E 04	0.22000E 00	0.39832E-04	0.39000E-01
-0.39811E 04	0.19400E 00	0.28363E-04	0.12570E-01
-0.50119E 04	0.16800E 00	0.19501E-04	0.40513E-02
-0.63096E 04	0.14900E 00	0.10672E-04	0.13496E-02
-0.79433E 04	0.13700E 00	0.65609E-05	0.46469E-03
-0.10000E 05	0.12500E 00	0.39968E-05	0.16000E-03
-0.12589E 05	0.11860E 00	0.22078E-05	0.76146E-04
-0.15849E 05	0.11220E 00	0.16716E-05	0.36239E-04
-0.19953E 05	0.10640E 00	0.11973E-05	0.19381E-04
-0.25119E 05	0.10120E 00	0.89906E-06	0.11648E-04
-0.31623E 05	0.96000E-01	0.68673E-06	0.70000E-05
-0.39811E 05	0.91200E-01	0.52363E-06	0.42410E-05
-0.50119E 05	0.86400E-01	0.38998E-06	0.25695E-05
-0.63096E 05	0.82200E-01	0.26847E-06	0.16651E-05
-0.79433E 05	0.78600E-01	0.19683E-06	0.11542E-05
-0.10000E 06	0.75000E-01	0.16502E-06	0.80000E-06
-0.12589E 06	0.71000E-01	0.13799E-06	0.54038E-06
-0.15849E 06	0.67000E-01	0.10961E-06	0.36502E-06
-0.19953E 06	0.63000E-01	0.87065E-07	0.24546E-06
-0.25119E 06	0.59000E-01	0.69158E-07	0.16432E-06
-0.31623E 06	0.55000E-01	0.52193E-07	0.11000E-06
-0.39811E 06	0.51400E-01	0.39273E-07	0.73394E-07
-0.50119E 06	0.47800E-01	0.29465E-07	0.48970E-07
-0.63096E 06	0.44600E-01	0.20652E-07	0.34467E-07
-0.79433E 06	0.41800E-01	0.15309E-07	0.25590E-07
-0.10000E 07	0.39000E-01	0.12160E-07	0.19000E-07
-0.12589E 07	0.36200E-01	0.96592E-08	0.14698E-07
-0.15849E 07	0.33400E-01	0.68517E-08	0.11370E-07

Table C.4. -- continued

Matric Potential (mm)	Water Content (mm/mm)	Specific Water Capacity (1/mm)	Hydraulic Conductivity (mm/hr)
-0.19953E 07	0.31200E-01	0.41365E-08	0.91745E-08
-0.25119E 07	0.29600E-01	0.27663E-08	0.77223E-08
-0.31623E 07	0.28000E-01	0.30197E-08	0.65000E-08
-0.39811E 07	0.25200E-01	0.30545E-08	0.50743E-08
-0.50119E 07	0.22400E-01	0.23398E-08	0.39613E-08

From Clark (1982)

Table C.5. Hydraulic Properties of Yolo Light Clay.

Matric Potential (mm)	Water Content (mm/mm)	Specific Water Capacity (1/mm)	Hydraulic Conductivity (mm/hr)
-0.12589E 02	0.49451E 00	0.13683E-03	0.29345E 00
-0.15849E 02	0.49401E 00	0.13683E-03	0.29010E 00
-0.19953E 02	0.49351E 00	0.10869E-03	0.28679E 00
-0.25119E 02	0.49301E 00	0.86337E-04	0.28351E 00
-0.31623E 02	0.49251E 00	0.68580E-04	0.28027E 00
-0.39811E 02	0.49201E 00	0.16972E-03	0.27707E 00
-0.50119E 02	0.48940E 00	0.22836E-03	0.26074E 00
-0.63096E 02	0.48674E 00	0.18292E-03	0.24512E 00
-0.79433E 02	0.48408E 00	0.19521E-03	0.23044E 00
-0.10000E 03	0.47960E 00	0.20809E-03	0.21297E 00
-0.12589E 03	0.47450E 00	0.21231E-03	0.19393E 00
-0.15849E 03	0.46729E 00	0.19763E-03	0.16724E 00
-0.19953E 03	0.46007E 00	0.22238E-03	0.14422E 00
-0.25119E 03	0.44685E 00	0.22920E-03	0.11295E 00
-0.31623E 03	0.43356E 00	0.18249E-03	0.88378E-01
-0.39811E 03	0.42027E 00	0.19528E-03	0.69149E-01
-0.50119E 03	0.39775E 00	0.19722E-03	0.46639E-01
-0.63096E 03	0.37475E 00	0.16179E-03	0.30888E-01
-0.79433E 03	0.35074E 00	0.95029E-04	0.19377E-01
-0.10000E 04	0.34000E 00	0.53042E-04	0.14800E-01
-0.12589E 04	0.32631E 00	0.47268E-04	0.10817E-01
-0.15849E 04	0.31260E 00	0.36235E-04	0.80175E-02
-0.19953E 04	0.29987E 00	0.26924E-04	0.62626E-02
-0.25119E 04	0.28786E 00	0.20223E-04	0.50334E-02
-0.31623E 04	0.27647E 00	0.16605E-04	0.40046E-02
-0.39811E 04	0.26367E 00	0.13418E-04	0.31320E-02
-0.50119E 04	0.25188E 00	0.10188E-04	0.24659E-02
-0.63096E 04	0.24016E 00	0.82332E-05	0.19556E-02
-0.79433E 04	0.22795E 00	0.67504E-05	0.15344E-02
-0.10000E 05	0.21547E 00	0.54232E-05	0.12000E-02
-0.12589E 05	0.20298E 00	0.40412E-05	0.93844E-03
-0.15849E 05	0.19204E 00	0.29316E-05	0.75562E-03
-0.19953E 05	0.18158E 00	0.22758E-05	0.61399E-03
-0.25119E 05	0.17113E 00	0.18078E-05	0.49890E-03
-0.31623E 05	0.16067E 00	0.14359E-05	0.40539E-03
-0.39811E 05	0.15022E 00	0.10071E-05	0.32941E-03
-0.50119E 05	0.14221E 00	0.69129E-06	0.28072E-03
-0.63096E 05	0.13426E 00	0.54733E-06	0.23946E-03
-0.79433E 05	0.12631E 00	0.42539E-06	0.20427E-03
-0.10000E 06	0.11870E 00	0.32897E-06	0.17555E-03
-0.12589E 06	0.11116E 00	0.26015E-06	0.15109E-03
-0.15849E 06	0.10362E 00	0.18607E-06	0.13003E-03

Table C.5. -- continued

Matric Potential (mm)	Water Content (mm/mm)	Specific Water Capacity (1/mm)	Hydraulic Conductivity (mm/hr)
-0.25119E 06	0.92927E-01	0.80438E-07	0.10520E-03
-0.31623E 06	0.88275E-01	0.63894E-07	0.95957E-04
-0.39811E 06	0.83622E-01	0.50753E-07	0.87521E-04
-0.50119E 06	0.78970E-01	0.39760E-07	0.79828E-04
-0.63096E 06	0.74446E-01	0.28574E-07	0.72995E-04

From Clark (1982)

REFERENCES

Aboukhaled, A., A. Alfaro, and M. Smith. 1982. Lysimeters. FAO irrigation and drainage paper 39. Food and Agric. Organization of the United Nations. Rome. 68 pages.

Amerman, C.R. 1976. Soil water modeling I: A generalized simulator of steady, two-dimensional flow. Transactions of the ASAE 19(3):466-470.

Belmans, C., J. Feyen, and D. Hillel. 1979. An attempt at experimental validation of macroscopic-scale models of soil moisture extraction by roots. Soil Sci. 127(3):174-186.

Brandt, A., E. Bresler, N. Diner, I. Ben-Asher, J. Heller, and D. Goldberg. 1971. Infiltration from a trickle source: I. Mathematical models. Soil Sci. Soc. Amer. Proc. 35:675-682.

Brooks, R.H. and A.T. Corey. 1966. Properties of porous media affecting fluid flow. J. Irrig. Drain. Div. Am. Soc. Civil Eng. 92(IR2):61-68.

Carnahan, B., N.A. Luther, and J.O. Wilkes. 1969. Applied numerical Methods. John Wiley and Sons, New York.

Childs, E.C. 1940. The use of soil moisture characteristics in soil studies. Soil Sci. 50:239-252.

Childs, E.C. 1957. The physics of land drainage. Ch. 1 in Drainage of agricultural lands, J.N. Luthin (ed.), Am. Soc. Agron., Madison, WI.

Chow, V.T. 1964. Handbook of applied hydrology. McGraw-Hill, New York.

Clark, G.A. 1982. Simulation of the sensitivity of water movement and storage in sandy soils to irriation application rate and depth. M.S. Thesis. Univ. of Florida, Gainesville, FL.

Clark, G.A. 1989. Personal communication. Assistant Professor of Agricultural Engineering, Univ. of Florida, Gainesville, FL.

Clayton, B.S., J.R. Neller, and R.V. Allison. 1942. Water control in the peat and muck soils of the Florida Everglades. Fla. Agr. Exp. Sta. Bul. 378, Univ. of Florida, Gainesville, FL.

Colman, E.A. and T.M. Hendrix. 1949. Fiberglass electrical soil moisture instrument. Soil Sci. 67:425-438.

Darcy, H. 1856. Determination of the laws of the flow of water through sand. The public fountains of the city of Dijon pp. 590-594, Victor Dalmont, Paris.

Denmead, O.T. and R.H. Shaw. 1962. Availability of soil water to plants as affected by soil moisture content and meteorological conditions. Agron. J. 45:385-390.

Feddes, R.A., P. Kowalik, S.P. Neuman, and E. Bresler. 1976. Finite difference and finite element simulation of field water uptake by plants. Hydrologic Sciences Bulletin 21(3):82-98.

Feddes, R.A., P.J. Kowalik, and H. Zaradny. 1978. Simulation of field water use and crop yield. Halsted Press, New York.

Freeze, R.A. and J.A. Cherry. 1979. Groundwater. Prentice-Hall, Englewood Cliffs, NJ.

Gardner, W.R. 1958. Some steady-state solutions of the unsaturated moisture flow equation with application to evaporation from a water table. Soil Sci. 85:228-232.

Gardner, W.R. 1960. Dynamic aspects of water availability to plants. Soil Sci. 89:63-73.

Gardner, W.R. 1964. Relation of root distribution to water uptake and availability. Agron. J. 56:41-45.

Gardner, W.R. and C.F. Ehlig. 1962. Some observations on water movement to plant roots. Agron. J. 54:453-456.

Gardner, W.R. and M. Fireman. 1958. Laboratory studies of evaporation from soil columns in the presence of a water table. Soil Sci. 85:244-249.

Gilley, J.R. and E.R. Allred. 1974. Infiltration and root extraction from subsurface irrigation laterals. Transactions of the ASAE 17(6):927-933.

Goldstein, A. (ed.). 1988. 1987 Irrigation survey. Irrig. J. 38(1):23-32.

Gradmann, H. 1928. Untersuchungen über die wasserverhältnisse des bodens als grundlage des pflanzenwachstums. Jahrb. Wiss. Bot. 69(1)1-100.

Green, R.E. and J.C. Corey. 1971. Calculation of hydraulic conductivity: a further evaluation of some predictive methods. Soil Sci. Soc. Am Proc. 35:3-8.

Hamon, W.R. 1966. Evapotranspiration and water yield predictions. Proceedings of the Conference on Evapotranspiration and Its Role in Water Resources Management, pp 8-13, ASAE, St. Joseph, MI.

Harrison, D.S., A.G. Smajstrla, R.E. Choate, and G.W. Isaacs. 1983. Irrigation in Florida agriculture in the '80s. Bulletin 196, Fla. Coop. Ext. Serv., Univ. of Florida, Gainesville, FL.

Haverkamp, R. and M. Vauclin. 1979. A Note on estimating finite difference interblock hydraulic conductivity values for transient unsaturated flow problems. Water Resour. Res. 15(1):181-187.

Haverkamp, R., M. Vauclin, J. Touma, P.J. Wierenga, and G. Vachaud. 1977. A comparison of numerical simulation models for one-dimensional infiltration. Soil Sci. Soc. Am. J. 41:285-294.

Hillel, D. 1980. Fundamentals of soil physics. Academic Press, New York.

Hornberger, G.M., I. Remson, and A.A. Fungaroli. 1969. Numeric studies of a composite soil moisture ground-water system. Water Resour. Res. 5:797-802.

Kidder. G. 1983. Interpretation of micronutrient soil tests. Notes in Soil Science No. 9, Coop. Ext. Ser., Inst. Food Agr. Sci., Univ. of Florida, Gainesville, FL

Klute, A. 1965. Water capacity. Ch. 18 in Methods of soil analysis, Part 1, C.A. Black et al. (eds.), Am. Soc. Agron., Madison, WI, p. 273-278.

Lomen, D.O. and A.W. Warrick. 1974. Time-dependent linearized infiltration: II. Line sources. Soil Sci. Soc. Amer. Proc. 38(4):568-572.

Marthaler, H.P., W. Vogelsanger, F. Richard, and P.J. Wierenga. 1983. A pressure transducer for field tensiometers. Soil Sci. Soc. Amer. Proc. 47:624-627.

Millington, R.J. and J.P. Quirk. 1961. Permeability of porous solids. Trans. Faraday Soc. 57:1200-1206.

Molz, F.J. 1981. Models of water transport in the soil-plant system: A review. Water Resour. Res. 17(5):1245-1260.

Molz, F.J. and I. Remson. 1970. Extraction term models of soil moisture use by transpiring plants. Water Resour. Res. 6(5):1346-1356.

Molz, F.J., I. Remson, A.A. Fungaroli, and R.L. Drake. 1968. Soil moisture availability for transpiration. Water Resour. Res. 4(6):1161-1169.

Moore, R.E. 1939. Water conduction from shallow water tables. Hilgardia 12:383-426.

Mualem, Y. 1976. A new model for predicting the hydraulic conductivity of unsaturated porous media. Water Resour. Res. 12:513-522.

Mualem, Y. 1986. Hydraulic conductivity of unsaturated soils: prediction and formulas. Ch. 31 in Methods of soil analysis, Part 1, A. Klute, (ed.), American Society of Agronomy, Madison, WI.

Newman, E.I. 1969. Resistance to water flow in soil and plant. I. Soil resistance in relation to amounts of root: theoretical estimates. J. Appl. Ecol. 6:1-12.

Nimah, M.N. and R.J. Hanks. 1973a. Model for estimating soil water, plant, and atmospheric interrelations: I. Description and sensitivity. Soil Sci. Soc. Amer. Proc. 37:522-527.

Nimah, M.N. and R.J. Hanks. 1973b. Model for estimating soil water, plant, and atmospheric interrelations: II. Field test of model. Soil Sci. Soc. Amer. Proc. 37:528-532.

Oron, G. 1981. Simulation of water flow in the soil under sub-surface trickle irrigation with water uptake by roots. Agric. Water Manage. 3:179-193.

Penman, H.L. 1970. The water cycle. Sci. Am. 222:99-108.

Perrens, S.J. and K.K. Watson. 1977. Numerical analysis of two-dimensional infiltration and redistribution. Water Resour. Res. 13(4): 781-790:

Philip, J.R. 1959. Theory of infiltration. Advances in Hydroscience 5:215-296.

Poulovassilis, A. 1962. Hysteresis of pore water, an application of the concept of independent domains. Soil Sci. 93:405-412.

Raats, P.A.C. 1970. Steady infiltration from line sources and furrows. Soil Sci. Soc. Amer. Proc. 34(5):709-714.

Ragab, R., J. Feyen, and D. Hillel. 1984. Simulating infiltration into sand from a trickle line source using the matric flux potential concept. Soil Sci. 137(2):120-127.

Reddell, D.L. and D.K. Sunada. 1970. Numerical simulation of dispersion in groundwater aquifers. Hydrology paper 41, Colorado State Univ., Fort Collins, CO.

Richards, L.A. 1931. Capillary conductivity of liquids through a porous medium. Physics 1:318-333.

Ritchie, J.T. 1973. Influence of soil water status and meteorological conditions on evaporation from a corn canopy. Agron. J. 65:893-897.

Rubin, J. 1966. Theory of rainfall uptake by soils initally drier than their field capacity and its application. Water Resour. Res. 2(4): 739-749.

Rubin, J. 1968. Theoretical analysis of two-dimensional, transient flow of water in unsaturated and partly unsaturated soils. Soil Sci. Soc. Amer. Proc. 32(5):607-615.

Rubin, J. and R. Steinhardt. 1963. Soil water relations during rain infiltration: I. Theory. Soil Sci. Soc. Amer. Proc. 27:246-251.

Shih, S.F., G.J. Gascho, and J.W. Mishoe. 1977. A lysimeter system for water table control. ASAE Paper No. 77-2575. Amer. Soc. Agr. Eng., St. Joseph, MI.

Slack, D.C. 1975. Modeling the uptake of soil water by plants. Ph.D. Dissertation. Univ. of Kentucky, Lexington, KY.

Slack, D.C., C.T. Haan, and L.G. Wells. 1977. Modeling soil water movement into plant roots. Transactions of the ASAE 20(5):919-927.

Smajstrla, A.G. 1982. Irrigation management for the conservation of limited water resources. Office of Water Research and Technology of the Department of Interior Water Conservation Research Program (WRC-80).

Smajstrla, A.G. 1985. A field lysimeter system for crop water use and water stress studies in humid regions. Proc. Soil & Crop Sci. Soc. Fla. 44:53-59.

Speir, W.H. 1962. Installation and operation of non-weighing lysimeter. Proc. Soil & Crop Sci. Soc. Fla. 22:167-176.

Steinhardt, R., R.R. Van der Ploeg, and W. Ehlers. 1982. Comparing forms and solutions of the single root soil water extraction model. Soil Tillage Res. 2:347-357.

Stephens, J.M. 1984. Tomatoes in the Florida garden. Vegetable Crops Fact Sheet No. 8, Coop. Ext. Ser., Inst. Food Agr. Sci., Univ. of Florida, Gainesville, FL.

Stone, K.C. 1987. Measurement and simulation of soil water status under field conditions. Ph.D. Dissertation. Univ. of Florida, Gainesville, FL.

Stone, K.C., A.G. Smajstrla, and F.S. Zazueta. 1985. Microcomputer-based data acquisition system for continuous soil water potential measurements. Proc. Soil & Crop Sci. Soc. Fla. 44:49-53.

Taylor, S.A. and G.L. Ashcroft. 1972. Physical edaphology. W.H. Freeman and Company, San Fransisco.

Thomas, A.W., H.R. Duke, D.W. Zachman, and E.G. Kruse. 1976. Comparisons of calculated and measured capillary potentials from line sources. Soil Sci. Soc. Amer. J. 40(1):10-14.

Thomas, A.W., E.G. Kruse, and H.R. Drake. 1974. Steady infiltration from line sources buried in soil. Transactions of the ASAE 17(1):125-128, 133.

Thomson, S.J., E.D. Threadgill, and J.R. Stansell. 1982. Field test of a microprocessor based center pivot irrigation controller. ASAE Paper No. 82-2535, ASAE, St. Joseph, MI.

Tollner, E.W. and F.J. Molz. 1983. Simulating plant water uptake in moist, ligther textured soils. Transactions of the ASAE 26(1):87-99.

van den Honert, T.H. 1948. Water transport as a catenary process. Faraday Soc. Discuss. 3:146-153.

van Genuchten, M.Th. 1980. A closed-form equation for predicting the hydraulic conductivity of unsaturated soils. Soil Sci. Soc. Am. J. 44:892-898.

Warrick, A.W. 1974. Solution to the one-dimensional linear moisture flow equation with extraction. Soil Sci. Soc. Amer. Proc. 38(4):573-576.

Warrick, A.W., A. Amoozegar-Fard, and D.O. Lomen. 1979. Linearized moisture flow from line sources with water extraction. Transactions of the ASAE 22(3):549-553, 559.

Warrick, A.W. and D.O. Lomen. 1977. Flow from a line source above a shallow water table. Soil Sci. Soc. Am. J. 41(5):849-852.

Whisler, F.D., A. Klute, and R.J. Millington. 1970. Analysis of radial, steady-state solution, and solute flow. Soil Sci. Soc. Amer. Proc. 34:382-387.

Zachmann, D.W. and A.W. Thomas. 1973. A mathematical investigation of steady infiltration from line sources. Soil Sci. Soc. Amer. Proc. 37(4):495-500.

Zaradny, H., 1978. Boundary conditions in modeling water flow in unsaturated soil. Soil Sci. Soc. 125(2):75-82.

BIOGRAPHICAL SKETCH

George Vellidis was born October 21, 1962, at Kitwe, Zambia. In 1971, he and his family moved to Greece, their native country, where they now live.

George completed his secondary education in Thessaloniki in 1979. That same year, he began his college education at Virginia Polytechnic Institute and State University where he received a B.Sc. degree in agricultural engineering in June, 1983, and a M.S. degree in agricultural engineering in June, 1985. He enrolled at the University of Florida in July, 1985, to pursue a Ph.D. degree in agricultural engineering.

I certify that I have read this study and that in my opinion it conforms to acceptable standards of scholarly presentation and is fully adequate, in scope and quality, as a dissertation for the degree of Doctor of Philosophy.

Allen G. Smajstrla, Chair
Professor of Agricultural Engineering

I certify that I have read this study and that in my opinion it conforms to acceptable standards of scholarly presentation and is fully adequate, in scope and quality, as a dissertation for the degree of Doctor of Philosophy.

Gary A. Clark
Assistant Professor of Agricultural Engineering

I certify that I have read this study and that in my opinion it conforms to acceptable standards of scholarly presentation and is fully adequate, in scope and quality, as a dissertation for the degree of Doctor of Philosophy.

Dorota Z. Haman
Assistant Professor of Agricultural Engineering

I certify that I have read this study and that in my opinion it conforms to acceptable standards of scholarly presentation and is fully adequate, in scope and quality, as a dissertation for the degree of Doctor of Philosophy.

Fedro S. Zazueta-Ranahan
Associate Professor of Agricultural Engineering

I certify that I have read this study and that in my opinion it conforms to acceptable standards of scholarly presentation and is fully adequate, in scope and quality, as a dissertation for the degree of Doctor of Philosophy.

Joseph J. Delfino
Professor of Environmental Engineering Sciences

This dissertation was submitted to the Graduate Faculty of the College of Engineering and to the Graduate School and was accepted as partial fulfillment of the requirements for the degree of Doctor of Philosophy.

May 1989

Dean, College of Engineering

Dean, Graduate School